POLITECNICO DI TORINO

Department of Chemical and Materials Engineering

Master Degree

in Chemical and Sustainable Process Engineering

Master Degree Thesis

Combinatorial Deposition of Thin Films: Study of pH Variation Using Fluorescent Dyes

Supervisors

Prof. Sabrina Grassini

Prof. Yuval Golan

Candidate

Angela Di Lorenzo

July 2024

Contents

1. Introduction 1
1.1. Organic dyes 2
1.2. Techniques for Measuring pH 4
1.2.1. Electrochemical method 4
1.2.2. Non electrochemical method 5
1.3. Fluorescence 6
1.3.1. Fluorescence-influencing factors 12
1.4. Investigation of Temperature Effects on Dyes 14
2. Materials and methods 19
2.1. Selection of dyes 20
2.1.1. Rhodamine B 20
2.1.2. Rhodamine 6G 21
2.1.3. Indigo Carmine 22
2.1.4. Titan Yellow 22
2.2. Preparation of solutions at different pH 24
2.3. Fluorescence Analysis 25
2.3.1. Lab setup 25
2.3.2. How to interpret fluorescence peaks 28
2.4. Temperature analysis 29
2.4.1. Optical interrogator 29
2.4.2. Temperature compensation 32
2.5. Effect of Metal Cations on Dye Fluorescence 33
2.6. Kinetic Studies 35
3. Results 37
3.1. Fluorescence Analysis 37
3.1.1 Rhodamine B 37
3.1.2. Indigo Carmine 41
3.1.3 Rhodamine 6G 45
3.1.4. Titan Yellow 50
3.2. Mixing 52
3.3. Temperature analysis 55
3.4. Stability over time 59
3.4.1. Rhodamine 6G 59
3.4.2. Rhodamine B 62

3.5. Effect of Metal Cations on Dye Fluorescence 64
3.5.1. Rhodamine 6G 64
3.5.3. Rhodamine B 66
3.6. Kinetic study 67
3.6.1. Rhodamine 6G 67
3.6.1. Rhodamine B 70
3.7. Florescence Intensity Analysis of Rhodamine 6G with pH 71
4. Conclusion 75
5. Bibliography 77
Acknowledgements 81

Abstract

Combinatorial thin-film deposition is an innovative technique for the synthesis and discovery of new materials, designed to efficiently explore a wide range of compositions and process parameters. This is a technique widely used in various areas of chemical engineering to create nanometer-thick layers of material on a substrate.

Research teams from Ben-Gurion University of Negev (Beersheva, Israel) and the Polytechnic of Turin recently collaborated to study combinatorial in-flow deposition of thin films, publishing the results in the paper *"A Combinatorial Approach for the Solution Deposition of Thin Films."* The research offers a combinatorial method for the deposition of thin films from solution that allows two crucial parameters - temperature and deposition time - to be examined simultaneously on a single sample.

This thesis aims to develop innovative combinatorial deposition systems for multicomponent thin films and to study the impact of reagents concentration changes on film properties. The challenge is to create and measure a pH gradient using a linear alkaline solution blower and optical fibers to monitor pH changes through the solution optical transmittance, using fluorescent dyes. Light reflected from the sample surface is directed to an array of photodiodes to measure changes in optical transmittance as a function of time. The thesis employs a continuous flow reactor developed at Ben Gurion University's Department of Materials Engineering, designed to establish a pH gradient within an alkaline range from pH 12.5 to 14.25.

The investigated dyes are Rhodamine B, Rhodamine 6G, Indigo Carmine, and Titan Yellow. The effect of pH on fluorescence was analyzed by examining the changes in fluorescence intensity and in characteristic wavelength of the peak_for each dye once added to alkaline solutions. All tests were conducted in cuvettes, and signal acquisition was performed by an Avantes spectrometer. To simulate the behavior of the dyes within the continuous flow reactor as accurately as possible, several key parameters were examined: Temperature, stability over time, mixing, stability in the presence of metallic cations (Pb^{2+} and Sn^{4+}) and kinetic response.

The analyses identified Rhodamine 6G as the most suitable dye for the application, demonstrating enhanced stability in the presence of metal cations and over time. Additionally, Rhodamine 6G showed a rapid and reliable kinetic response to pH changes compared to the other dyes analyzed.

Abstract (italiano)

La deposizione combinatoria di film sottili è una tecnica innovativa per la sintesi e la scoperta di nuovi materiali, progettata per esplorare una vasta gamma di composizioni e parametri di processo. Si tratta di una tecnica ampiamente utilizzata in vari settori dell'ingegneria chimica per creare strati di materiale di spessore nanometrico su un substrato.

I gruppi di ricerca dell'Università Ben-Gurion del Negev (Beersheva, Israele) e del Politecnico di Torino hanno recentemente collaborato per studiare la deposizione combinatoria in flusso di film sottili, pubblicando i risultati nell'articolo "*A Combinatorial Approach for the Solution Deposition of Thin Films".* La ricerca propone un metodo combinatorio per la deposizione di film sottili da soluzione che consente di esaminare simultaneamente due parametri cruciali - temperatura e tempo di deposizione - su un singolo campione.

Questa tesi mira a sviluppare sistemi innovativi di deposizione combinatoria per film sottili multicomponente e a studiare l'impatto delle variazioni di concentrazione dei reagenti sulle proprietà dei film. La sfida consiste nel creare e misurare un gradiente di pH utilizzando un soffiatore lineare di soluzione alcalina e fibre ottiche per monitorare i cambiamenti di pH tramite la trasmissione ottica della soluzione, con l'uso di coloranti fluorescenti. La luce riflessa dalla superficie del campione è diretta verso una serie di fotodiodi per misurare le variazioni nella trasmissione ottica nel tempo. La tesi utilizza un reattore a flusso continuo, sviluppato presso il Dipartimento di Ingegneria dei Materiali dell'Università Ben Gurion, progettato per stabilire un gradiente di pH compreso tra 12,5 e 14,25.

I coloranti studiati sono: Rhodamine B, Rhodamine 6G, Indigo Carmine e Titan Yellow. L'effetto del pH sulla fluorescenza è stato analizzato esaminando le variazioni di Intensità della fluorescenza e Lunghezza d'onda del picco per ciascun colorante una volta aggiunto a soluzioni alcaline. Tutti i test sono stati condotti in cuvette e l'analisi della fluorescenza è stata eseguita con uno spettrometro Avantes. Per simulare il comportamento dei coloranti all'interno del reattore a flusso continuo nel modo più accurato possibile, sono stati esaminati diversi parametri chiave: Temperatura, stabilità nel tempo, miscelazione, stabilità in presenza di cationi metallici (Pb^{2+} e Sn^{4+}) e risposta cinetica.

Le analisi hanno identificato Rhodamine 6G come il colorante più adatto per l'applicazione della tesi, dimostrando una maggiore stabilità in presenza di cationi metallici e nel tempo.

Inoltre, la Rhodamine 6G ha mostrato una risposta cinetica rapida e affidabile ai cambiamenti di pH rispetto agli altri coloranti analizzati.

1. Introduction

Combinatorial thin-film deposition is an innovative technique for the synthesis and discovery of new materials, designed to efficiently a wide range of compositions and process parameters. This is a technique widely used in various areas of chemical engineering to create nanometer-thick layers of material on a substrate.

This method enables the systematic study of the effect of various deposition parameters (namely temperature, deposition time, pH, and reagent concentration) on the properties of thin films and allows identification of optimal combinations of reagents and deposition parameters. Research teams at Ben-Gurion University of Negev (Beersheva, Israel) and the Polytechnic of Turin recently collaborated to study combinatorial in-flow deposition of thin films.

The results were published in the paper *"A Combinatorial Approach for the Solution Deposition of Thin Films."* [1]

The research offers a combinatorial method for thin-film deposition from solution that enables the examination of two crucial parameters - temperature and deposition time - to be examined simultaneously on a single sample. The method creates a horizontal temperature gradient varied by adding cold solution to a heated reactor.

The reactor used in the research establishes regulated conditions for deposition, maintains temperature gradients, and guarantees uniformity of the deposition process and facilitates the systematic investigation of the impact of the crucial parameters on thin film growth.

(Figure 1.1.1).

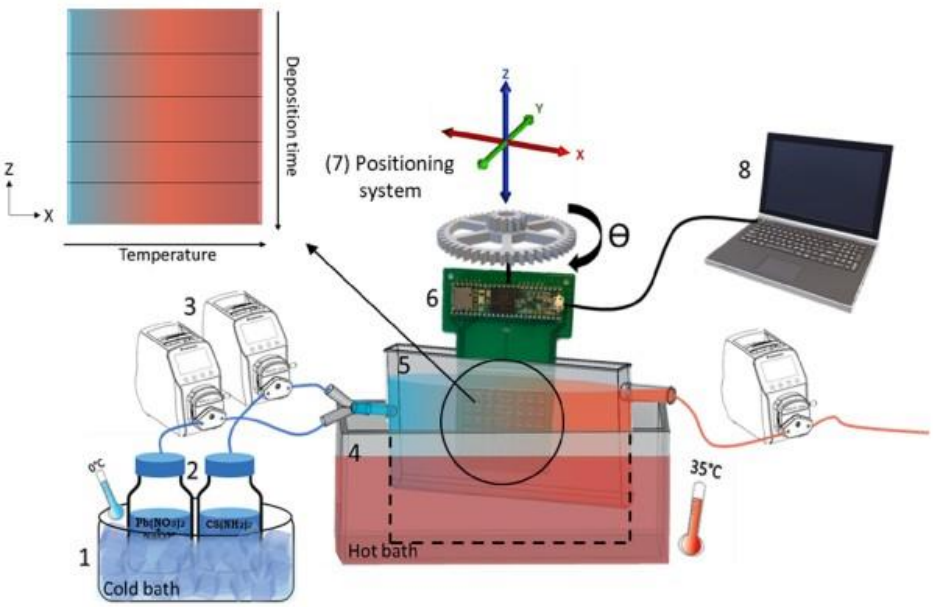

Figure 1.1.1. A schematic illustration of the experimental conditions depicting discrete deposition time steps along the z-axis and the temperature gradient along the x-axis. Blue represents the cold solution temperature, and red represents the hot solution temperature. Image taken from [1].

This thesis aims to develop innovative combinatorial deposition systems for multi-component thin films and study the impact of concentration changes on the film properties.

The challenge is to create and measure a pH gradient along the flow direction by adding a horizontal, linear showerhead that introduces concentrated alkaline solutions along the flow direction. To assess the pH gradient, fluorescent organic dyes were employed in the solution within the reactor. The pH is measured at designated points along the horizontal direction of the sample by using a linear array of fiber optic light sources that will emit monochromatic light onto the sample. The light reflected from the sample surface will be directed to a corresponding array of photodiodes for measuring time-dependent changes in optical transmittance.

The reactor used in this study is a custom-designed open-top continuous flow reactor. This open design facilitates access and manipulation of the substrate during deposition, and it is designed to maintain uniform and constant deposition conditions throughout the process.

By placing the optical sensor outside the glass reactor, out of direct contact with the solution, it avoids interference with the ongoing chemical process. This is an advantage over traditional pH sensors that require immersion in the environment to be perform the measurement.

1.1. Organic dyes

Fluorescent organic dyes are preferred for their cellular characteristics, simplicity, and sensitivity. They were chosen for the following properties:

- They rely on pH-induced changes in electronic structure that alter fluorescence characteristics for pH measurement and adjust their emitted light in reaction to pH change.

- They are sensitive to pH over a wide range of concentration, from acidic to alkaline values.

- They are unaffected by the presence of common ions, allowing accurate measurements even in the presence of interfering species.

-The fluorescent response of the dyes is reversible to changes in pH. This allows real-time tracking of pH variations throughout the process. [2][3]

Organic fluorescent dyes, such as coumarins, BODIPY dyes, fluoresceins, cyanines, and rhodamines, are frequently employed as fluorescent markers in a range of applications. [4][7]

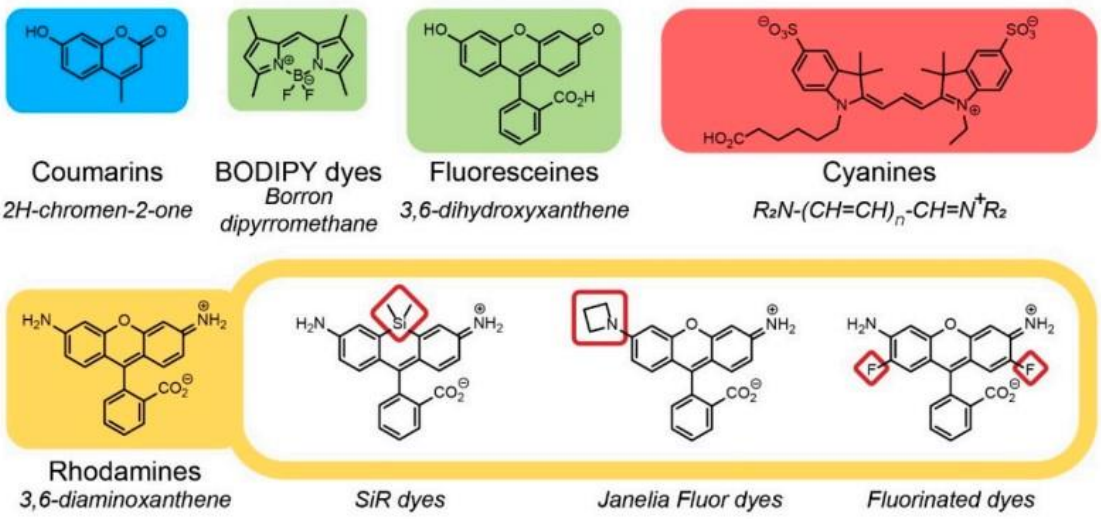

Figure 1.1.2. "Examples of fluorescence dyes with the background colored according to the wavelength maxima of fluorescence emission and examples of modifications of the rhodamines dye family." Image taken from [7].

- Coumarins are blue fluorescent dyes that can be excited by UV light and have short emission wavelengths, approximately between 390 and 480 nm. They are helpful for direct imaging of high-abundant targets, cell tracking, and the detection of enzyme activity. They are frequently employed for labeling biomolecules such as antibodies, proteins, nucleic acids, and oligonucleotides. [4][8]

- The extremely adaptable class of fluorophores known as BODIPY (boron-dipyrromethene) dyes is distinguished by its vivid fluorescence and resistance to environmental fluctuations. [5]

- Green fluorescent dyes such as fluoresceines are frequently utilized as fluorescent markers because of their high quantum yields and extinction coefficients. They are frequently used with other dyes in multicolor fluorescence applications. [5]

- A class of fluorescent dyes known as cyanine dyes emits light at a variety of wavelengths, ranging from blue to near-infrared. They are frequently employed in FRET-based applications and as luminous markers. [5]

- Reddish-orange fluorescent dyes called rhodamines are highly photostable and brilliant. They are widely employed as fluorescent markers for nucleic acids, peptides, and proteins.[5][6]

1.2. Techniques for Measuring pH

pH plays a critical role in many aspects of environmental, chemical and biological fields, as well as in industry and in the development of new materials.

The pH measurement methods are of two types: electrochemical and non-electrochemical. **(Figure 1.2.1)**

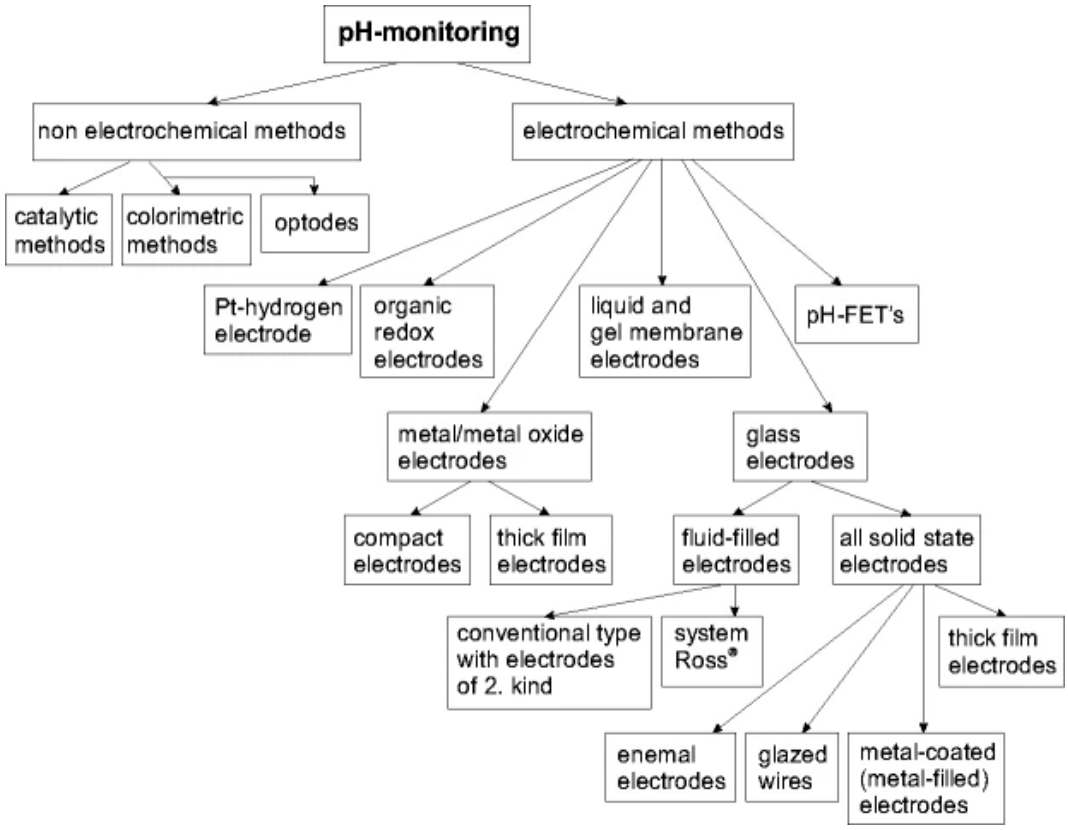

Figure 1.2.1. Techniques for Measuring pH Levels. Image taken from [34].

1.2.1. Electrochemical method

These systems utilize the electrical properties of solutions to determine pH, relying on the measurement of the potential difference between electrodes immersed in the solution.

Among electrochemical methods, the most widely used is the glass electrode method, which employs glass electrodes to measure pH.

The glass pH electrode is able to detect pH from acid to neutral and alkaline conditions with performance, offering a low detection limit, long-term stability and high reproducibility.

In its simplest form, the glass electrode is a thin glass bulb filled with a pH-controlled solution, typically hydrochloric acid or a phosphate buffer containing potassium chloride.

This solution contains an electrode, usually silver coated with silver chloride.

The electrode response is generated by the exchange of ions in the glass membrane.

The pH-sensitive tip is stored in a buffer solution containing potassium chloride at pH 7. **(Figure 1.2.2.)**

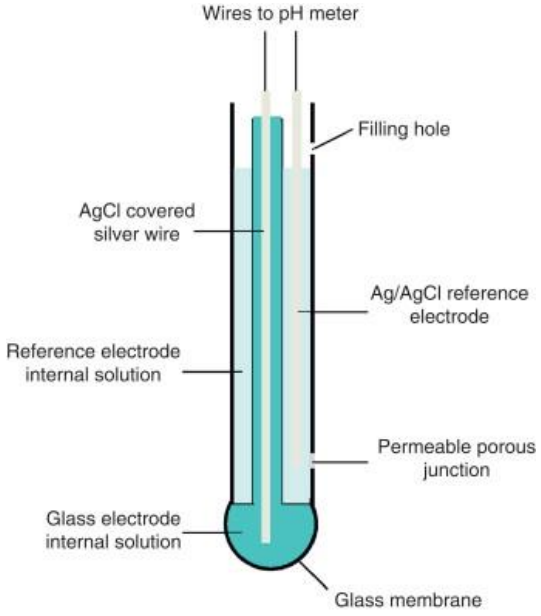

Figure 1.2.2. Glass electrode system. Image taken from [33].

This type of system presents some limitation:

- Glass electrodes must always be calibrated before use using standard buffer solutions, due to the existence of an asymmetry potential in the glass/liquid interface.

- The internal solution undergoes a constant degradation by diffusion inside and outside the electrode over several months, resulting in a decrease in the inclination of the electrodes response.

- The mechanical structure is fragile.

- It is difficult to manufacture pH electrodes of small size to measure small-volume samples.

1.2.2. Non electrochemical method

Among the non-electrochemical methods, optodes are the most widespread for pH measurement. They are optical systems that are based on fluorescence change or absorption of pH-sensitive indicators in response to changes in H^+ ions in the solution to be analyzed. The basic equipment for optical sensing includes a light source, an adjustable monochromator, a sample holder and a detector, with the monochromators selecting the

excitation and emission wavelengths and monitoring the variations in the light intensity of the source. **(Figure 1.2.3.)** Fluorescence-based indicators are more sensitive than absorption-based ones and require a lower concentration of the indicator, offering high sensitivity, quick response times, and technical simplicity. The pollution of the sample and diffused or dispersed light can compromise the accuracy of the instrument. The emission spectrum of the sample and the reference sample must be accurately assessed to ensure the reliability of the measurements. [33] [34] [35]

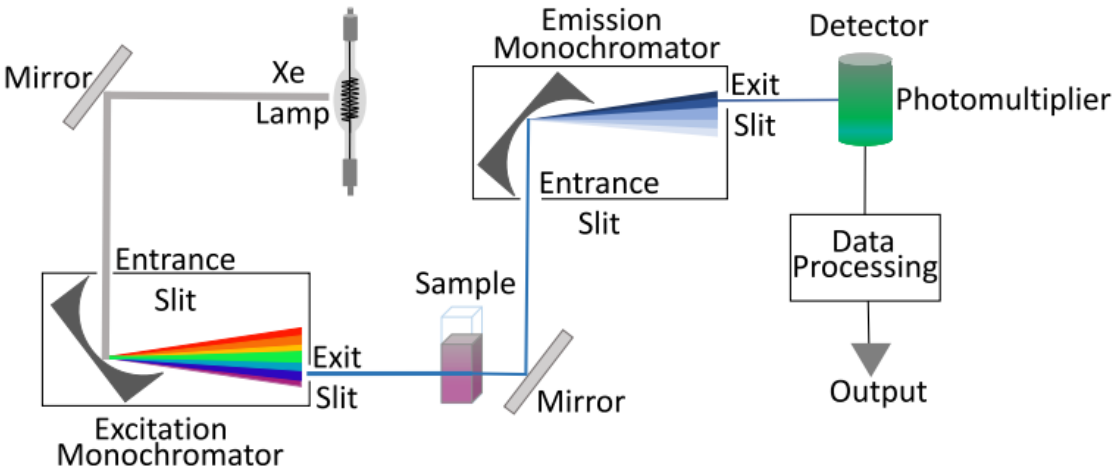

Figure 1.2.3. Optical Systems for pH Measurement. Image taken from [35].

1.3. Fluorescence

Theoretical background

Fluorescence is a phenomenon whereby light is absorbed by a substance at one wavelength then emitted at a longer wavelength. When photons strike a fluorescent molecule, it absorbs the light's energy and becomes excited, elevating it to a higher electronic state. The molecule eventually relaxes by emitting a photon as it returns to the ground state, often emitting in the visible light spectrum. The precise wavelengths involved in absorption and emission determine the observed color of fluorescence.

Luminescence is a process where light is released by certain materials when electronically stimulated. It encompasses both fluorescence and phosphorescence, which differ in their excited state properties. Phosphorescence occurs when the electron remains in an electronically excited state for an extended time following excitation before releasing energy. Fluorescence differs in that the time period spent in the excited state is typically extremely short.

Fluorescence is prevalent in both natural and manufactured materials, including minerals, biological systems, and man-made materials such as fluorescent lighting and dyes. Fluorescence has a wide range of practical uses, including mineralogy, gemology,

medicine, chemical sensors, biological detectors, and cosmic ray detection. It is also employed in daily products like fluorescent lights and LED bulbs, which transform UV or blue light into longer wavelengths and generate white light.

Fluorescence generally arises from aromatic molecules. **Figure 1.3.1** illustrates some typical fluorescent substances known as fluorophores. [9]

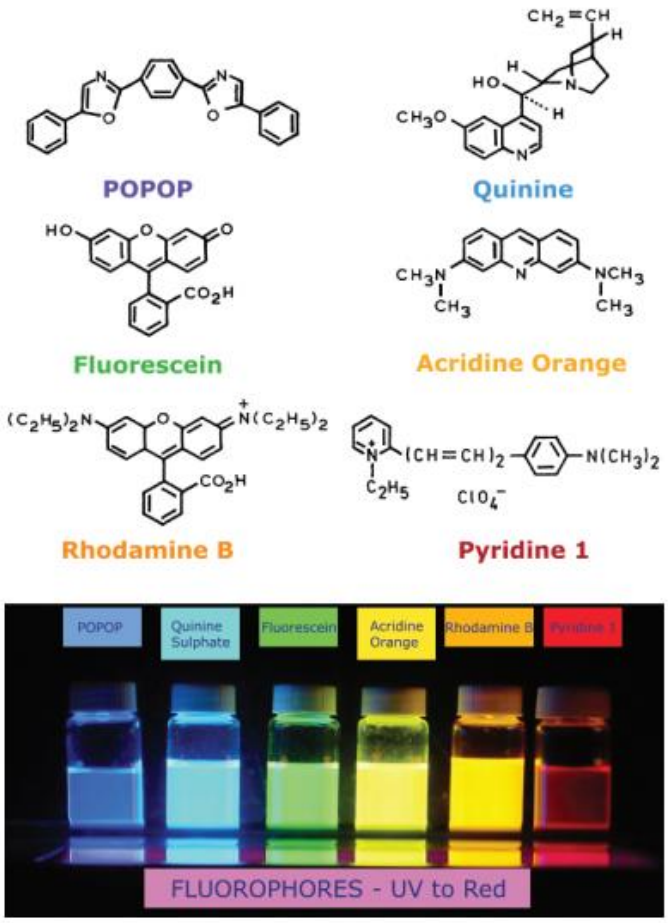

Figure 1.3.1. Chemical configurations of common fluorescent substances. Image taken from [9].

Jablonski diagrams

Jablonski diagrams are often used to represent the shift from light absorption to emission and is an effective tool for visualizing the various transitions that may occur after a molecule has been photoexcited. These diagrams illustrate the processes of light absorption and emission, highlighting molecular events that occur in excited states. [10][11] **Figure 1.3.2** depicts a typical Jablonski diagram, with explanations of the diagram's essential components and transitions below.

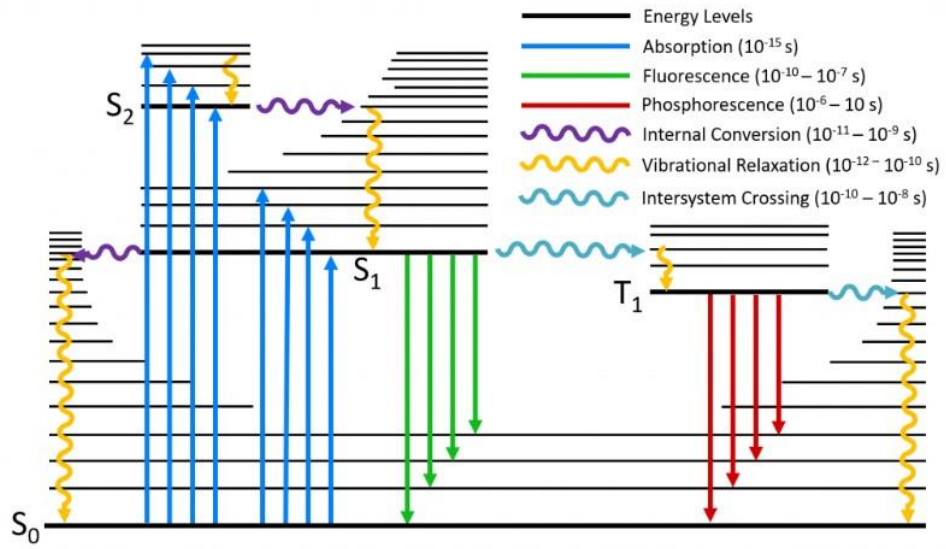

Figure 1.3.2. Jablonski diagram. Image taken from [10].

Energy Levels

The horizontal black lines represent a molecule's energy levels, which increase down the diagram's vertical axis. The bold lines reflect each electrical state's lowest vibrational level, whereas thinner lines represent higher vibrational levels.

As energy grows, the vibrational levels become closer together and finally form a continuum.
The electronic states are named for their spin angular momentum configurations.

Singlet states (a total spin angular momentum of zero) are designated by an S, and triplet states (a total spin angular momentum of one) by a T.

S0 represents the molecule's singlet ground state;

S1 is the first excited singlet state;

Sn is the nth excited singlet state;

T1 is the initial excited triplet state, while *Tn* is the subsequent excited triplet state.

Radiative and Non-radiative Transitions

The coloured arrows depict the various energy-transfer transitions between molecular states, which are classified as radiative or non-radiative. Radiative transitions are transitions between two chemical states in which photons emit or absorb the energy difference, and they are depicted by straight arrows on a Jablonski diagram. Non-radiative transitions are transitions between two chemical states that do not involve photon absorption or emission, and they are shown in a Jablonski diagram by undulating arrows.

Absorption

The absorption of a photon promotes a molecule from its ground state to a higher state, as

shown by the blue arrows in **Figure 1.3.2**. It is the fastest transition in the Jablonski diagram, with a timescale of 10^{-15} s. At normal temperature, the majority of molecules in a population will be in the lowest vibrational level of the ground state (Boltzmann distribution), indicating that absorption begins at this level. When a photon is absorbed, the molecule moves from S0 to a vibrational level of the singlet excited state (S1, S2, etc.).

Vibrational Relaxation

When a molecule is energized by absorption, it is in a non-equilibrium state. It eventually dissipates the energy obtained and returns to the ground state. The first way energy is lost is through vibrational relaxation (orange arrows), which occurs when excess vibrational energy is lost to vibrational modes within the same molecule (intramolecular) or to surrounding molecules (intermolecular) until the lowest vibrational level of the electronic state is achieved. Vibrational relaxation happens on a time scale of 10^{-12} to 10^{-10} s and outperforms all other transitions.

Internal Conversion

A molecule in a higher lying singlet electronic state can also undergo internal conversion to a lower lying singlet electronic state, as illustrated by the purple arrows in **Figure 1.3.2.** Vibrational relaxation to the electronic state's lowest vibrational level occurs immediately after internal conversion. The rate of internal conversion is inversely related to the energy difference between two electronic states. Internal conversion of the closely spaced higher lying singlet excited states ***(S3 → S2, S2 → S1, etc.)*** will occur fast on a timescale of 10^{-11} to 10^{-9} s. In contrast, the energy gap between S1 and S0 is substantially larger, and internal conversion between these states happens on a slower timeframe, competing with other transitions like fluorescence and intersystem crossover.

Stokes shift

Fluorescence is the emission of photons from the ***S1 → S0*** radiative transition on a timeframe of 10^{-10} to 10^{-7} s, as depicted by the green arrows in **Figure 1.3.2.**

Fluorescence occurs as a result of the quick vibrational relaxation and internal conversion processes outlined above, from the lowest vibrational level of the first electrically excited singlet state to the singlet ground state. [9]

The absorption and emission of energy are distinct features of a specific molecular structure. The Stokes shift refers to the energy differential (or wavelength) between absorbed and released photons, as seen in **Figure 1.3.3.** A large **Stokes shift** is frequently desired because it eliminates the need for optical filters, which are used to separate exciting light from fluorescence emission. The fluorescence process's efficiency is described by its quantum yield, which is the ratio of photons emitted to photons received.

$$\Phi = \frac{Number\ of\ photons\ emitted}{Number\ of\ photons\ absorbed} \qquad (1.3.1)$$

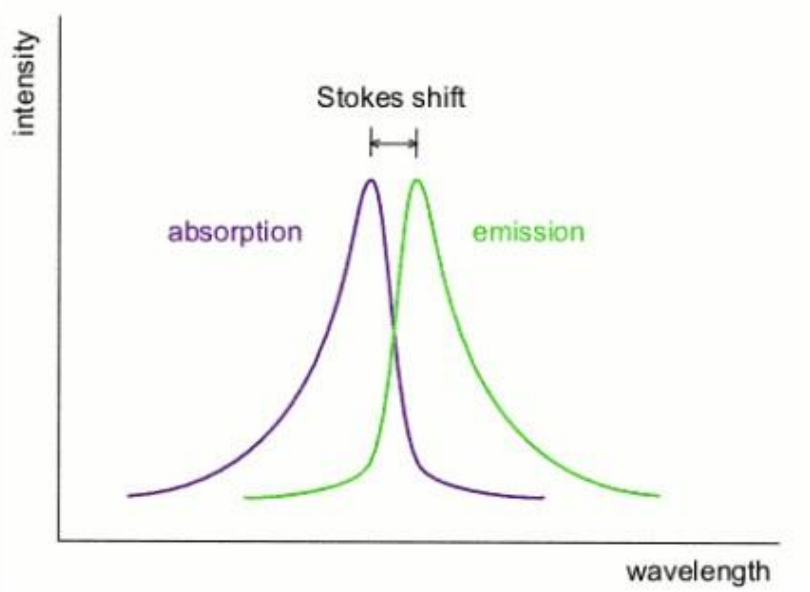

Figure 1.3.3. The absorption and emission bands of a molecule. The differences in wavelength between the peaks is known as Stokes shift. Image taken from [9].

The rates of radiative ***(k_r)*** and non-radiative ***(k_{nr})*** electron de-excitation can also be used to characterize this phenomenon.

$$\Phi = \frac{kr}{kr+knr} \qquad (1.3.2)$$

Quantum yield ranges from 0 to 1, with 0 indicating non-fluorescing materials and 1 indicating highly fluorescent materials that emit photons for every photon absorbed. The average duration a molecule spends in an excited state before emitting a photon is referred to as the lifetime. Fluorescence intensity decreases when excitation stops. This drop is proportional to the rate of electron de-excitation and can be described as

$$I_t = I_0 e^{\frac{-t}{\tau}} \qquad (1.3.3)$$

Where

$$\frac{1}{\tau} = kr + knr \qquad (1.3.4)$$

τ is the fluorescence lifetime and is in the range of 10^{-8} s.

Figure 1.3.4. illustrates the decline of fluorescence intensity and the calculation of lifetime using *Eqn. (2.3.4)*. After a short pulse of electromagnetic radiation, the fluorescence intensity reaches its peak, known as ***$I_{max.}$***

The intensity gradually drops to zero, and the time it takes to attain $\frac{Imax}{e}$ is defined as the lifetime ***(τ)***. [9][14]

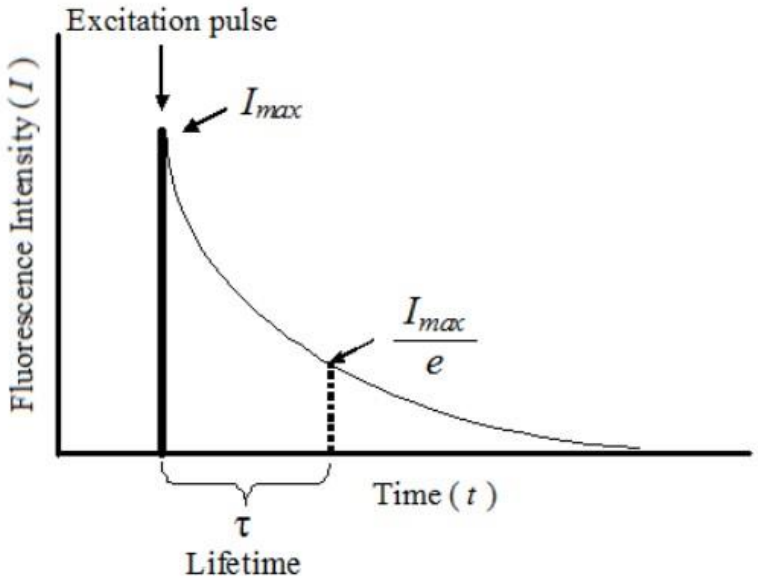

Figure 1.3.4. Fluorescence intensity exponential decay after excitation with a short excitation pulse. Image taken form [9].

Franck Condom principle

The intensity of vibronic transitions, or the absorption or emission of a photon, is described by the Franck-Condon Principle. It affirms that a molecule's nuclear configuration does not significantly alter when it goes through an electronic transition, such as ionization. This is because the electronic transition occurs faster than the nuclei can react, and nuclei are way more massive than electrons. According to theory, a vibration must occur in the nucleus as it realigns itself with the new electrical arrangement. It asserts that a molecule's nuclear configuration does not significantly alter when it goes through an electronic transition, such as ionization.

In **Figure 1.3.5**, the nuclear axis illustrates the effect of internuclear separation, and the vibronic transition is represented by the blue and green vertical arrows.

This figure shows three concepts:

-Absorption leads to a higher energetic state.

- Fluorescence leaves to a lower energy state.

- The change of the nuclear coordinates between the fundamental state and the excited state indicates a new balance position for the potential of nuclear interaction.

The lower length of the arrow of the fluorescence than that of the absorption indicates that the fluorescent has less energy, i.e. a larger wavelength.

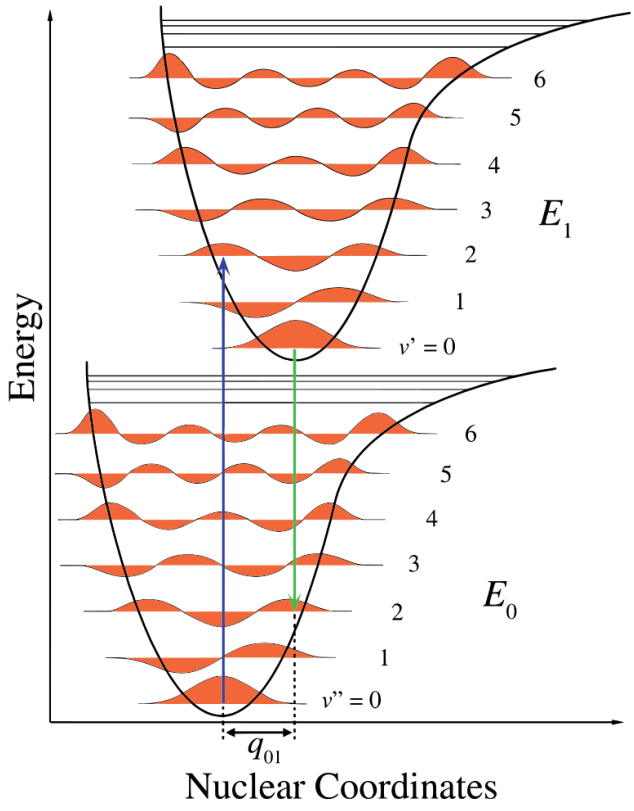

Figure 1.3.5. Transitions between different electronic states occur very quickly compared to nuclear movements. Vibrational levels are favored when they involve minimal changes in nuclear coordinates. Image taken from [37].

1.3.1. Fluorescence-influencing factors

Quenching

The intensity of fluorescence can be decreased by a wide variety of processes. Such decreases in intensity are called quenching.

The interactions between fluorophores and other molecular entities make fluorescence environmentally sensitive. Fluorescence quenching occurs when molecular species absorb the fluorophore's energy. Quenching can be:

- *Static or contact:* Non-fluorescent complexes arise as a result of contact with a quenching molecule.

- *Dynamic or collisional*: when energy is removed from the stimulated molecule through collision. [15]

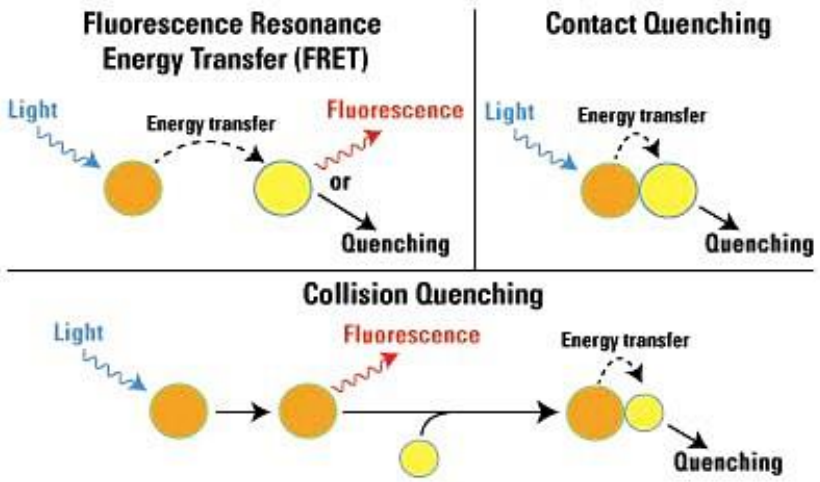

Figure 1.3.6. The operation of contact and collisional quenching. Image taken from [15].

Reabsorption

In fluorescence, reabsorption is the phenomenon by which the light emitted by a substance is again absorbed by the same substance, reducing the intensity of the observed fluorescence and causing a possible shift in the peak wavelength (increase of Stokes shift). This phenomenon is due to the transfer of resonance energy (RET). Reabsorption is most pronounced when the spectra of excitation and emission of a substance significantly overlap. The smaller the Stokes shift (the distance between the wavelengths of excitation and emission), the greater the reabsorption. In a more concentrated solution, there are more excited phosphorus that can be reabsorbed, causing a shift in the peak emission wavelength towards larger wavelengths.

Figure 1.3.7 illustrates this phenomenon. In the example of Rhodamine 6G, the absorption and emission spectra overlap considerably, with a Stokes shift of only 23 nm. Reabsorption may also occur for other reasons related to the concentration of the solution:

-Increased path length: in a highly concentrated solution, the length of the path through the fluorescence emitted is greater due to the high density of fluorophores.

As a result, there is a greater likelihood that reabsorption will occur along this longer route.

- Higher probability of collisions: in highly concentrated solutions, the molecular density is higher, leading to more frequent collisions between fluorophores. These collisions can lead to energy transfer processes such as Förster Resonance Energy Transfer (FRET) or Dexter Energy Transfer, contributing to resorption events.

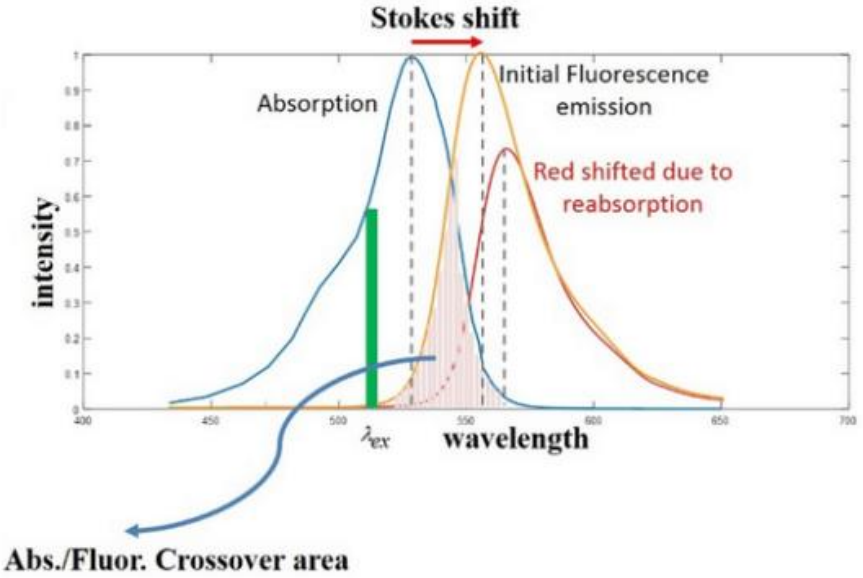

Figure 1.3.7. Illustration of the reabsorption phenomenon, showing that fluorophores emitted at overlapping wavelengths can be reabsorbed. Image taken from [9].

Temperature

The quantum efficiency of fluorescence decreases with rising temperature. As the temperature rises, the number of collisions rises, increasing the likelihood of deactivation by external conversion. Solvents with lower viscosity are more susceptible to deactivation through external conversion. A molecule's fluorescence reduces when its solvent contains heavy atoms like carbon tetrabromide and ethyl iodide, or when heavy atoms are substituted into the fluorescing compound. Orbital spin interactions cause a rise in the rate of triplet production, reducing the chance of fluorescence. Heavy atoms are generally added into the solution to improve the phosphorescence.

Time, mixing and contact with metal cations are other factors that influence fluorescence. The subsequent paragraphs and chapters in the results will go into additional detail about these subjects.

1.4. Investigation of Temperature Effects on Dyes

A temperature change was found to be connected with an intensity fluctuation that was observed during the fluorescence investigation of the selected dyes. Remarkably, the warming of the cuvettes by the LED was linked to an increase in temperature. Bragg fibers were used to thoroughly examine this temperature change.

Theoretical background

Distributed Bragg reflector

Bragg fibers (FBGs) are symmetrical microstructures several millimeters long that are photo-inscribed onto a single-mode fibre. The inscription of these gratings causes a local change in the refractive index of the core. In this region, the fiber functions as a filter, allowing for the selection of specific wavelengths. Specifically, when light contacts a grating fringe (showing a change in refractive index), it is partially reflected **(Figure 2.4.1)**

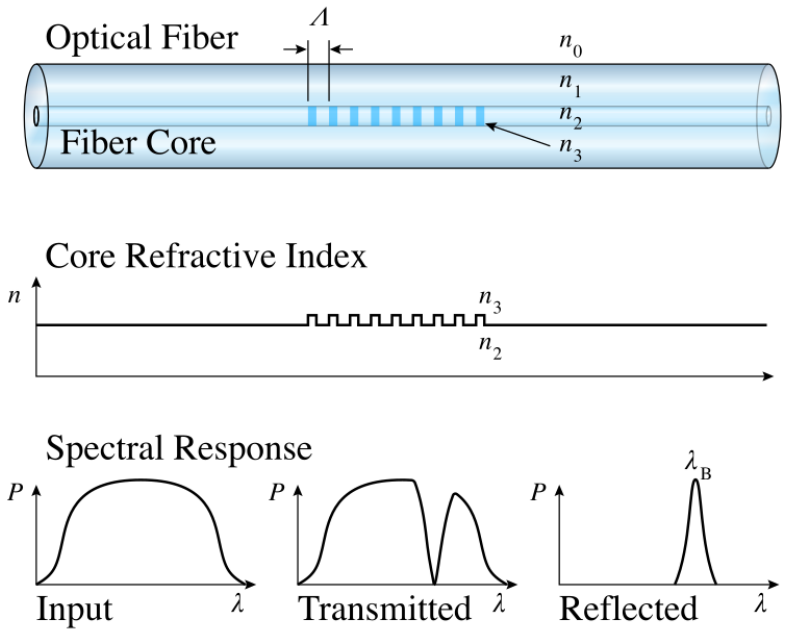

Figure 2.4.1. "A Fiber Bragg Grating structure, with refractive index profile and spectral response." Image taken from [26].

Reflection occurs at wavelengths close to the grating's Bragg wavelength ***(λ_B)***, which is determined by the grating pitch ***(Λ)*** and effective refractive index ***(n_{eff})***. Changing the physical or mechanical parameters of the grating will affect the Bragg wavelength ***(λ_B)***. Applying strain or a temperature gradient to the sensor can change the grating pitch ***(Λ)*** and effective refractive index ***(n_{eff})***. As a result, FBG sensors are particularly well-suited to monitoring deformations and temperatures.

$$\lambda_B = 2n_{eff}\Lambda \qquad (2.4.1)$$

The intensity of the sensor's response, or the intensity of the peak reflected by the grating, is proportional to the length of the FBG. Each fringe reflects a small fraction of the incident signal, which adds up; increasing the length increases the number of fringes and hence the intensity of the reflected wavelength. [29]

The infinitesimal Bragg wavelength variation due to strain and temperature is derived by deriving the wavelength expression:

$$d\lambda_B = \frac{\partial \lambda_B}{\partial \varepsilon} \cdot d\varepsilon + \frac{\partial \lambda_B}{\partial T} \cdot dT = \left[\frac{\partial}{\partial \varepsilon} 2n_{eff}\Lambda\right] \cdot d\varepsilon + \left[\frac{\partial}{\partial T} 2n_{eff}\Lambda\right] \cdot dT =$$
$$= [2n_{eff}\frac{\partial \Lambda}{\partial \varepsilon} + 2\Lambda\frac{\partial 2n_{eff}}{\partial \varepsilon}]d\varepsilon + [2n_{eff}\frac{\partial \Lambda}{\partial T} + 2\Lambda\frac{\partial 2n_{eff}}{\partial T}]dT \qquad (2.4.2)$$

Expressing it as the relative change in Bragg wavelength, it is divided by λB, yielding:

$$\frac{d\lambda_B}{\lambda_B} = [\frac{1}{\Lambda}\frac{\partial \Lambda}{\partial \varepsilon} + \frac{1}{n_{eff}}\frac{\partial n_{eff}}{\partial \varepsilon}]d\varepsilon + [\frac{1}{\Lambda}\frac{\partial \Lambda}{\delta T} + \frac{1}{n_{eff}}\frac{\partial n_{eff}}{\partial T}]dT \qquad (2.4.3)$$

The Bragg wavelength variations can then be expressed as a function of strain and temperature changes *(Eq. 2.4.4):*

$$\Delta\lambda_B = k_\varepsilon \varepsilon + k_T T \qquad (2.4.4)$$

where:

- k_ε is the strain sensitivity, equal to 1 pm/με;
- k_T is the sensitivity to temperature, equal to 10 pm/°C;

The structure of the FBG varies according to the refractive index of the core and the spatial periodicity of the grating. There are various sorts of gratings based on their spatial periodicity **(Fig. 2.4.2)**:

- *Uniform:* both the periodicity and the refractive index modulation remain constant.

- *Tilted:* the periodicity remains constant, but the refractive index modulation is slanted relative to the core axis.

- *Chirped:* the periodicity and refractive index modulation vary and are not uniformly adjusted.

- *Superstructure*: Refractive index modulation is dispersed in superstructures along the fiber.

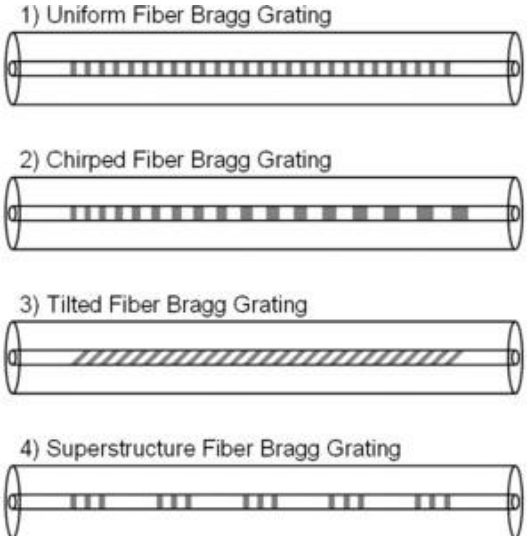

Figure 2.4.2. Types of Bragg gratings according to spatial periodicity. Image taken from [26].

The change in refractive index can be **(Figure 2.4.3)**:

1. Uniform positive, if it is constant for each period, with positive offset.
2. Gaussian-apodized, if it has a longitudinal Gaussian shape, with positive offset.
3. Raised-cosine-apodized, if it has a longitudinal raised-cosine shape, with null offset.
4. Discrete phase shift, if the two halves of the structure are in phase opposition, with positive offset.

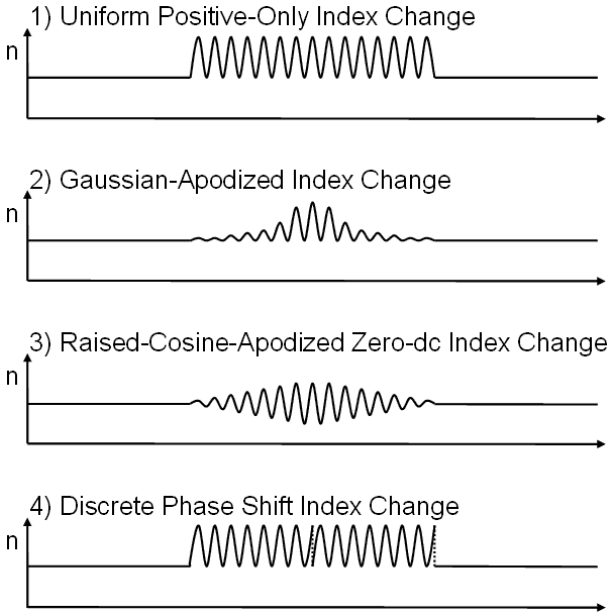

Figure 2.4.3. "Refractive index profile in the core of, 1) a uniform positive-only FBG, 2) a Gaussian-apodized FBG, 3) a raised-cosine-apodized FBG with zero-dc change, and 4) a discrete phase shift FBG." Image taken from [26].

2. Materials and methods

The thesis employs a continuous flow thin deposition reactor developed at Ben Gurion University's Department of Materials Engineering, designed to establish a pH gradient within an alkaline range, specifically ranging from pH 12.5 to 14.25.

This reactor is housed within the Department of Materials Engineering at Ben Gurion University of Negev.

The initial step involved searching the literature for dyes most suitable for this pH range. This exploration revealed that dyes specifically designed for an extremely alkaline environment are still relatively scarce. However, among the compounds available, the following dyes were selected for their compatibility with alkaline conditions:

Rhodamine B, Rhodamine 6G, Indigo Carmine, and Titan Yellow. [16][17][18][19]

The following paragraphs describe the successive procedures used:

2.1 Selection of Dyes

2.2 Preparation of solutions at different pH

2.3 Fluorescence Analysis

2.4 Temperature Analysis

2.5 Effect of Metal Cations on Dye Fluorescence

2.6 Kinetic Studies

2.1. Selection of dyes

2.1.1. Rhodamine B

Rhodamine B, a xanthene dye, is commonly employed as a fluorescent tracer in biology and medicine. It has a high quantum yield and is extremely soluble in water, making it an excellent choice for staining cells and tissues.

Its luminescence quantum yield is 0.65 in basic ethanol *[21],* 0.49 in ethanol *[22],* and 0.68 in 94% ethanol *[23].*

Rhodamine B is also employed in dye lasers, as a sensitizer in photodynamic therapy.

Figure 2.1.1. Rhodamine B solution in water. Image taken from [20].

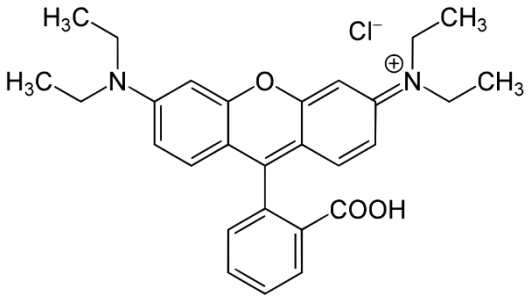

Figure 2.1.2 Chemical structure of Rhodamine B. Image taken from [20].

Table 2.1.1. Rhodamine B properties. [20]

PROPERTIES:

Chemical formula:	**$C_{28}H_{31}ClN_2O_3$**
Molar mass:	**479.02 g/mol**
Appearance	**red to violet powder**
Melting point	**210 to 211°C**
Solubility in water	**8 to 15 g/L (20°C)**

Rhodamine B can exist in two states of equilibrium: "open"/fluorescent and "closed"/nonfluorescent spirolactone. The "open" form predominates under acidic conditions, whereas the "closed" form is colorless in basic conditions **(Figure 2.1.3)**. [24]

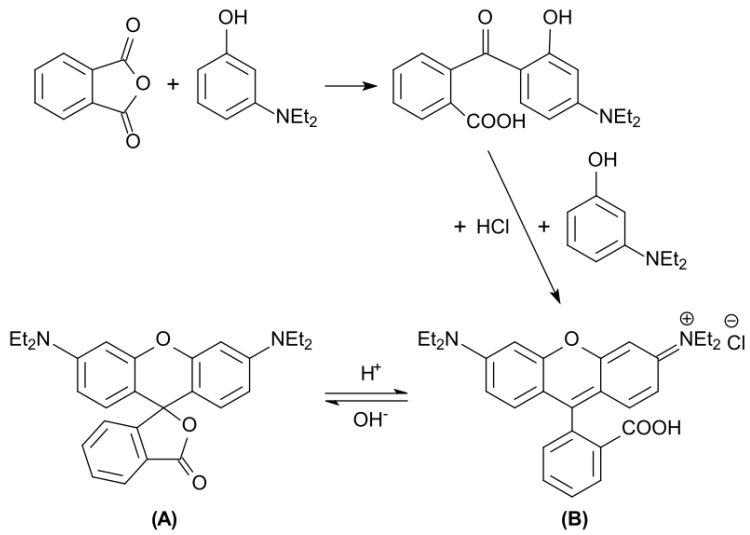

Figure 2.1.3. Rhodamine B has two forms: closed (A) and open (B). Image taken from [24].

2.1.2. Rhodamine 6G

Rhodamine 6G, another xanthene dye, is widely employed as a fluorescent tracer and sensitizer. Its high absorption coefficient and long fluorescence lifetime, make it valuable in applications such as flow cytometry and fluorescence microscopy.

The dye exhibits a relatively high photostability and high fluorescence quantum yield (0.95). [21]

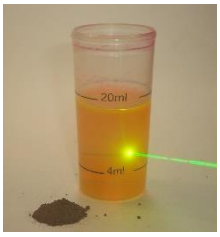

Figure 2.1.4. Rhodamine 6G chloride powder combined with methanol emits yellow light under green laser illumination. Image taken from [25].

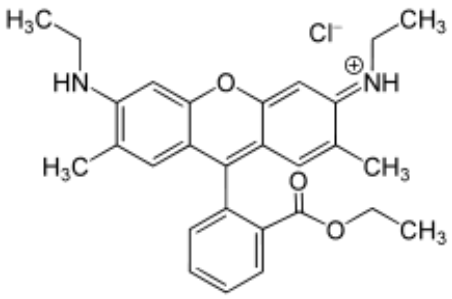

Figure 2.1.5.
Chemical structure of Rhodamine 6G. Image taken from [25].

Table 2.1.2. Rhodamine 6G properties. [25]

PROPERTIES:

Chemical formula:	**$C_{28}H_{31}N_2O_3Cl$**
Molar mass:	**479.02 g/mol**
Appearance	**dark reddish purple, brown or black crystalline solid**
Solubility in water	**20 g/L (25 °C)**

2.1.3. Indigo Carmine

Indigo Carmine is an indigoid dye that is often used to measure pH and stain tissues and cells. It has a pKa of approximately 12.0, making it suitable for staining basic structures like proteins and nucleic acids.

In a 0.2% aqueous solution, Indigo Carmine is blue at 11.4 pH and yellow at 13.0. Indigo carmine is also a redox indicator, turning yellow after reduction. [26]

It is also used as a food dye, as well as a textile and paper dye.

Figure 2.1.6. Indigo Carmine solution in water. Image taken from [27].

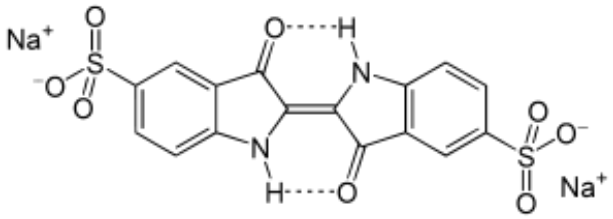

Figure 2.1.7. Chemical structure of Indigo Carmine. Image taken from [26].

Table 2.1.3. Indigo Carmine properties. [26]

PROPERTIES:

Chemical formula:	**$C_{16}H_8N_2Na_2O_8S_2$**
Molar mass:	**466.36 g/mol**
Appearance	**Purple solid**
Melting point	**>300°C**
Solubility in water	**10 g/L (25°C)**

2.1.4. Titan Yellow

Titan Yellow is a pH indicator with a transition range of 11.0 to 13.0. Titan Yellow is used as a stain and fluorescent indicator in microscopy, and its hue shifts from yellow to red between pH 12 and 13.

It has an absorbance peak at 403 nm and is also called Thiazol Yellow G.

Figure 2.1.8. Titan Yellow solution in water.

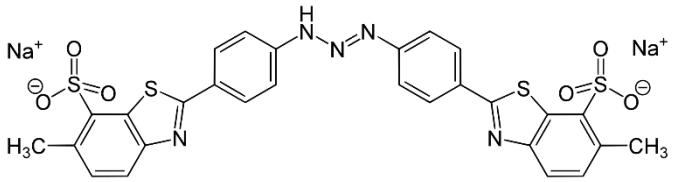

Figure 2.1.9. Chemical structure of Titan Yellow. Image taken from [26].

Table 2.1.4. Titan Yellow properties. [27]

PROPERTIES:

Chemical formula:	**$C_{28}H_{19}N_5Na_2O_6S_4$**
Molar mass:	**695.720 g/mol**
Appearance	**Yellow in water**
Solubility in water	**0.1 g/10 mL**

For all these compounds, concentrated solutions were prepared by dissolving 50 mg of dyes in distilled water and adjusting the final volume to 100 ml.

Each solution was then aliquoted with micropipettes and blended into multiple solutions of variable pH levels to achieve the necessary dye concentration for fluorescence investigations.

Additional information and photographs are supplied in the outcomes chapter.

2.2. Preparation of solutions at different pH

The second step is to prepare solutions at different pH levels.

The solutions were prepared using sodium hydroxide (NaOH). The resultant solutions have pH values of 12.5, 13, 13.5, 13.8, 13.9, 14.0, 14.1, and 14.25. The following approach was used to calculate the molarity of each solution and the amount of NaOH required:

1. Calculate pOH using

$$pOH = 14 - pH \qquad (2.2.1)$$

2. Calculate the **concentration of hydroxide ions [OH^-] and NaOH** using the equation

$$[OH^-] = [NaOH] = 10^{-pOH} \qquad (2.2.2)$$

3. Calculate the **molarity of the solution as [OH^-]**

4. Determine the number of **moles of NaOH necessary, which is equivalent to [OH-]**

5. To calculate **the stoichiometry of NaOH and hydroxide ions**, use the balanced chemical equation for dissociation

$$NaOH \rightarrow Na^+ + OH^-$$

Since one mole of NaOH generates one mole of OH^- ions, the number of **moles of NaOH needed is the same as [OH^-]**

6. Determine the needed **mass in grams of NaOH** based on its molar mass as the following way:

$$\text{g} = \text{Mole} \times \text{Molar Mass} \qquad (2.2.3)$$

2.3. Fluorescence Analysis

The effect of pH on fluorescence was analyzed by examining the changes in *intensity and wavelength of the peak* for each dye once added to alkaline solutions.
Each pH data point was measured in triplicate. The graphs in the results section show the average values and their corresponding standard deviations.

2.3.1. Lab setup

The laboratory setup consists of:

1) M450LP2 LEDs (nominal wavelength 450 nm) with LEDD1B driver (Thorlabs).

2) Avantes spectrometer (AvaSpec-3648) connected to PC with Avantes acquisition software installed.

3) Standard avantes fiber optic cable (multi-mode).

4) NeoLab E-1641 Disposable Cuvettes PS, Macro, 2.5-4.5 ml

5) Cuvette holder.

6) Micrometric and millimetric pipettes.

The AvaSpec-3648-USB2 is powered by USB and includes a USB interface cable, AvaSoft-basic, and a comprehensive manual. It is possible to externally couple up to 127 distinct USB2 spectrometers with various types of detectors.

The M450LP2 LED is designed to be installed on the cuvette holder. The M450LP2 has a broadband spectrum of roughly 100 nm.

The cuvette holder lacks an optical filter, requiring a post-processing (by means of a Matlab algorithm) to remove the signal related to the LED spectrum.

The optical fiber at one end of the cuvette holder collects the signal. The mounting location of the optical fiber is determined by the intensity of the LED and the cuvette. If the LED light is excessively bright, it should be put on a side that is not immediately facing the LED.

To eliminate any other light interference from the sides, the cuvette holder's unusable sides must be closed with a cap.

The optical fiber transmits light within the cuvette holder to the Avantes spectrometer and displays it on the AvaSoft acquisition program on the PC connected via a USB cable. [12]

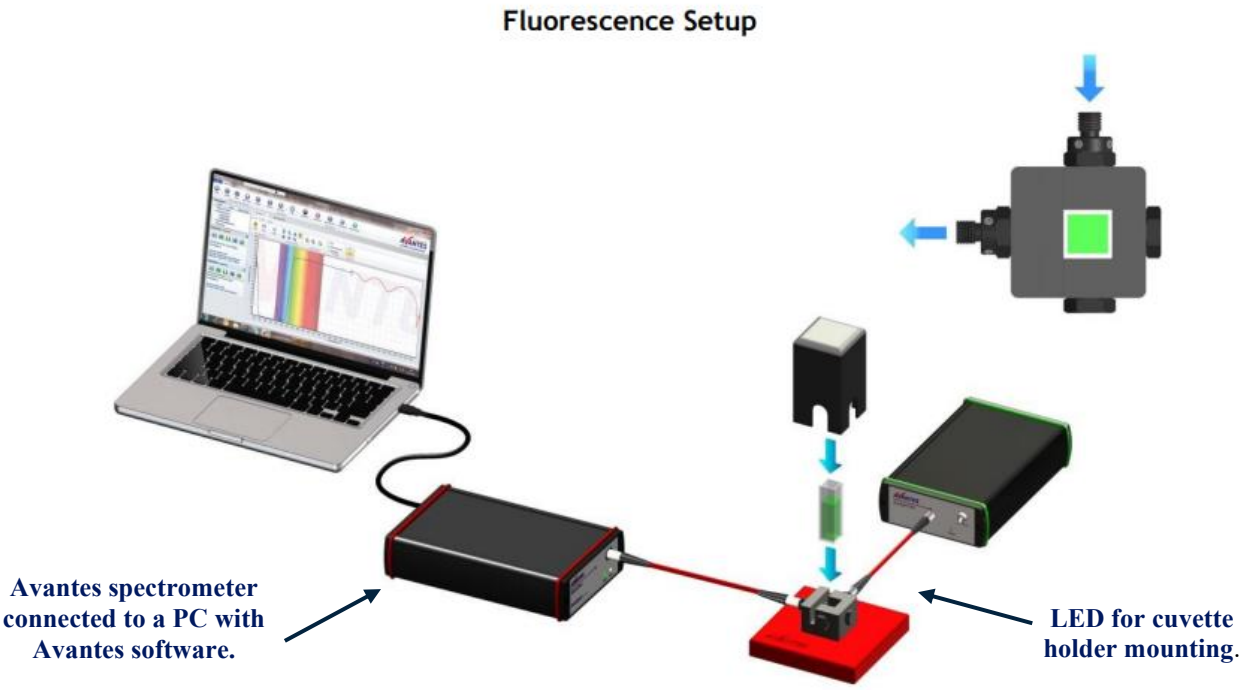

Figure 2.3.1. Fluorescence setup. Image modified from [12].

Avantes spectrometer

The overall operation of an Avantes spectrometer can be divided into four major steps:

1. ***Source Illumination***: A light source produces light radiation, which is delivered to the scattering system via optical fiber.

2. ***Light Dispersion:*** The light from the optical cable is passed via a diffraction grating or a prism, which divides it into distinct wavelengths. This occurs when the grating or prism deflects light beams in slightly varied ways based on their wavelength. This phase is critical in the spectrometer's ability to study the light spectrum.

3. ***Detection of Scattered Light***: After scattering, the light is detected by a detecting device such as a photodiode or camera. This apparatus measures the intensity of light at each wavelength.

4. ***Data Analysis:*** The data collected by the sensing device is processed by software linked to the Avantes spectrometer.

This software analyzes the acquired light spectrum and displays its intensity as a function of wavelength. This stage involves interpreting the data and presenting the results, allowing users to acquire useful insights into the qualities of the light being evaluated. [12] [13]

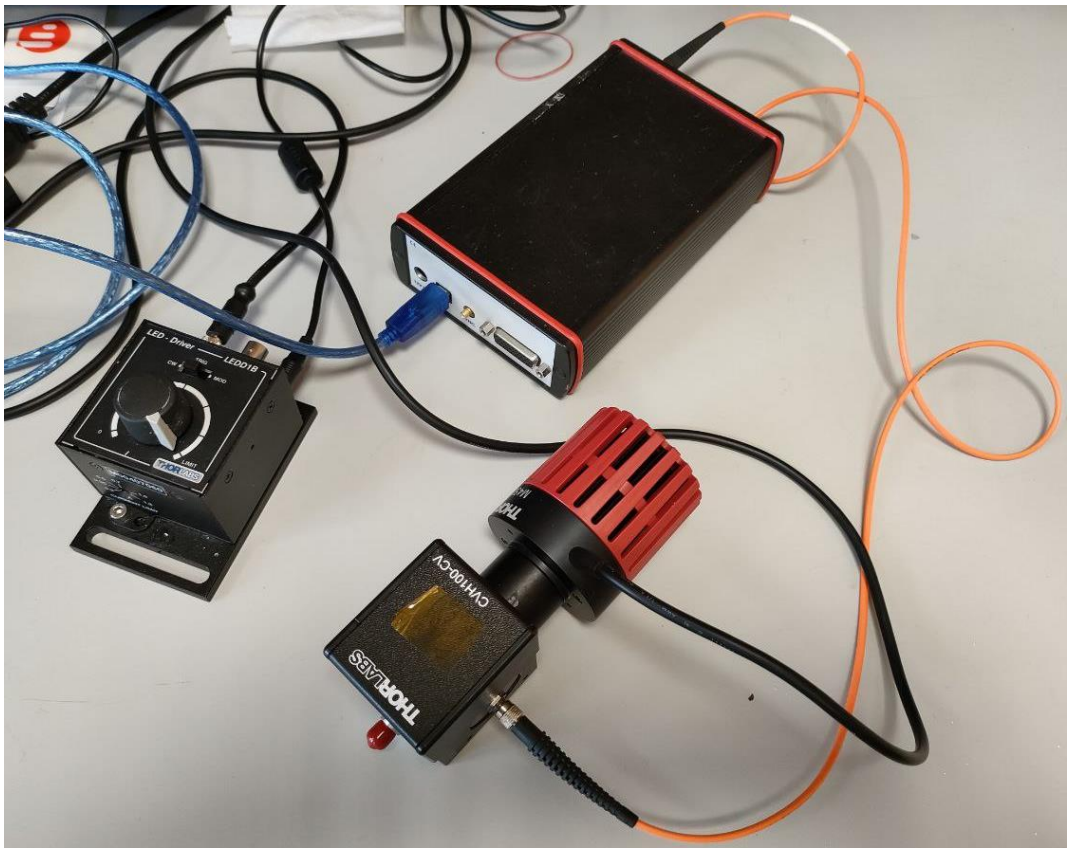

Figure 2.3.2. AvaSpec-3648-USB2 spectrometer connects to M450LP2 LED.

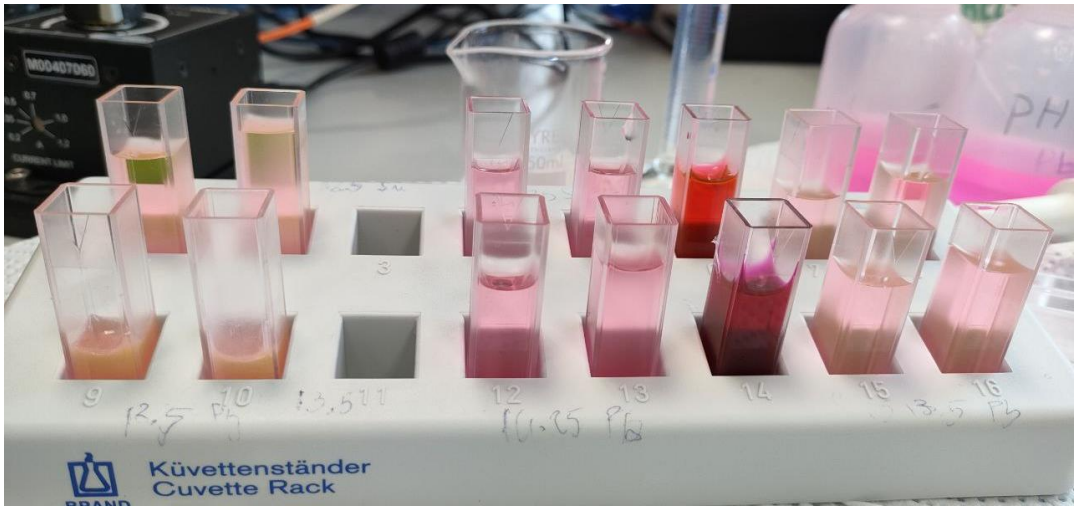

Figure 2.3.3. Cuvette holder.

Figure 2.3.4. pH solutions.

2.3.2. How to interpret fluorescence peaks

The image below depicts one of the experiments performed on Rhodamine 6G. Fluorescence data was collected with Avantes software.

Two peaks can be seen. The first peak is at the wavelength of the light source (~450 nm) used to illuminate the sample (*Excitation peak*). The dye (in this case, Rhodamine 6G) emits fluorescence, which causes the second peak. This peak occurs at a wavelength other than that of light and is determined by the substance being studied (*Compound emission peak*). **(Figure 2.3.5)**

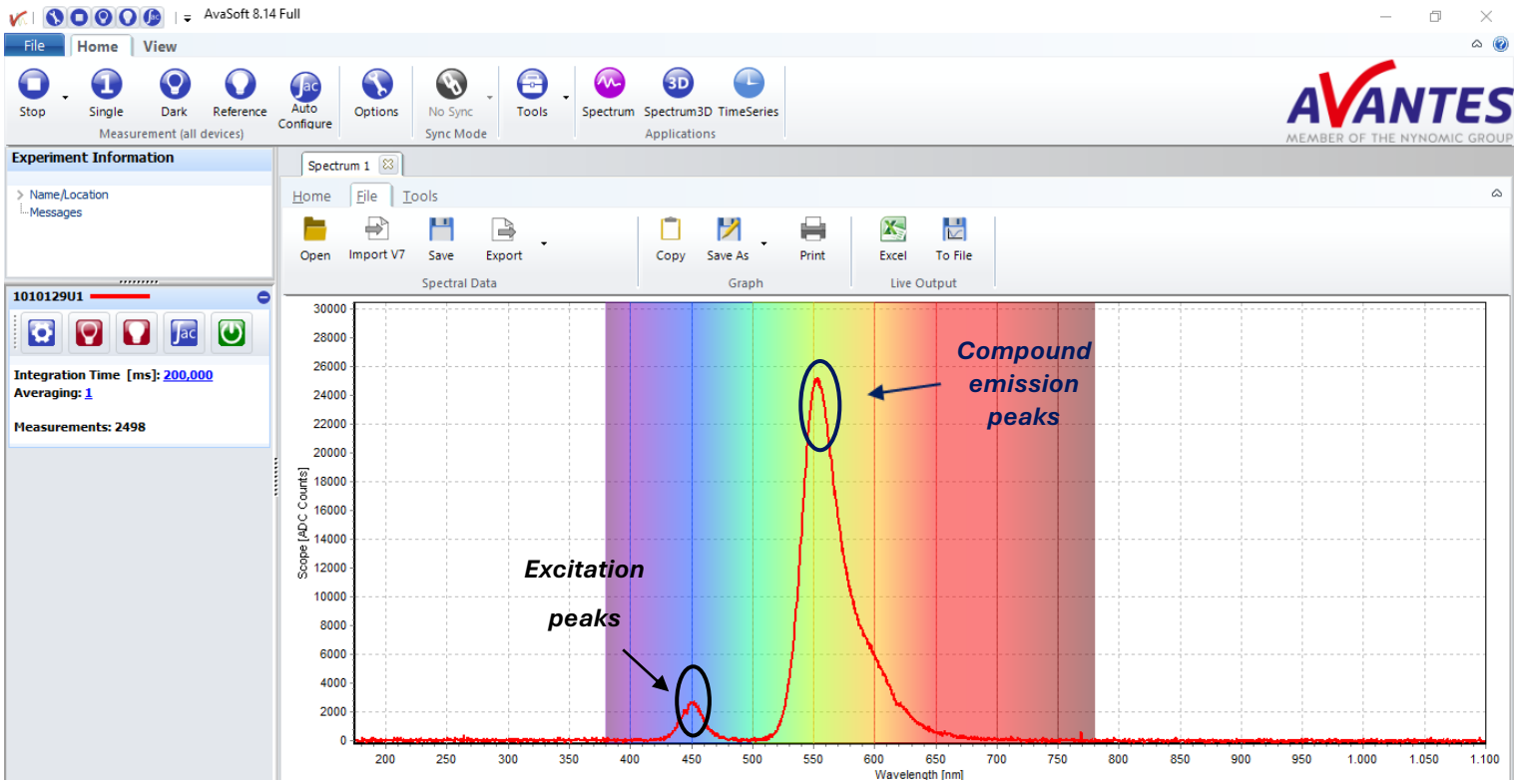

Figure 2.3.5. Experiment conducted to study the fluorescence of Rhodamine 6G.

2.4. Temperature analysis

During fluorescence tests, it was observed that illuminating the sample with the LED for a short period caused an increase in the temperature of the solution. This linear temperature increase led to a corresponding linear decrease in fluorescence intensity.

To accurately assess this effect, temperature sensors were integrated into the experimental setup. These sensors precisely recorded temperature variations throughout the experiment. To compensate for the thermal influence and isolate the specific effect of fluorescence, the mathematical model proposed by Watras et al. was employed.[36]

The mathematical model was subsequently validated through tests conducted under isothermal conditions.

Details of the model and its results are described in the following paragraphs.

2.4.1. Optical interrogator

The optical interrogator detects the Bragg wavelengths associated with gratings. It includes a light source, an optical isolator, a circulator, and wavelength filters. There are two types.

1. Broadband using LEDs or SLEDs;
2. Tunable lasers.

In broadband systems, light is steered through the circulator to the fiber, and reflected signals are routed through a narrowband optical filter to remove undesired spectral components. The filtered signal is then routed to a transimpedance amplifier, which converts current into an analog voltage proportionate to optical power.

Finally, an AC/DC converter converts voltage into digital signals.

A tunable laser optical interrogator with a narrowband light source eliminates spectral components, allowing reflected signals to be transmitted directly to the photodiode. This type of interrogator has a higher signal-to-noise ratio (SNR) because the emitted light signals from the source are consistent in intensity across all wavelengths. [30]

The optical interrogator employed for this thesis is the Micron Optics HYPERION

si155 from Luna Technologies® a tunable laser. This interrogator is operated via software "ENLIGHT Sensing Analysis Software" to which it is connected via an Ethernet network.

Software allows for real-time display of signals related to each channel and automatic detection of peaks at Bragg grating wavelengths.

The interrogator is very useful to visualize in real time the changes in the wavelengths of the Bragg wavelengths due to strain and/or temperature as that processing occurs in real time with the acquisition. **(Figure 2.4.1.)**

Figure 2.4.1. Optical interrogator Micron Optics HYPERION si155 from Luna Technologies®. Image taken from [31].

Table 2.4.1. Micron Optics HYPERION si155 specifications. [31]

Number of channels	From 1 to 4
Wavelength range	1500-1600 nm
Accuracy and stability	1 pm / 1 pm
Scanning speed	Until 5000 Hz
Data interface	Ethernet

In the image below, the spectrum of the sensor used for the analysis is represented, and there is a photo inserted of one of the tests conducted on a cuvette of an Indigo Carmine solution at pH 13.5, where the temperature is being monitored with the Bragg fiber:

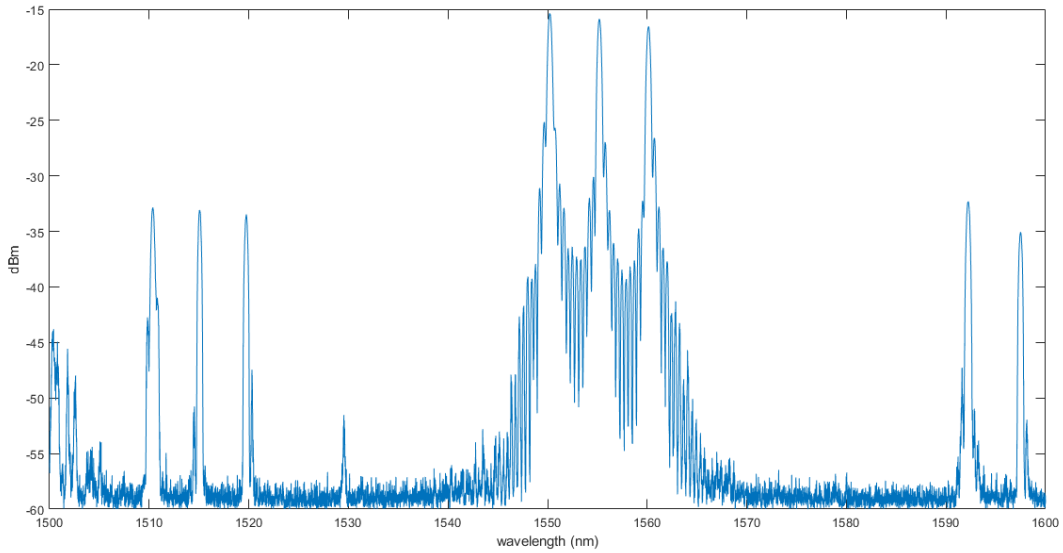

Figure 2.4.2. Spectrum of the sensor used for analysis.

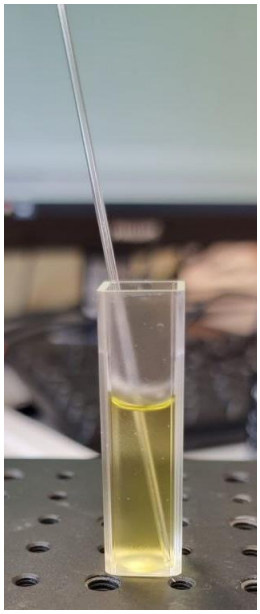

Figure 2.4.3. Experimental setup: Monitoring temperature with a Bragg fiber during analysis of an Indigo Carmine solution at pH 13.5.

2.4.2. Temperature compensation

To study the thermal influence and isolate the specific effect of fluorescence, the mathematical model proposed by Watras et al. (2011) was employed. [36]

This method is used to correct fluorescence measurements for temperature effects by referencing them to a standard, or reference, temperature.

The model is based on the following mathematical equation:

$$\frac{F_r}{F_m} = (1 - q)(T_m - T_r) \qquad (2.4.2)$$

Where:

- F_r is the fluorescence at the reference temperature.
- F_m is the measured fluorescence at the actual temperature.
- q is the temperature coefficient, which quantifies how much the fluorescence changes per degree Celsius.
- T_m is the measured temperature.
- T_r is reference temperature.

By applying this equation, Watras et al. were able to remove the temperature dependency in their fluorescence data (chlorophyll and phycocyanin) by referencing all the measured values to a standard temperature of 20° C.

This temperature referencing approach allows to compare fluorescence measurements made at different temperatures by normalizing them to a common reference point.

Figure 2.4.4 shows the evolution of phycocyanin fluorescence during a sequence of heating and cooling. It is evident how temperature variations influence fluorescence intensity.

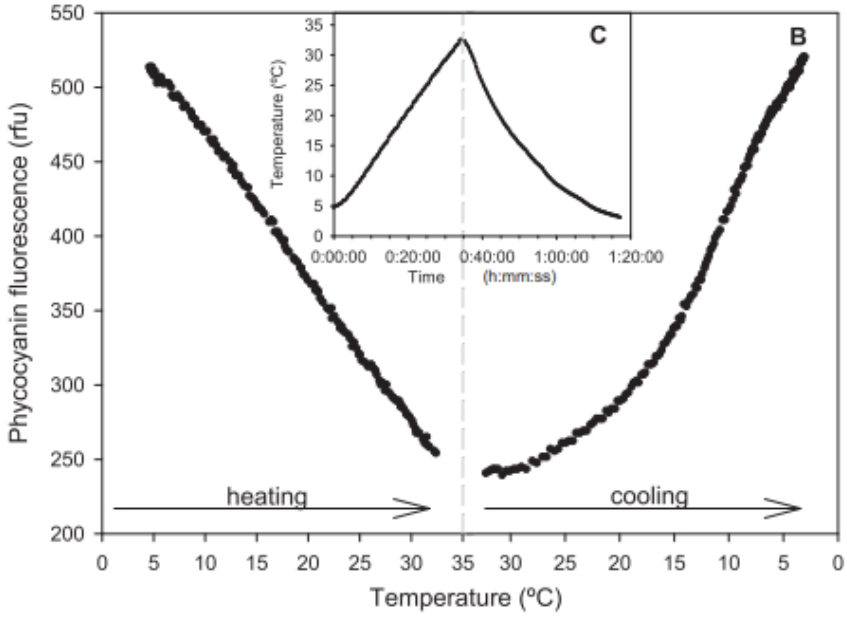

Figure 2.4.4. Evolution of phycocyanin fluorescence during a sequence of heating and cooling. Image taken from [36].

Figure 2.4.5 shows phycocyanin fluorescence data before (panel B) and after (panel D) temperature compensation to a standard temperature of 20°C, using Equation 2.4.2.

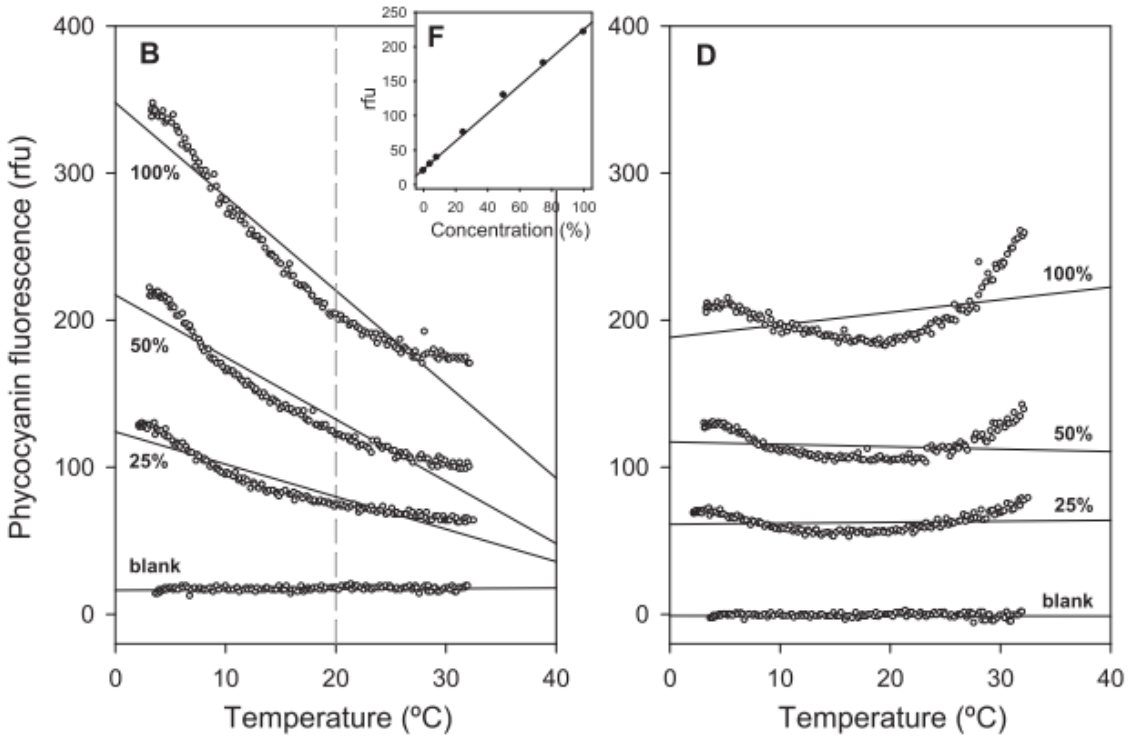

Figure 2.4.5. Temperature quenching of phycocyanin in panel B. in panel D the temperature quenching was removed by adjusting the raw data to a reference temperature of 20°C using Eq 2.4.1. Image taken from [36].

2.5. Effect of Metal Cations on Dye Fluorescence

One of the analyses involves determining the fluorescence of the dyes at various pH values in the presence of metal cations. This was done to simulate the dyes' action in the presence of metals inside the reactor. To do this, solutions containing 30 mM lead ions $\mathbf{Pb^{2+}}$ and tin ions $\mathbf{Sn^{4+}}$ were created.

Lead ions were introduced using $Pb(NO_3)_2$ (lead nitrate) while tin ions were introduced using $SnCl_4$ x $2H_20$ (Tin(IV) chloride hydrate)

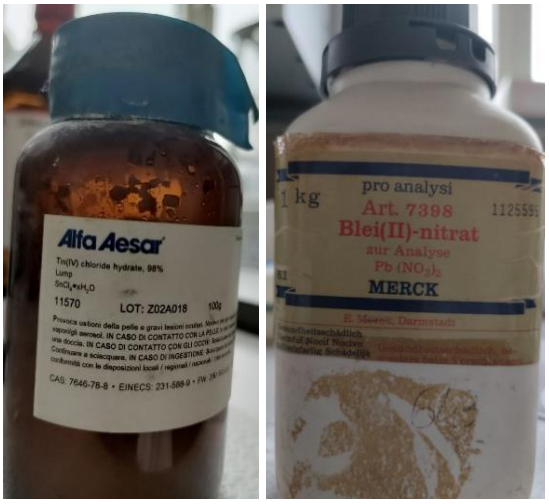

Figure 2.5.1. Lead nitrate and Tin(IV) chloride hydrate.

From the ion concentration, the required moles of Blei(II)-nitrate and Tin(IV) chloride hydrate were calculated, utilizing the formula:

$$\text{Molar Concentration} = \frac{\text{Number of moles}}{\text{Solution volume}} \qquad (2.5.1)$$

Given a solution volume of 40 mL and the molar concentration, the moles required were determined using the formula *(2.5.1)*.

From the mole value, the necessary grams were calculated, considering the molar mass of the compounds as follows:

$$\text{g} = \text{Mole} \times \text{Mass Molar} \qquad (2.5.2)$$

For thorough mixing of the compounds with the pH solutions, a Stuart Hot Plate and Stirrer was utilized.

Figure 2.5.2. Stuart Hot Plate and Stirrer.

2.6. Kinetic Studies

The final analysis was conducted to study the kinetics of the fluorescence phenomenon. This section will outline the preparation of the solutions, the addition of the dye, and the procedure followed to monitor the system's response in terms of the rate of intensity change.

1. Preparation of Solutions:

- Three solutions were prepared:
  - One with a pH of 12.5.
  - One with a pH of 13.5.
  - One with a concentration of 2.37 M.

The solutions were prepared following the procedure described in paragraph *2.2.*

2. Addition of the Dye:

The dye was added to all three prepared solutions to achieve a concentration of $1.0438\ 10^{-5}$ M.

3. Kinetics Study:

First Phase:

- Started with 3 mL of the pH 12.5 solution.
- 100 µL of the 2.37 molar concentration solution was added every 30 seconds.
- The addition continued until the pH reached 13.5.
- Throughout this process, the fluorescence intensity of the system was constantly monitored.

Second Phase:

- Started with 2 mL of the pH 13.5 solution.
- 200 µL of the 2.37 molar concentration solution was added until the pH reached 14.
- In this phase as well, the fluorescence intensity of the system was constantly monitored.

4. Comparison of Results:

- The values obtained from the two phases were compared with the intensity values obtained from previously prepared solutions.

The results obtained from the kinetic analyses are presented in the results paragraph.

3. Results

The effect of pH on fluorescence was analyzed by examining the changes in Intensity and Wavelength of the peak of each dye once added to alkaline solutions.

To simulate the behavior of the dyes within the continuous flow reactor as accurately as possible, several key parameters were examined: Temperature, stability over time, mixing, stability in the presence of metallic cations and kinetic response.

3.1. Fluorescence Analysis

3.1.1 Rhodamine B

The fluorescence of Rhodamine B was analyzed at the following pH points: 12.5, 13.0, 13.5, 13.8, 13.9, 14.0, 14.1, 14.25.

The concentration of Rhodamine B is $1.0438\ 10^{-5}$ M, which was chosen because it was identified as the minimum concentration at which the fluorescence peak of the compound could be detected.

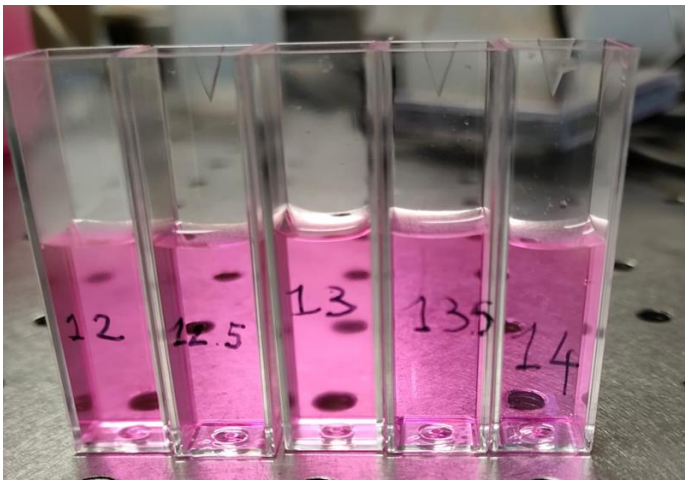

Figure 3.0.1. Solutions of Rhodamine B.

Figure 3.0.2 shows the fluorescence spectrum of Rhodamine B at the specified pH points. The data reveals that the intensity decreases as the pH increases.

In **Figure 3.0.4**, the change in intensity with pH is plotted with the standard deviations.

This trend has also been confirmed in the scientific literature in the paper "*Comparison of rhodamine 6G, rhodamine B, and rhodamine 101 spirolactam based fluorescent probes: A case of pH detection"*, where the variation of Rhodamine fluorescence with pH is analyzed. [32] **(Figure 3.0.3).**

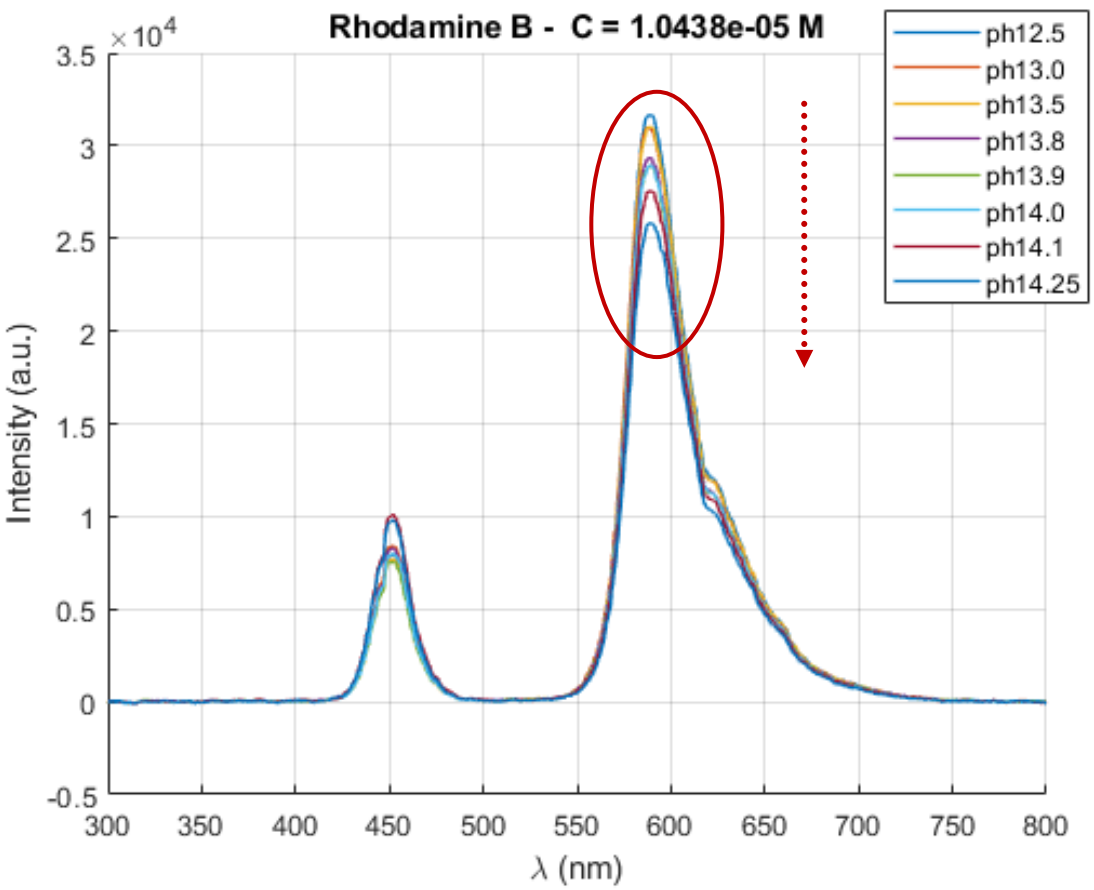

Figure 3.0.2. Spectrum of Fluorescence of Rhodamine B.

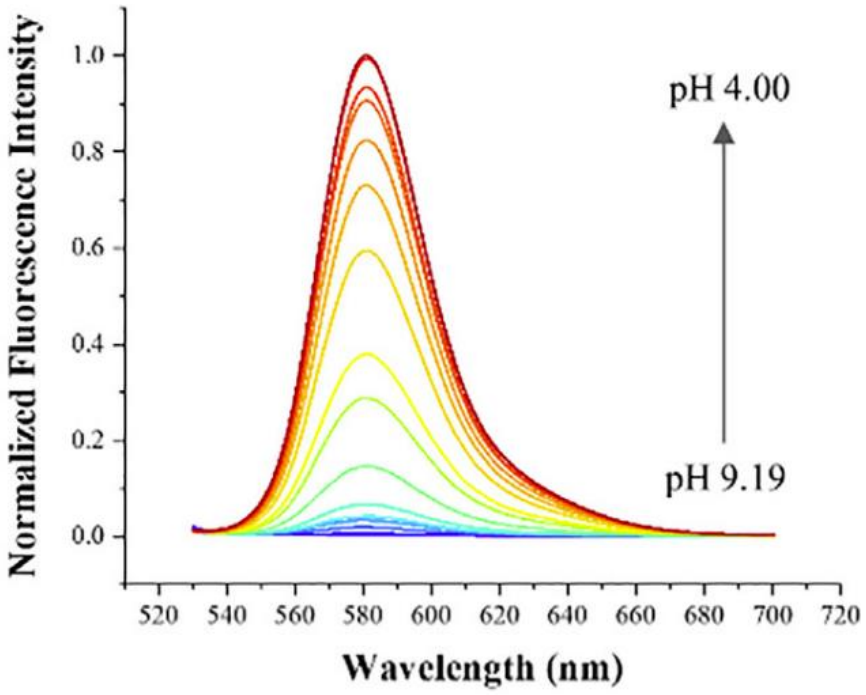

Figure 3.0.3. Fluorescence spectrum of Rhodamine B. Image taken from [31].

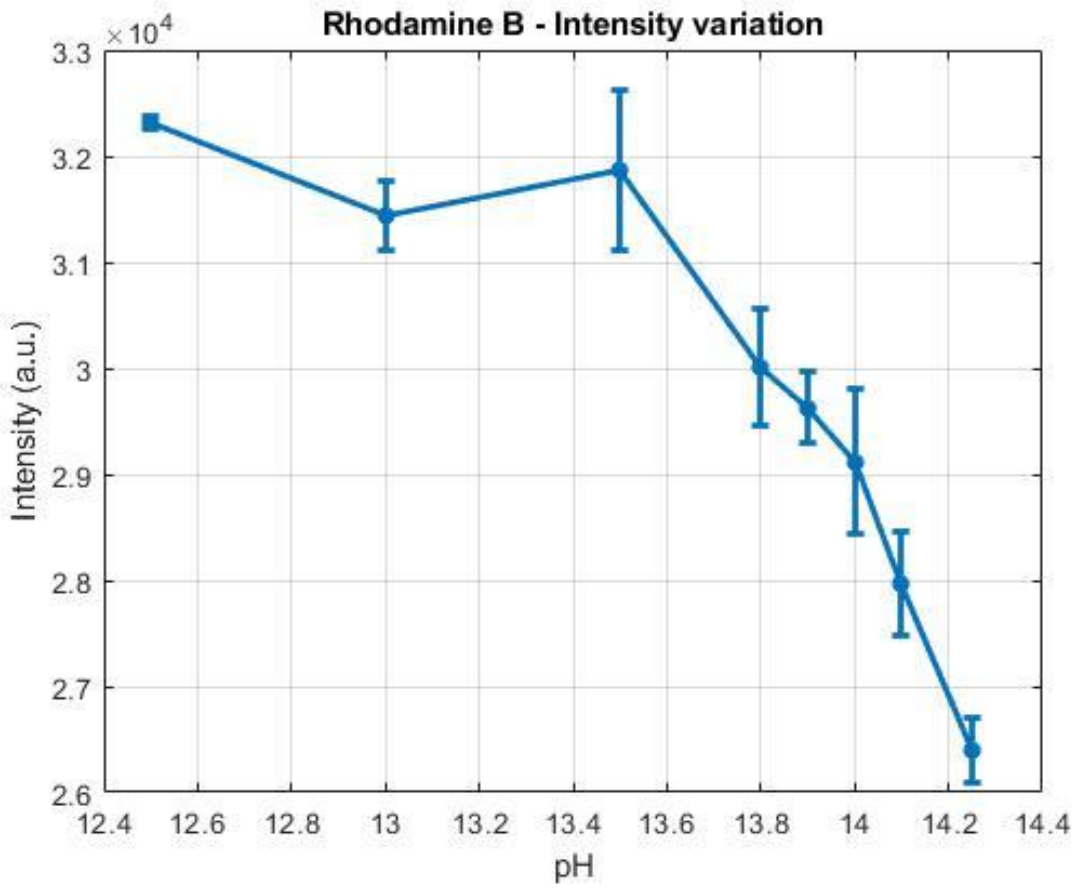

Figure 3.0.4. Intensity-pH variation with the standard deviations of Rhodamine B.

Linearity was observed in the pH range between 13.5 and 14.25. **Figure 3.0.5** shows the linear polynomial that fits the data.

Equation of linear polynomial:

$$y = -7000.06\,x + 126078.28 \qquad (3.1.1)$$

Coefficient of determination:

$$R^2 = 0.9604$$

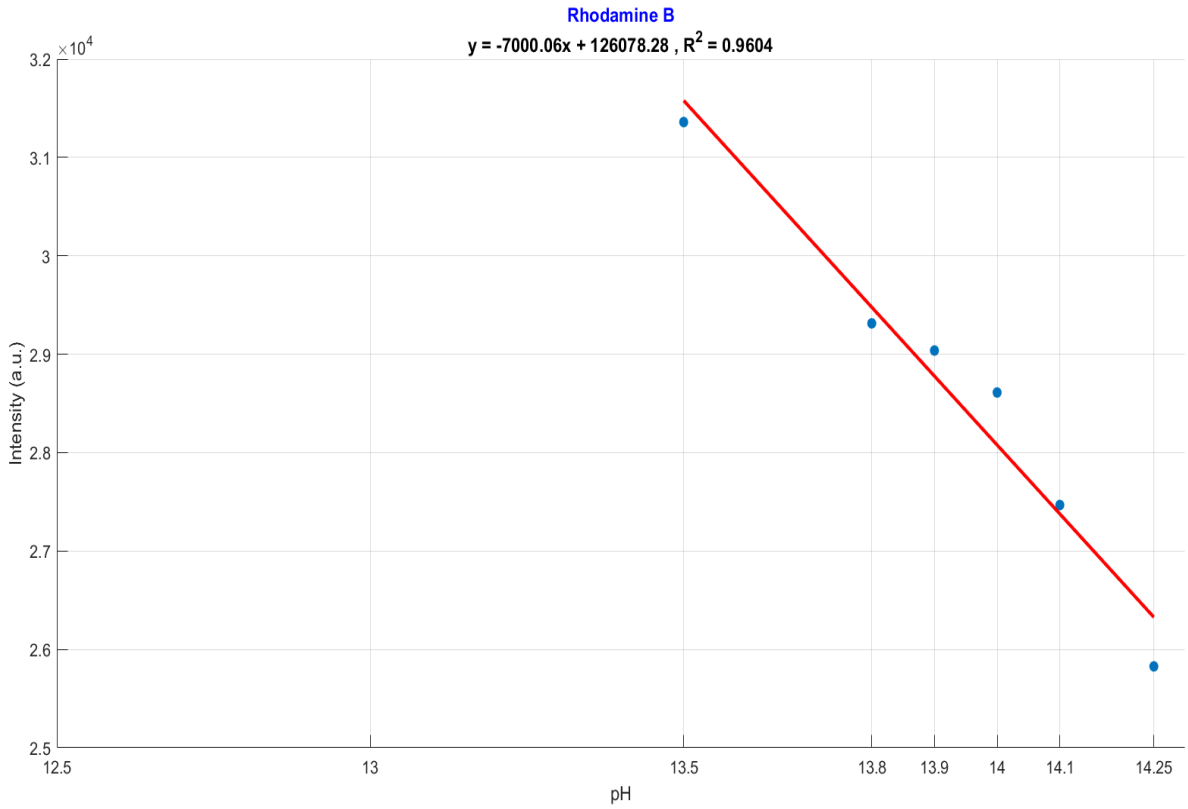

Figure 3.0.5. Linear polynomial interpolation in the range between 13.5 and 14.25.

Regarding the variation of the peak wavelength, it was observed that it does not change with pH, and it is identified at 590 nm. **(Figure 3.0.6).**

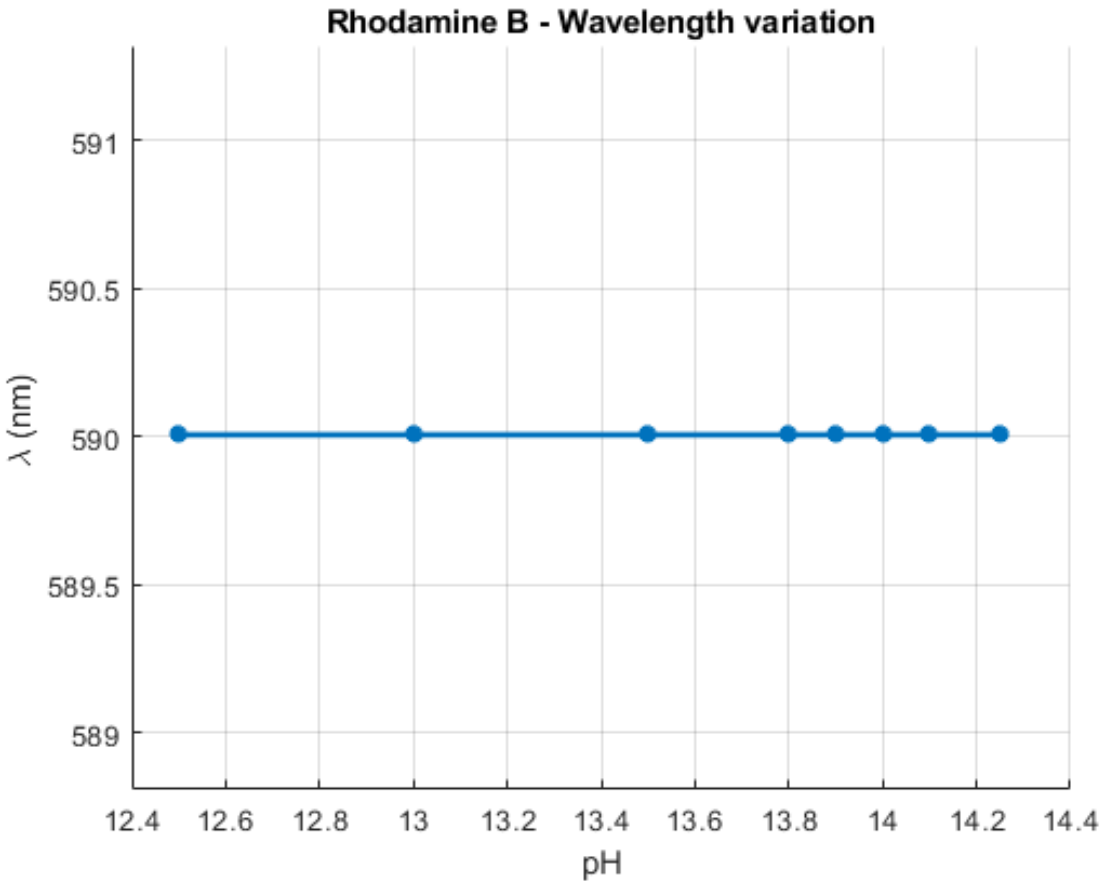

Figure 3.0.6. Variation of wavelength of the peak of Rhodamine B.

3.1.2. Indigo Carmine

The fluorescence of Indigo Carmine was analyzed at the following pH points: 12.5, 13.0, 13.5, 13.8, 13.9, 14.0, 14.1, 14.25.

The concentration of Indigo Carmine is $4.2886\ 10^{-5}$ M, which was chosen because it was identified as the minimum concentration at which the fluorescence peak of the compound could be detected.

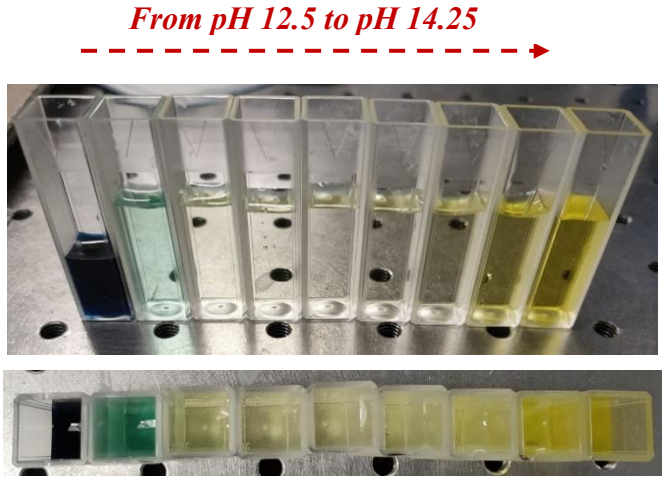

Figure 3.0.7. Indigo Carmine in alkaline solutions.

Figure 3.0.8 shows the fluorescence spectrum of Indigo Carmine at the specified pH points. The data reveal that the intensity increases as the pH increases.

In **Figure 3.0.9**, the change in intensity with pH is plotted with the standard deviations.

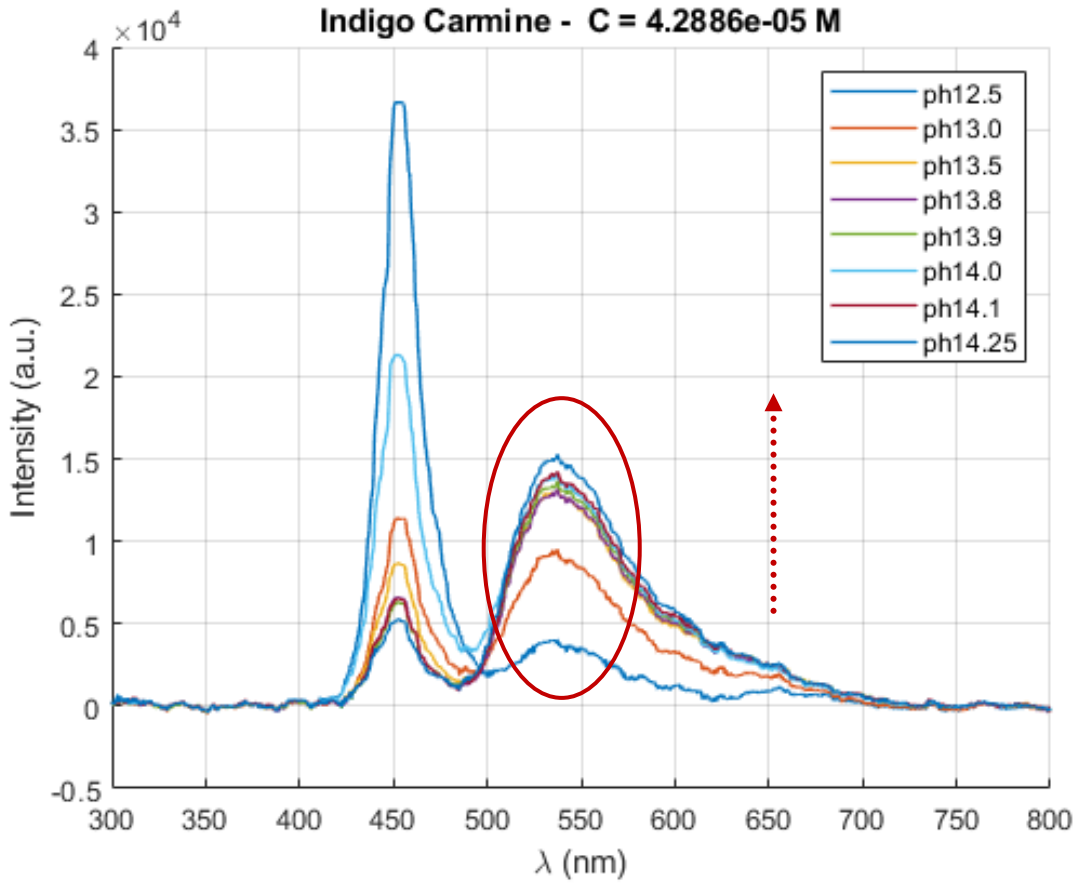

Figure 3.0.8. Spectrum of Fluorescence of Indigo Carmine.

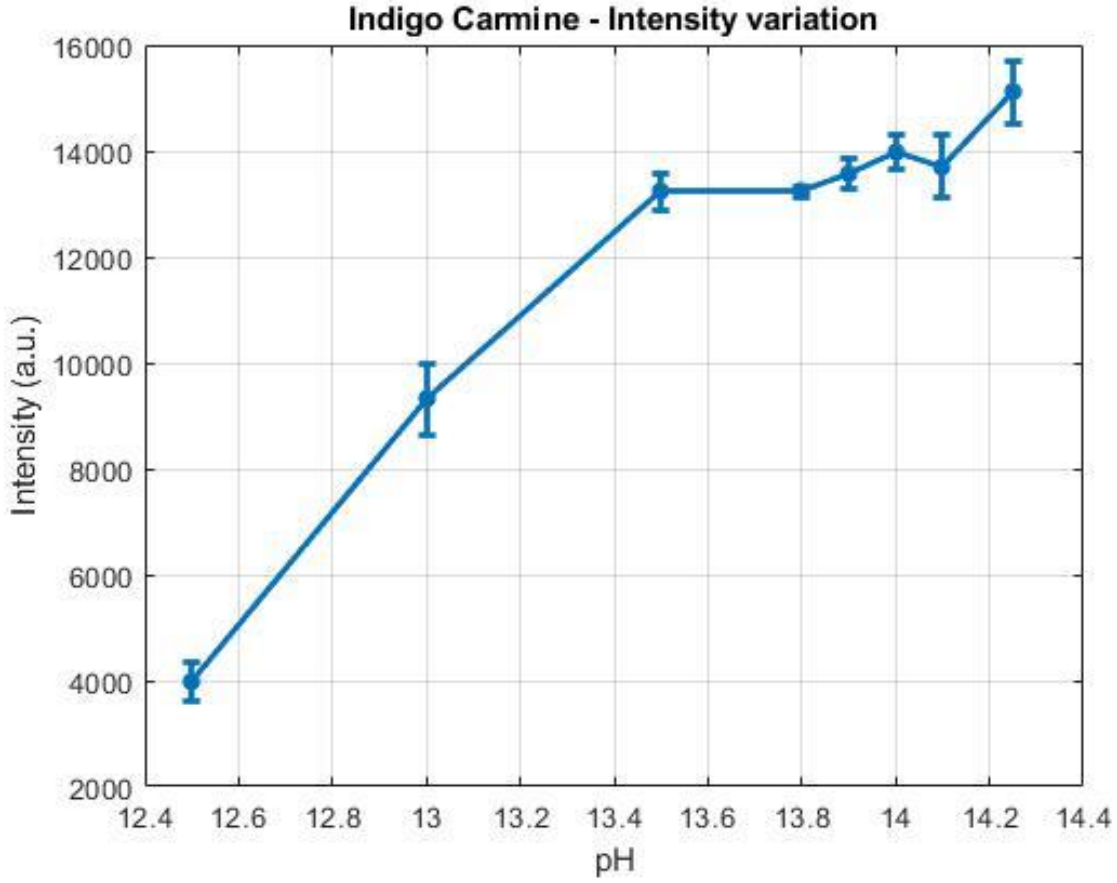

Figure 3.0.9. Intensity-pH variation with the standard deviations of Indigo Carmine.

Linearity was observed in the pH range between 12.5 and 13.5. **Figure 3.1.1** shows the linear polynomial that fits the data.

Equation of linear polynomial:

$$y = 9253.38\,x - 111449.39 \qquad (3.1.2)$$

Coefficient of determination:

$$R^2 = 0.9925$$

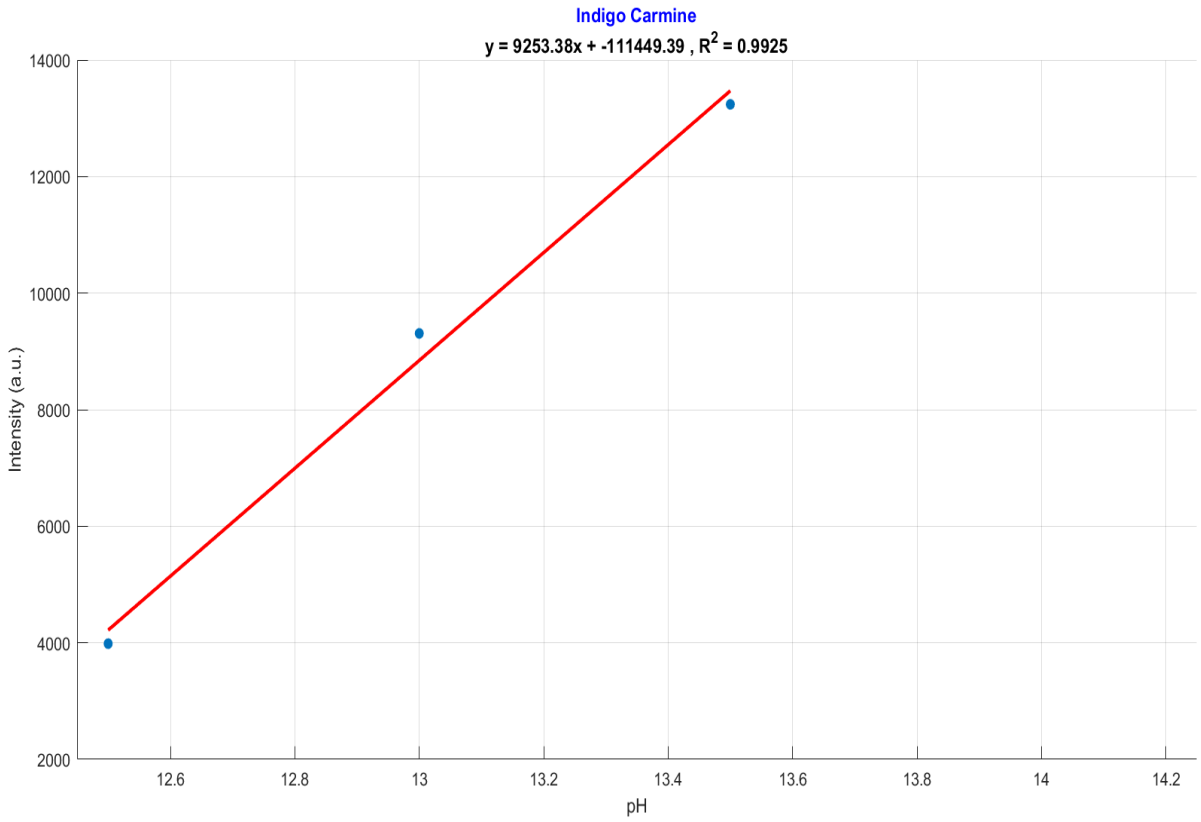

Figure 3.1.1. Linear polinomial interpolation in the range between 12.5 and 13.5.

Regarding the variation of the peak wavelength, it was observed that it does not change with pH, and it is identified around 537 nm. **(Figure 3.1.2).**

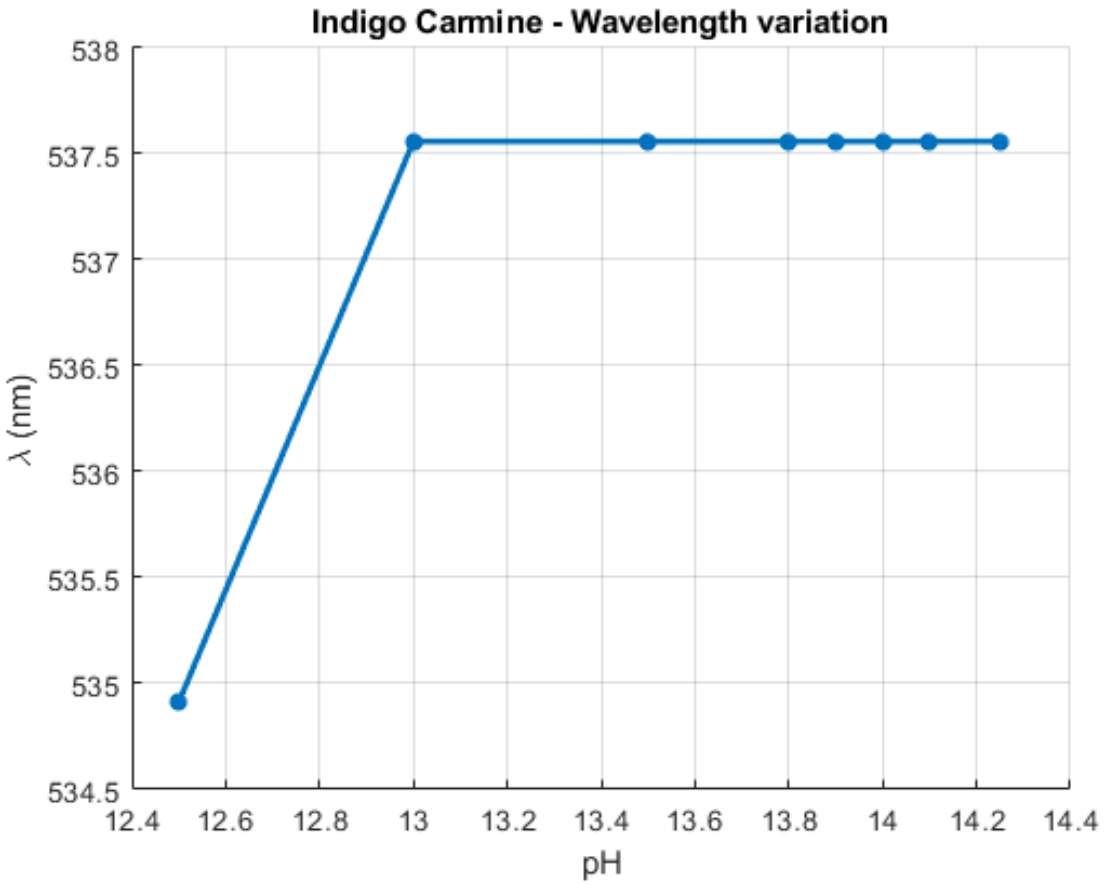

Figure 3.1.2. Variation of wavelength of the peak of Indigo Carmine.

3.1.3 Rhodamine 6G

The fluorescence of Rhodamine B was analyzed at the following pH points: 12.5, 13.0, 13.5, 13.8, 13.9, 14.0, 14.1, 14.25.

The concentration of Rhodamine 6G used was the same as that of Rhodamine B, which was $1.0438\ 10^{-5}$ M.

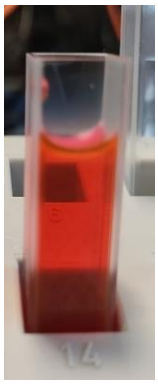

Figure 3.1.3. Solution of Rhodamine 6G.

Figure 3.1.4 shows the fluorescence spectrum of Rhodamine 6G at the specified pH points. The data reveals that the intensity decreases as the pH increases.

In **Figure 3.1.5**, the change in intensity with pH is plotted with the standard deviations.

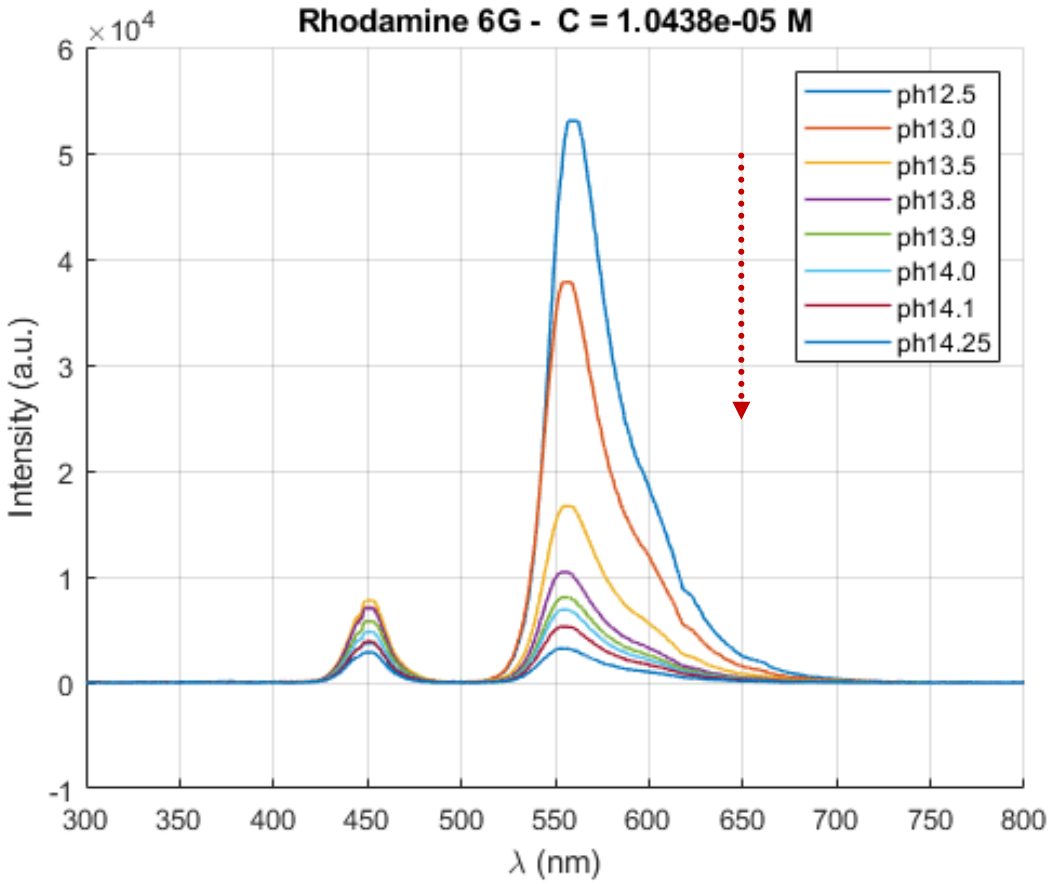

Figure 3.1.4. Spectrum of Fluorescence of Rhodamine 6G.

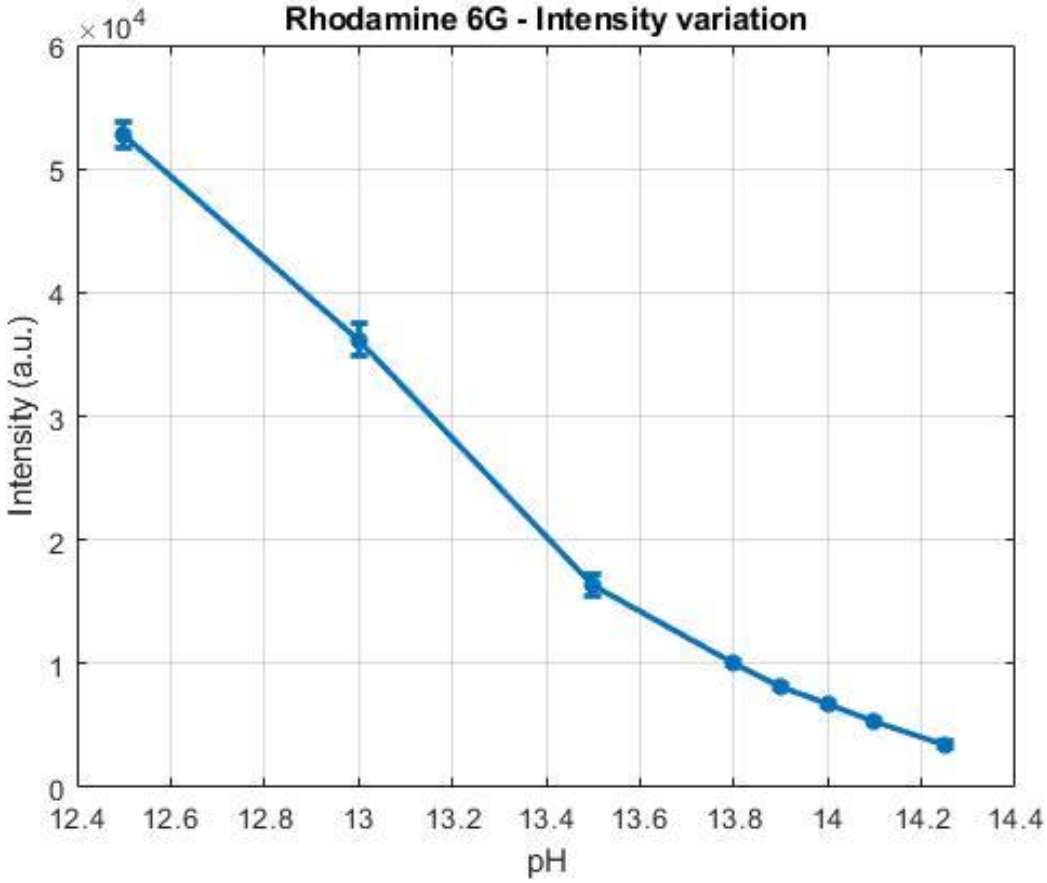

Figure 3.1.5. Intensity-pH variation with the standard deviations of Rhodamine 6G.

Both linear and second-order polynomials that fit the data of intensity variation were plotted. The linear polynomial was constructed by interpolating the data in the pH range of 13.5 to 14.25 **(figure 3.1.6)**, while the second-order polynomial was fitted to the data spanning the pH range from 12.5 to 14.25. **(Figure 3.1.7)**

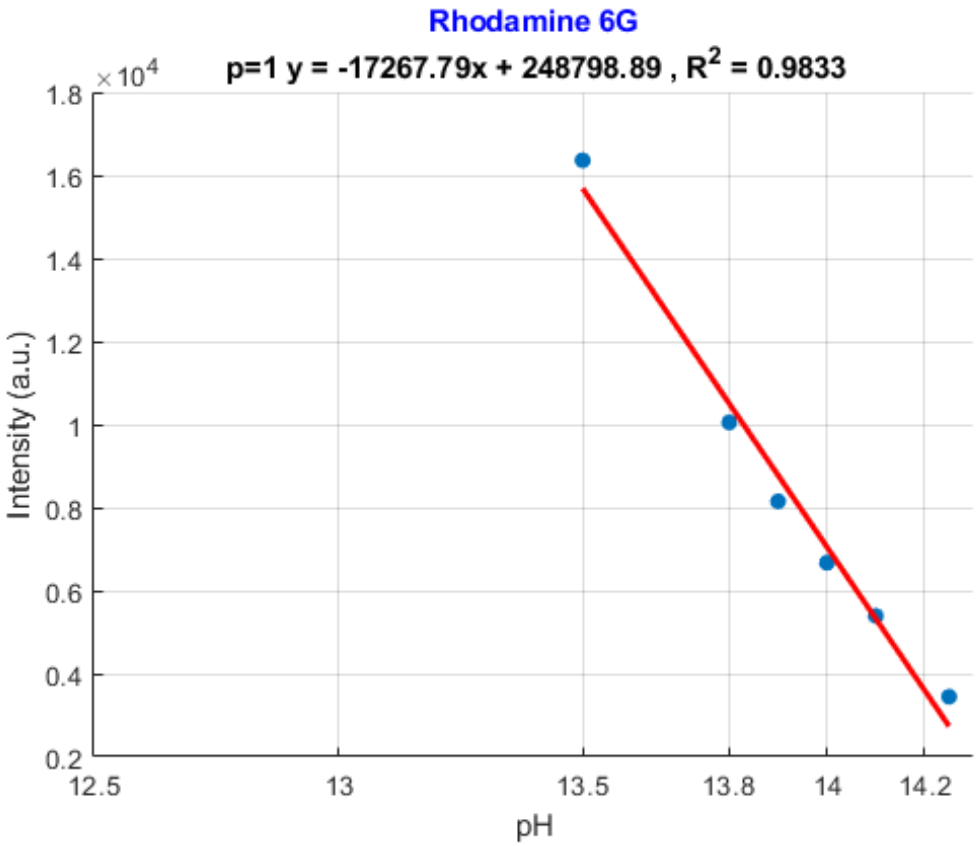

Figure 3.1.6. Linear polynomial interpolation in the range between 12.5 and 14.25.

Equation of linear polynomial:

$$y = -17267.79\,x - 111449.39 \qquad (3.1.3)$$

Coefficient of determination:

$$R^2 = 0.9833$$

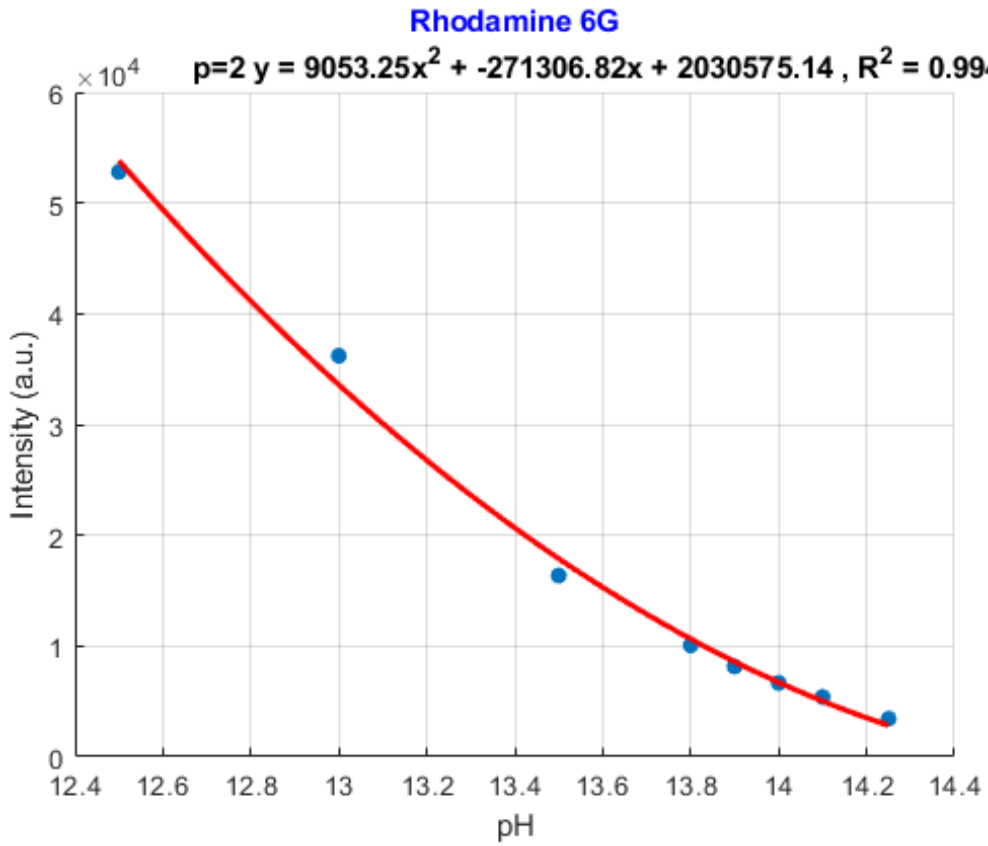

Figure 3.1.7. Second-order polynomial interpolation between pH 12.5 and 14.25.

Equation of second-order polynomial:

$$y = 9053.25\,x^2 - 271306.82x + 2030575.14 \qquad (3.1.4)$$

Coefficient of determination:

$$R^2 = 0.9949$$

Regarding the variation of the peak wavelength, it was observed that it does not change with pH, and it is identified around 560 nm. **(Figure 3.1.8).**

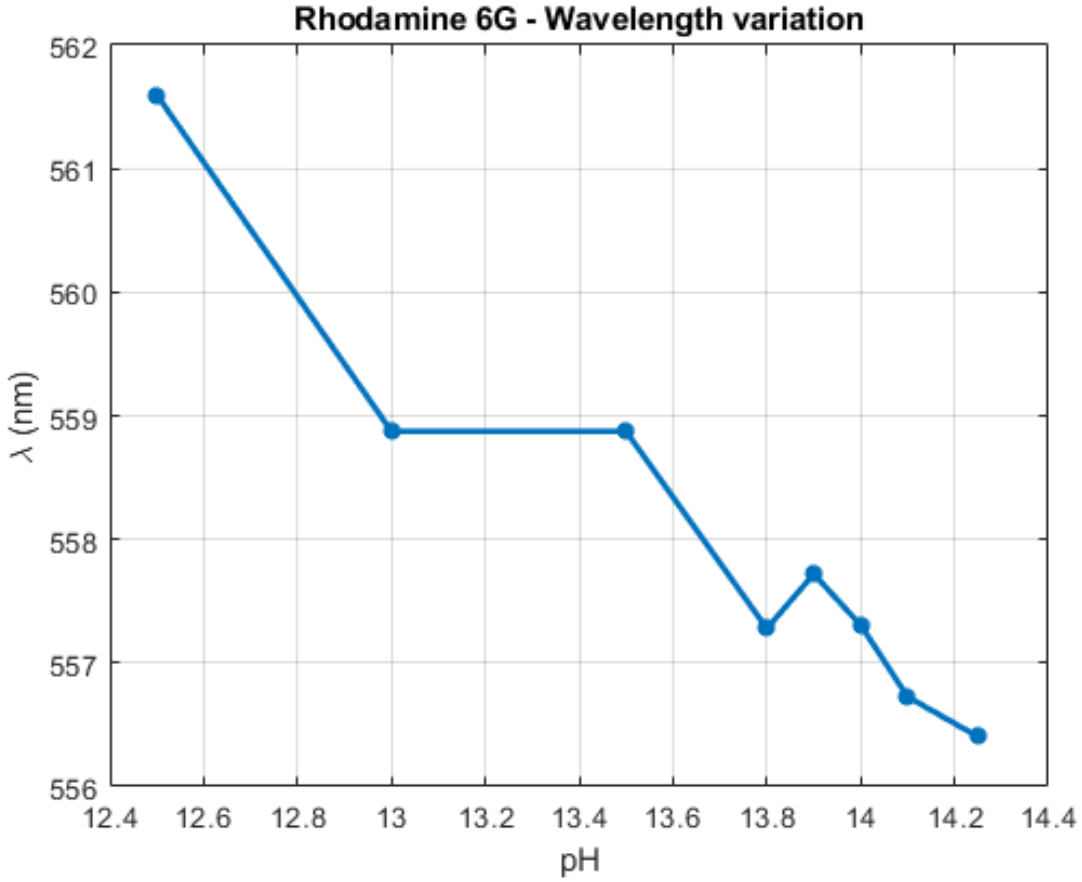

Figure 3.1.8. Variation of wavelength of the peak of Rhodamine 6G.

3.1.4. Titan Yellow

The fluorescence of Titan Yellow was analyzed at the following pH points: 12.5, 13.0, 13.5, 13.8, 13.9, 14.0, 14.1, 14.25.

The concentration of Titan Yellow is 3.5934 10^{-5} M. **(Figure 3.1.9)**

The intensity values associated with this dye are notably lower compared to those observed with previous dyes.

When the Thiazole concentration was increased to 2.8747 10^{-4} M only a minimal increase in intensity was observed, as depicted in **Figure 3.2.1** and separation between the solution and the dye **(Figure 3.2.2)**

Subsequent analyses exclude Titan Yellow due to noted limitations.

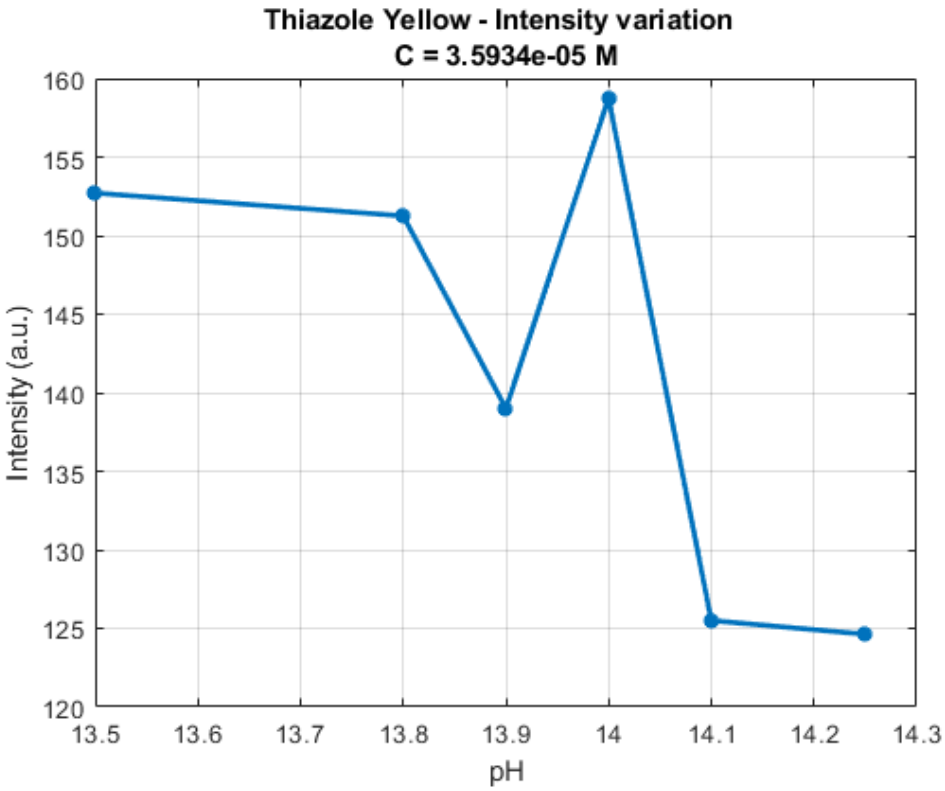

Figure 3.1.9. Intensity-pH variation with the standard deviations of Titan Yellow.

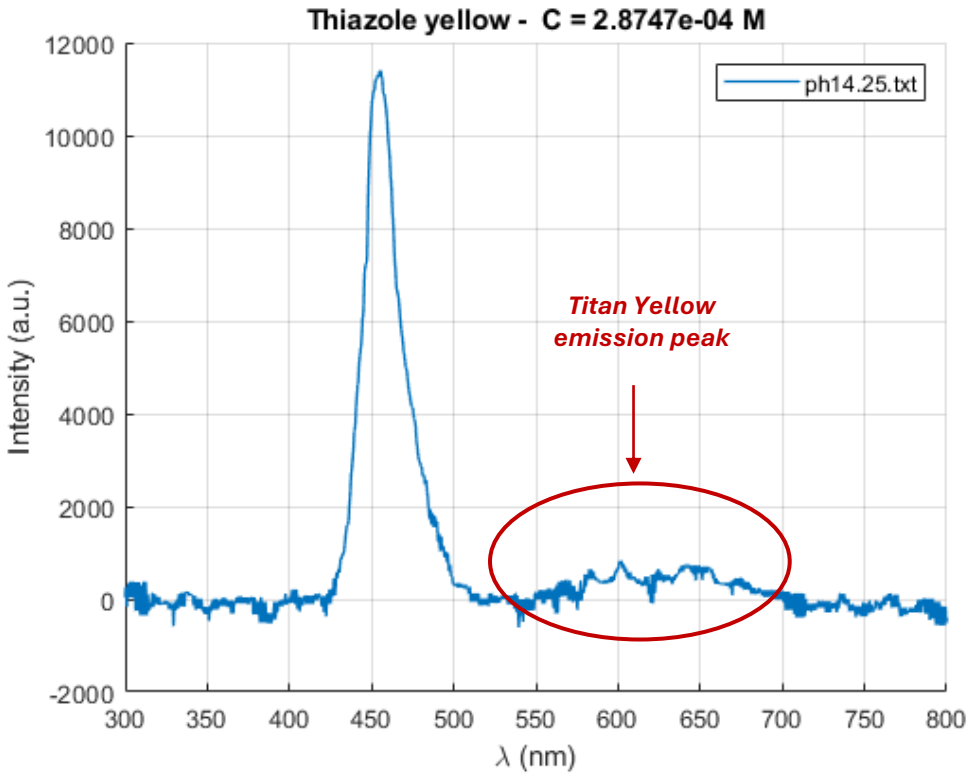

Figure 3.2.1. Spectrum of Fluorescence of Titan Yellow with a concentration of 2.8747 10^{-4} M for at pH 14.25

Figure 3.2.2. Titan Yellow solution, a separation is observed.

3.2. Mixing

During the previous analyses, it was noted that the fluorescence intensity occasionally changed over a few minutes, varying from one solution to another. To better understand this phenomenon, the effect of solution mixing was examined.

Solutions of the same dye subjected to accurate mixing and poor mixing have been compared to examine the effects of mixing on fluorescence intensity.

Figure 3.2.3 shows a solution of Rhodamine B with an accurate mixing, while **Figure 3.2.4** that shows a solution of Rhodamine B with an inadequate mixing.

The results show that without an accurate mixing, the intensity fluctuates randomly over time.

In contrast, these fluctuations do not exist when the solution is adequately mixed.

Furthermore, after 45 minutes, the mixing effect appears to be diminished, with the solution exhibiting behavior similar to that of well-mixed solutions. **(Figure 3.2.5)**

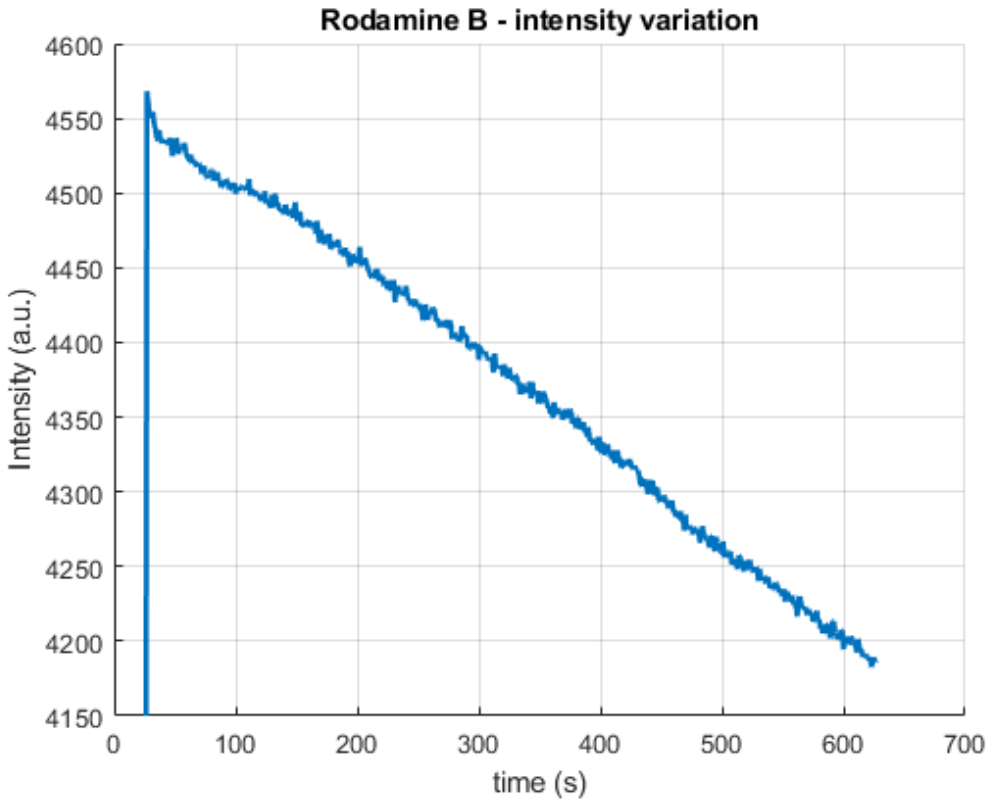

Figure 3.2.3. Intensity- Time variation of the solution of Rhodamine B with an accurate mixing.

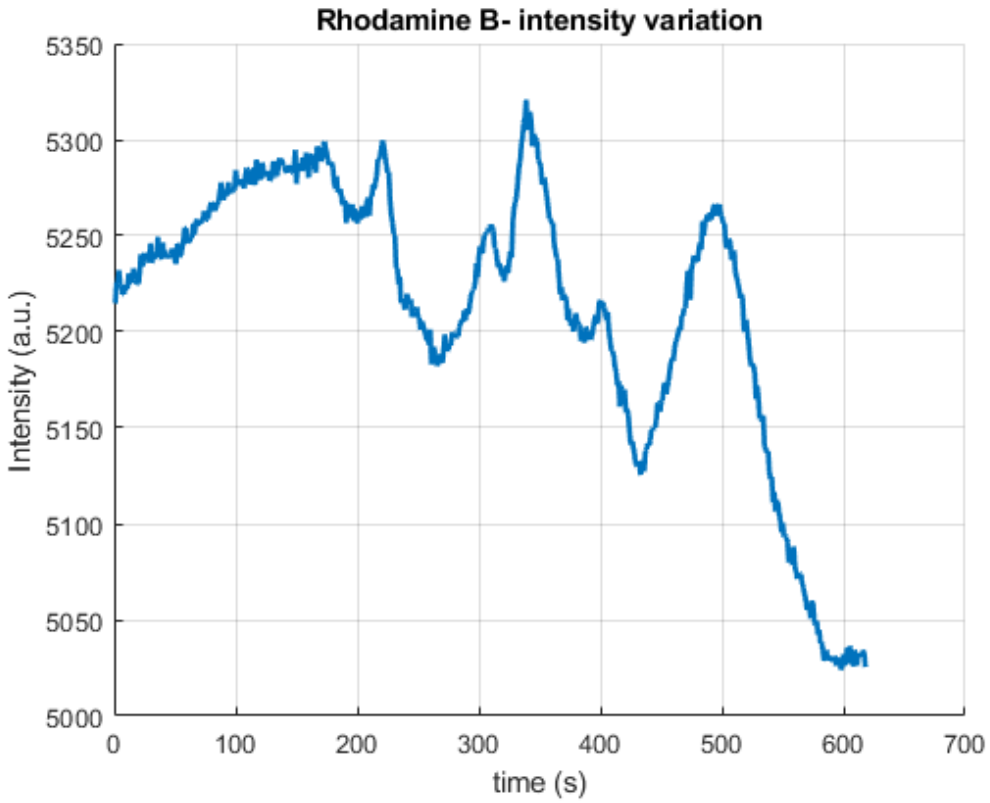

Figure 3.2.4. Intensity-Time variation of a solution of Rhodamine B with poor mixing.

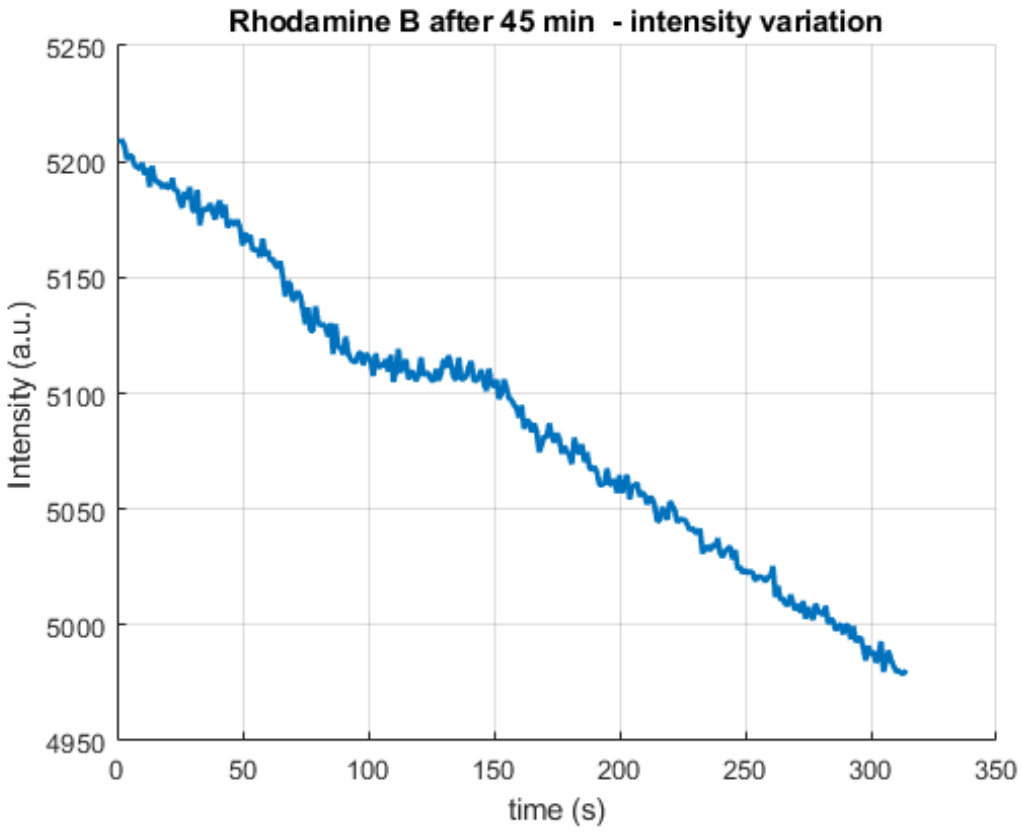

Figure 3.2.5. Intensity- Time variation of the solution of Rhodamine B with poor mixing after 45 minutes.

3.3. Temperature analysis

As indicated in *paragraph 2.4 of Materials and Methods*, the relation between fluorescence and temperature has been examined. During the analysis of pH solutions, a decrease in the intensity of fluorescence of dyes and an increase in temperature was observed.
To understand whether the temperature increase was due to the heating of the solution by the LED of the instrument or an exothermic reaction between the dye and the pH solution, several tests were conducted.

In the first test, the temperature of a solution of Rhodamine B exposed to the LED of the Avantes instrument for 1000 s was analyzed. It showed an increase of about 9°C. **(Figure 3.3.1)**

Subsequently, the temperature change of a new solution of Rhodamine B was monitored for the same period, without led exposure. This second test highlighted an almost constant temperature over time with negligible variations.

(Figure 3.3.2)

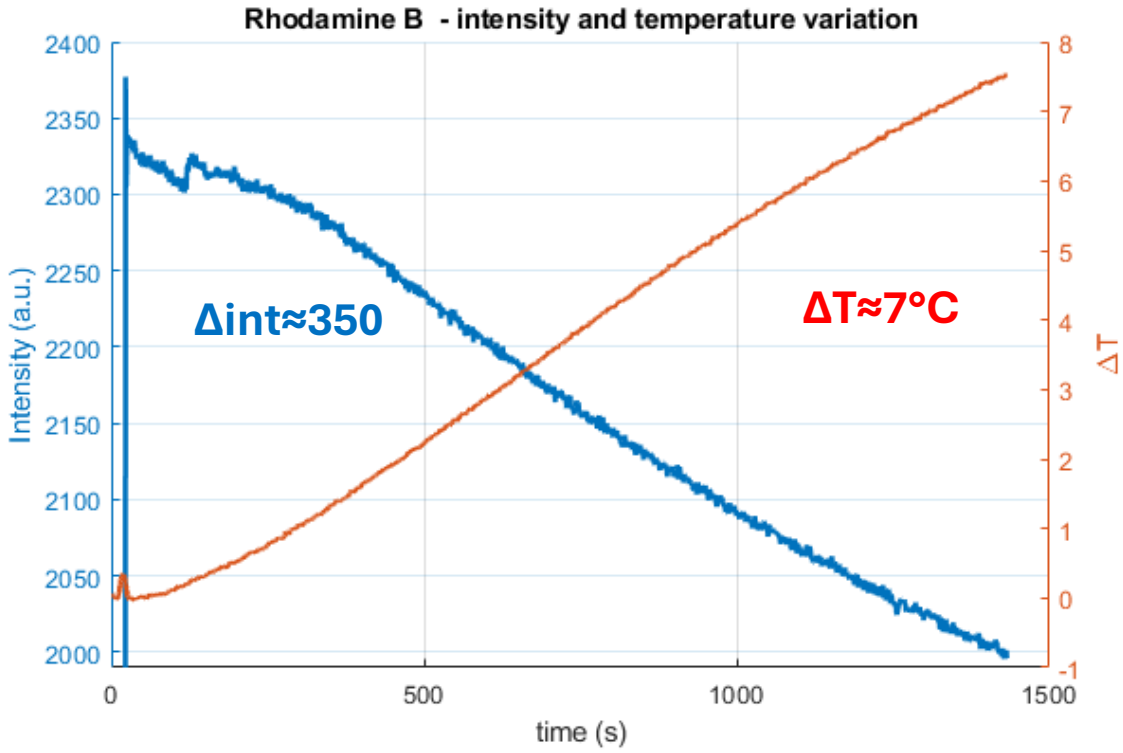

Figure 3.3.1. Rhodamine B intensity and temperature variation over time when exposed to the LED of the Avantes instrument.

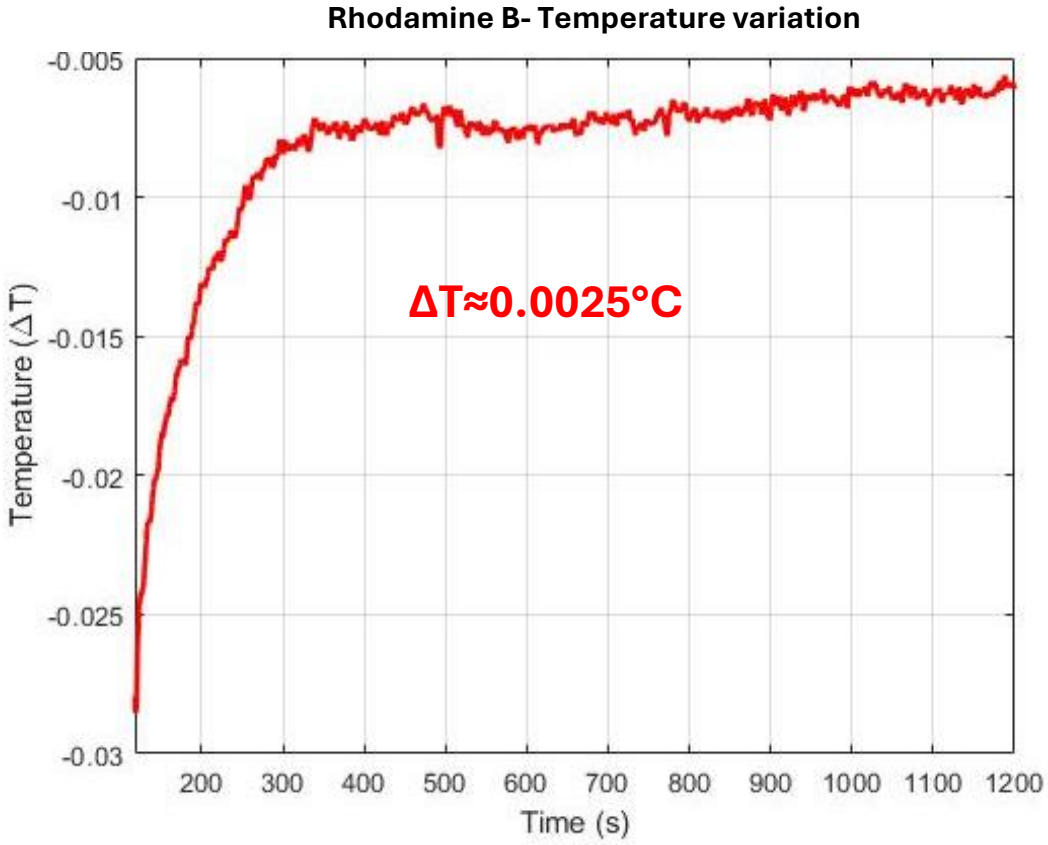

Figure 3.3.2. Temperature variation of Rhodamine B exposed to room temperature.

To confirm that the temperature increase was caused by the LED of the Avantes instrument, a solution with pH 13.5 without dye was exposed to the LED light. This also showed an increase in temperature over time **(figure 3.2.3).**

It clarified that the temperature increase was caused by the led.

Subsequently, the mathematical model of temperature compensation for Rhodamine B solutions was adapted. By compensating the temperature in relation to the surrounding environment, as proposed by Watras et al. (2011) [36], the results were consistent with the expected behavior. **(Figure 3.2.4)**

To validate the method over time, tests were conducted in isothermal conditions in the following section.

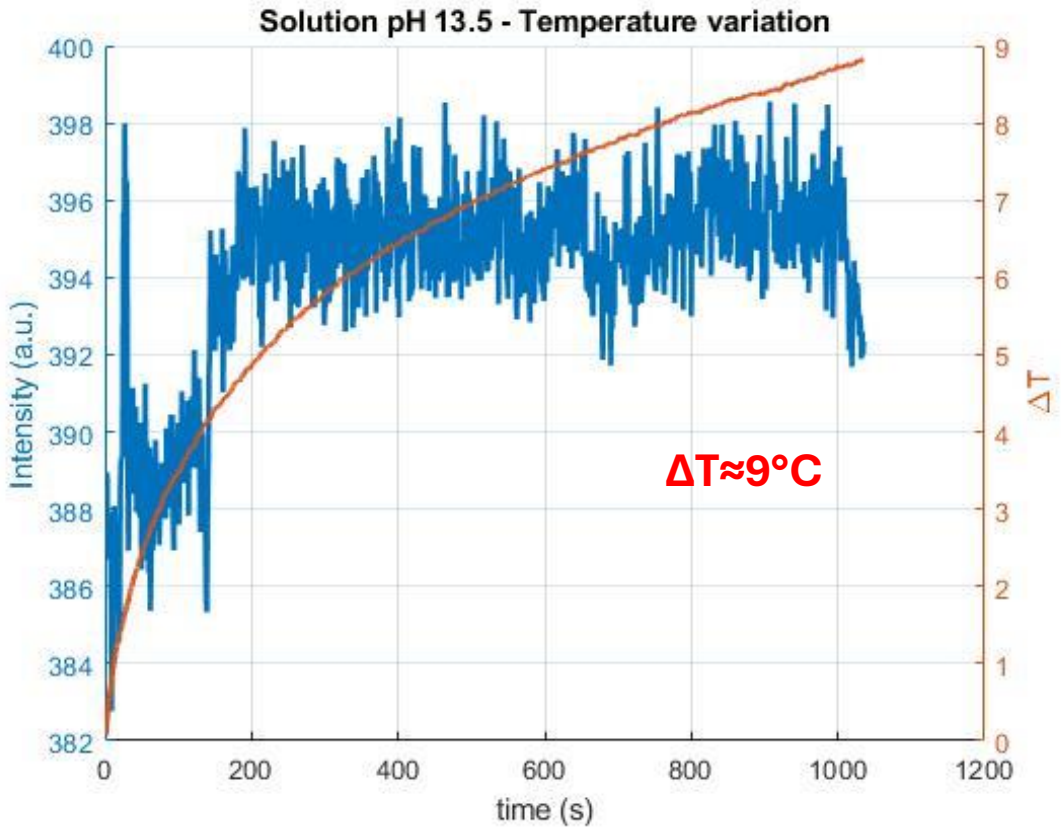

Figure 3.2.3. A solution with pH 13.5 without dye exposed to the LED light.

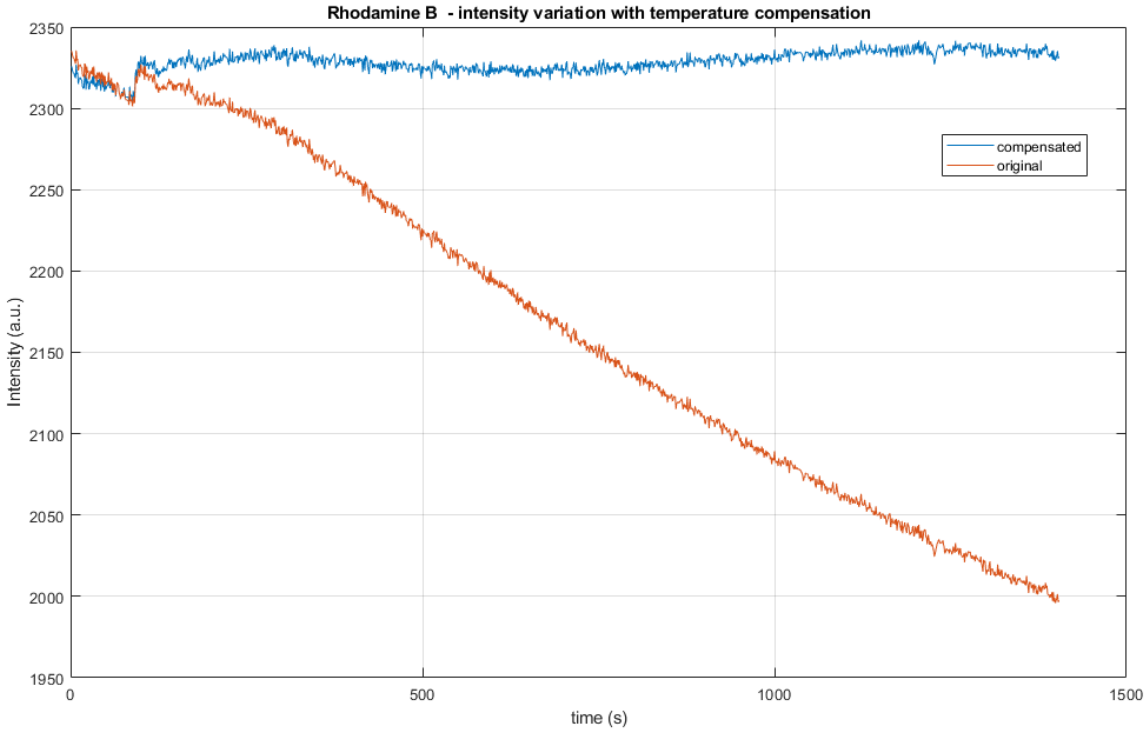

Figure 3.2.3. Curves depicting the temperature-influenced data and the compensated data using the mathematical model proposed by Watras et al. (2011) [36].

Regarding the Indigo Carmine solution, it was observed that the fluorescence followed the same pattern over time **(Figure 3.2.4),** but a color change occurred 10 minutes after the solution was prepared.

To determine if this phenomenon was related to temperature, two identical solutions of indigo carmine with a pH of 13.5 were prepared: one was placed on a heating plate with an increase of temperature of 4-5°C, and the other was left at room temperature. In both cases, a color change was observed, occurring more rapidly in the heated solution.

In **Figure 3.2.5** shows a new prepared Indigo Carmine solution and the two solutions after 10 minutes: the cuvette on the left was kept at room temperature, and the one on the right was placed on the heating plate.

This has detected the instability of the Indigo Carmine indicator over time, leading to its exclusion from further analyses.

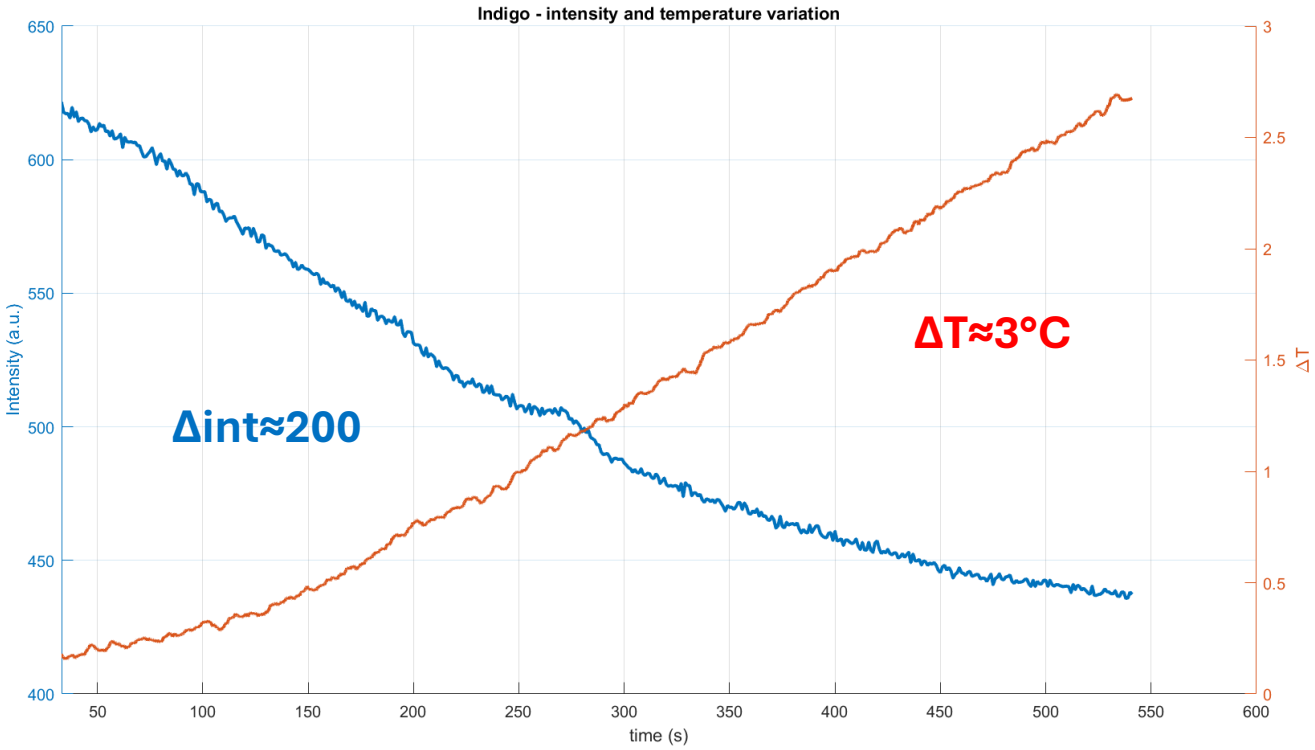

Figure 3.2.4. Indigo Carmine intensity and temperature variation over time when exposed to the LED of the Avantes.

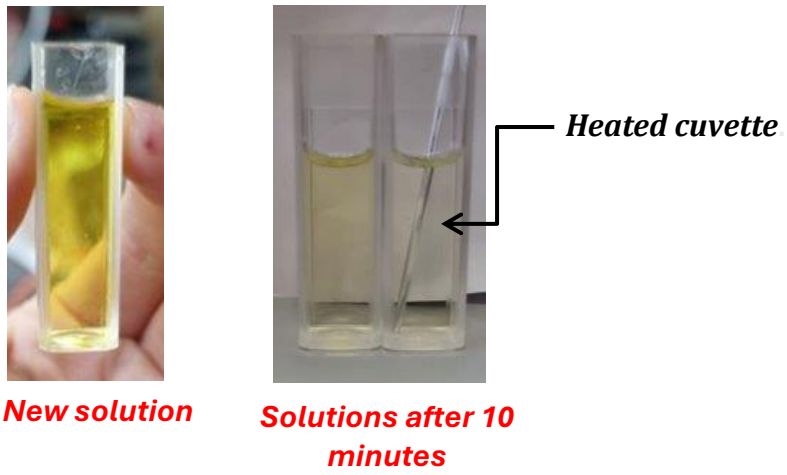

Figure 3.2.5. The images display a new Indigo Carmine solution and two solutions observed after 10 minutes. The cuvette on the left was kept at room temperature, while the one on the right was placed on a heating plate.

3.4. Stability over time

The tests were conducted to evaluate the stability of Rhodamine B and Rhodamine 6G over time in isothermal conditions at three pH levels: 12.5, 13.5, and 14.25, each lasting two hours. For each pH point, the tests were conducted in triplicate.

To simulate an environment as isothermal as possible, the LED of Avantes instrument was turned on and off to capture a singles acquisition.

Data were analyzed with higher frequency during the initial 10 minutes and then at a reduced frequency for the entire two-hour duration, enabling the construction of time-dependent curves.

3.4.1. Rhodamine 6G

The graphs showed that the Rhodamine 6G presents an initial transient phase in which the intensity increases, followed by a plateau in which it remains stable for at least two hours.

It was observed that the duration of the transitional phase decreases as the pH increases: at pH 12.5 it occurred around 4000 s **(Figure 3.4.1)**, at pH 13.5 about 800 s **(Figure 3.4.2)**, and at pH 14.25 about 300 s **(Figure 3.4.3)**.

Figure 3.4.4 displays the average intensity-time curves for Rhodamine 6G at each pH point. The three curves are clearly distinct and well-separated, showing a significant shift between each pH level.

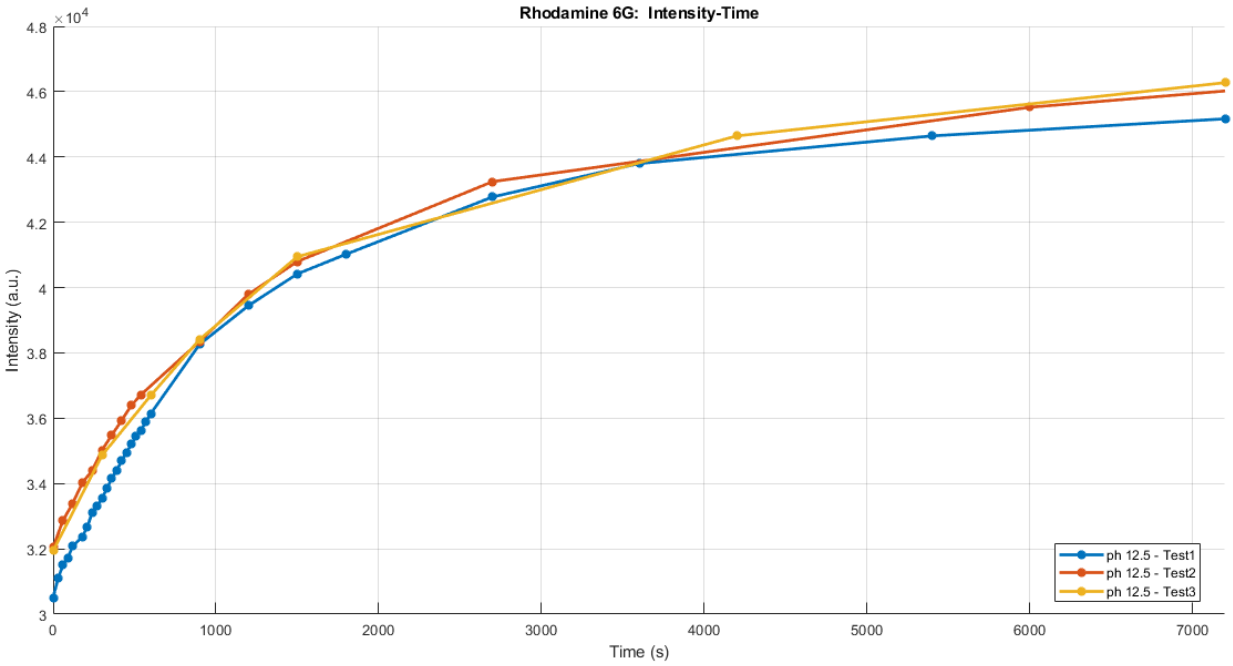

Figure 3.4.1. Rhodamine 6G intensity-time variation for three tests in solution at pH 12.5.

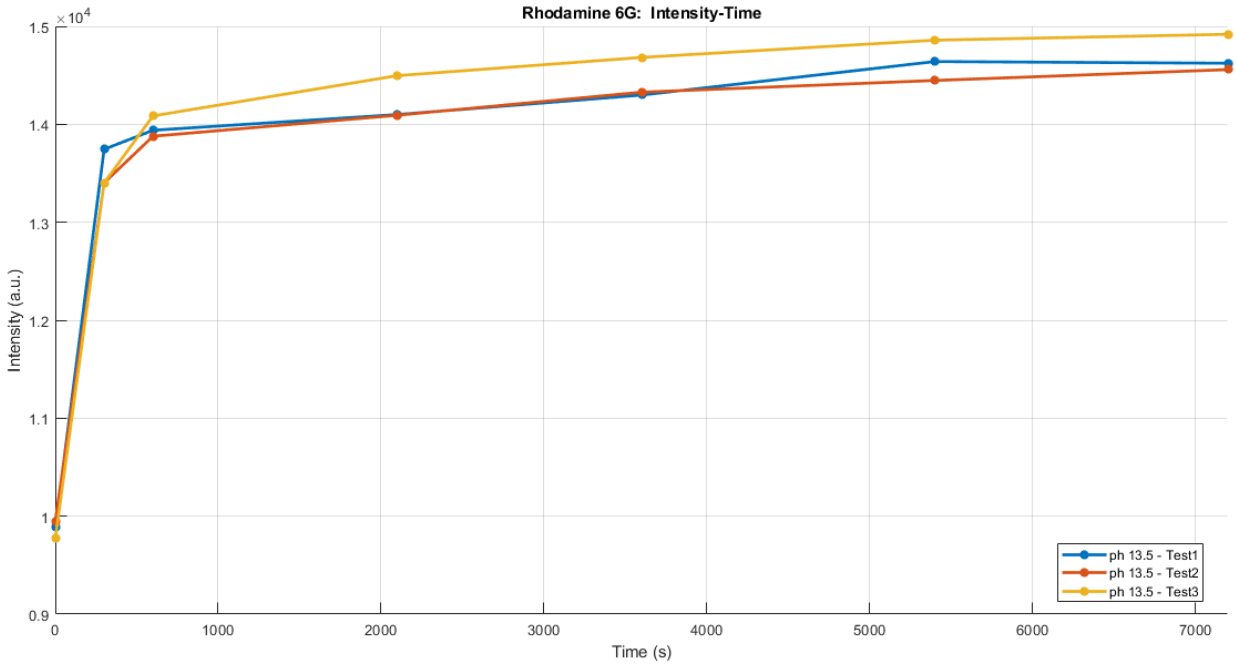

Figure 3.4.2. Rhodamine 6G intensity-time variation for three tests in solution at pH 13.5.

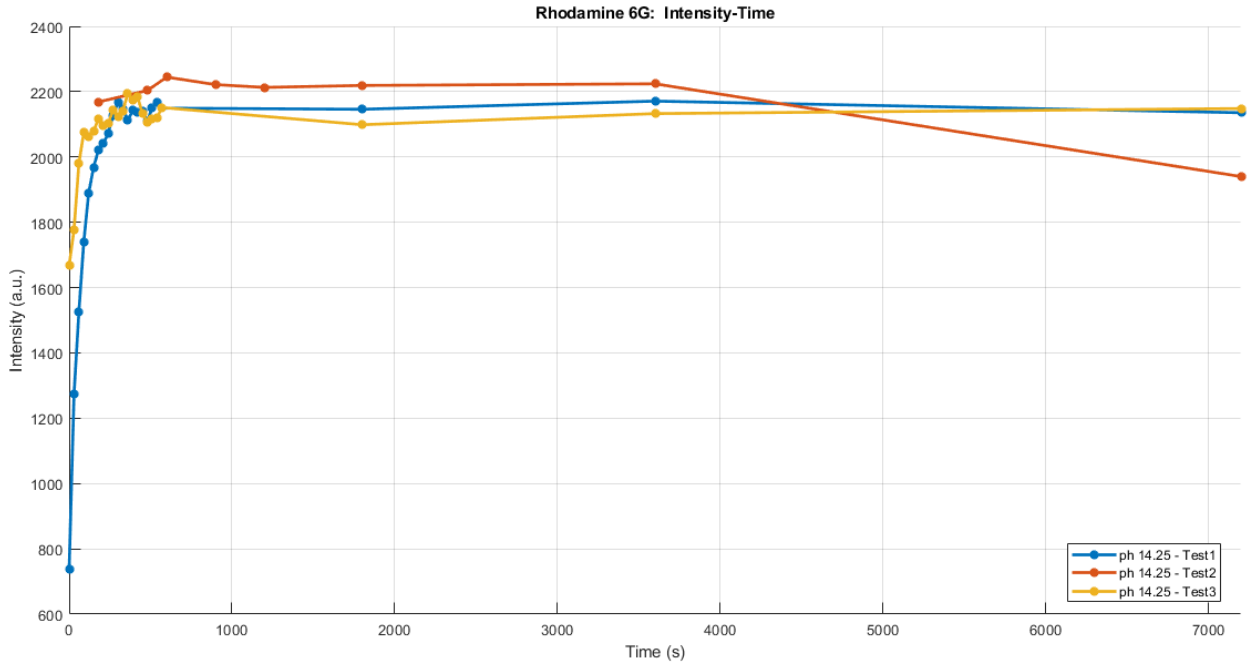

Figure 3.4.3. Rhodamine 6G intensity-time variation for three tests in solution at pH 14.25.

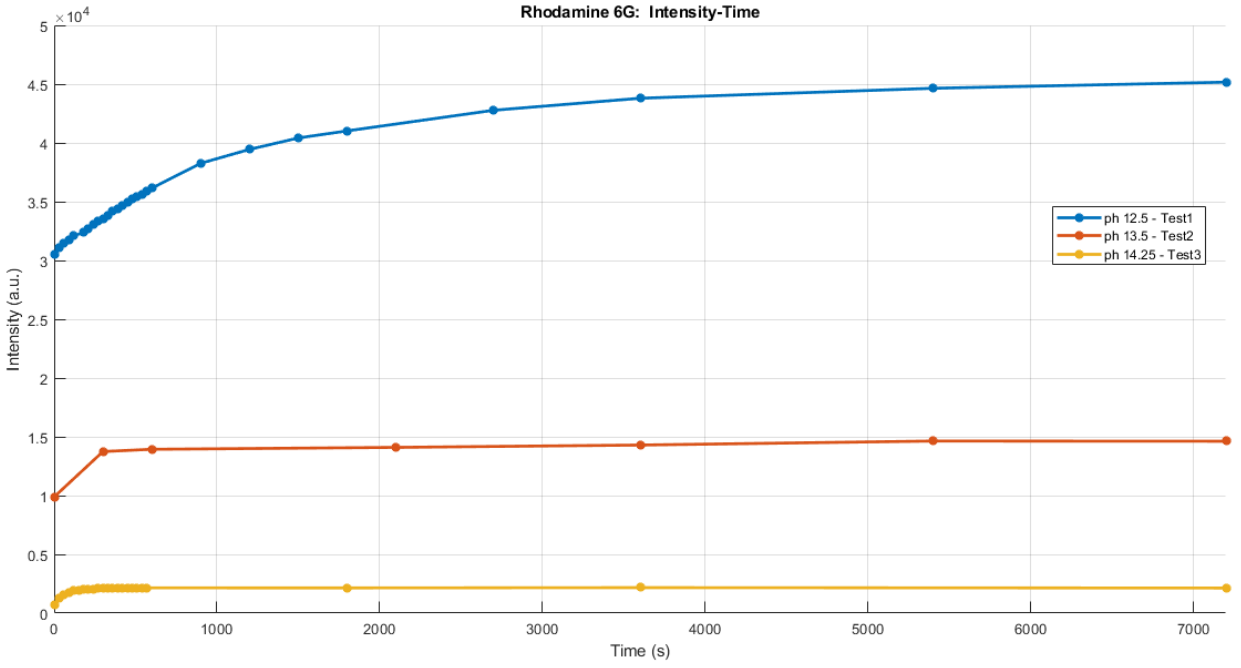

Figure 3.4.4 displays the average intensity-time curves for Rhodamine 6G at each pH point.

3.4.2. Rhodamine B

The same tests were conducted on Rhodamine B. In contrast to the Rhodamine 6G, the B immediately showed a plateau, with the intensity oscillating within a negligible range. **Figure 3.4.5**, **Figure 3.4.6**, and **Figure 3.4.7** represent the three tests conducted at pH 12.5, pH 13.5 and pH 14.25 respectively.

Figure 3.4.8 shows the average intensity curves over time for each pH point. The curves for the different pH levels tend to oscillate and intersect at certain points, which makes it challenging to distinguish the three curves.

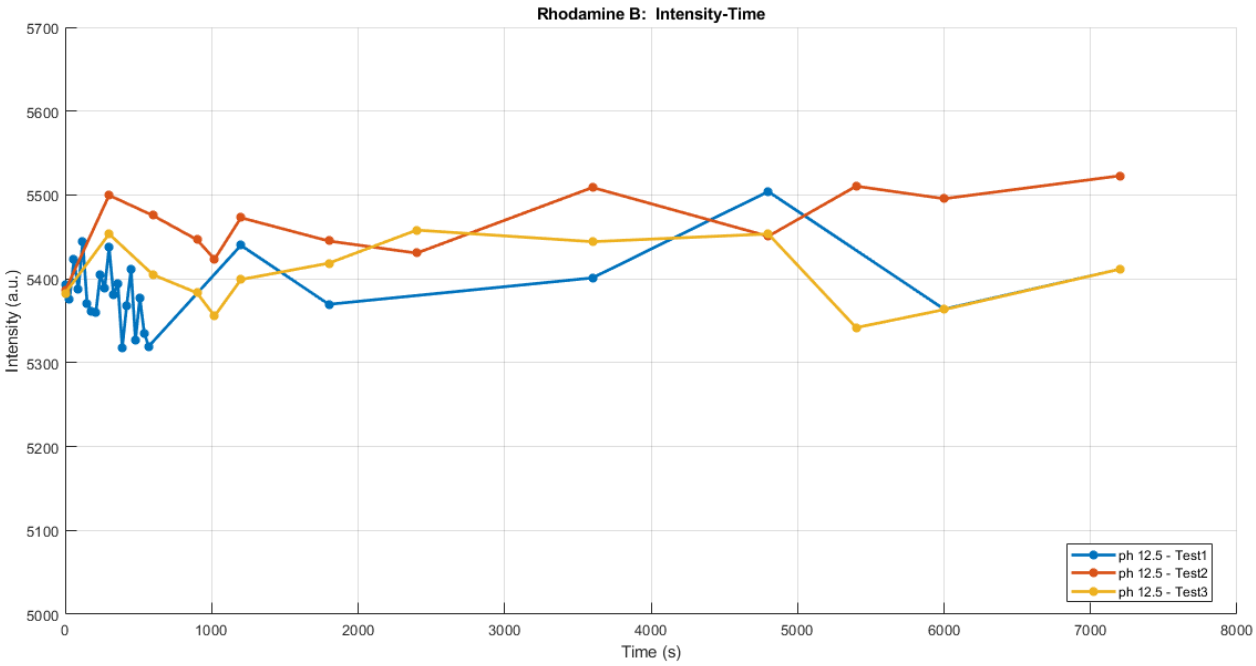

Figure 3.4.5. Rhodamine B intensity-time variation for three tests in solution at pH 12.5.

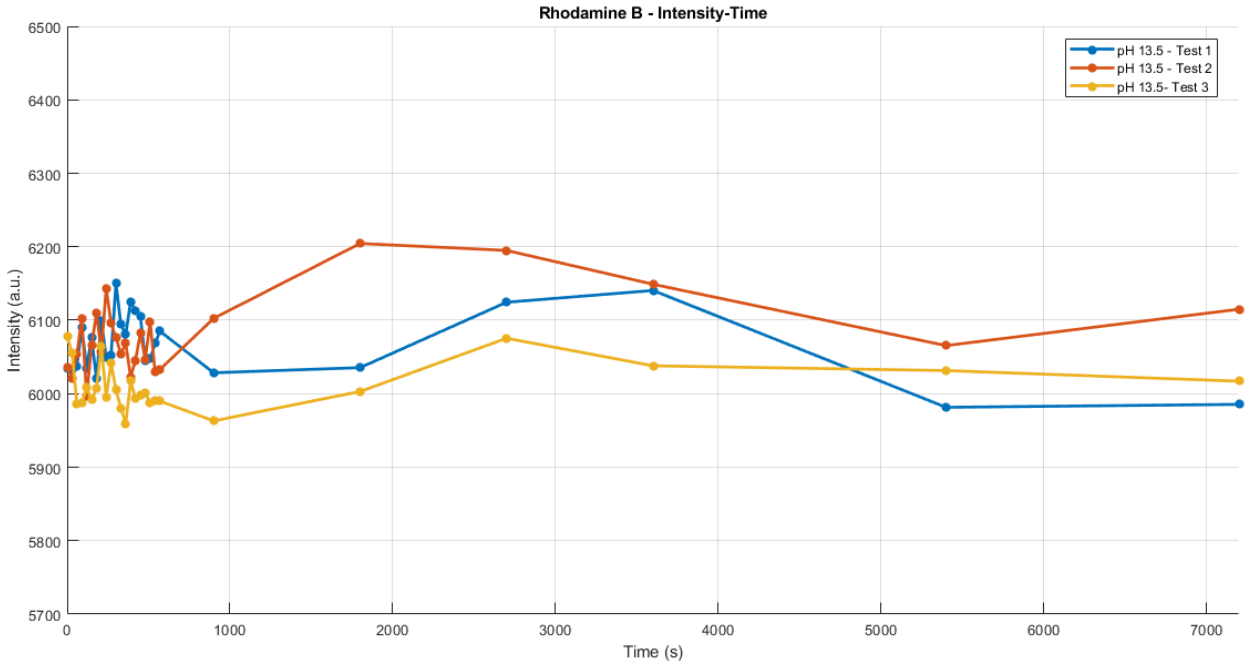

Figure 3.4.6. Rhodamine B intensity-time variation for three tests in solution at pH 13.5.

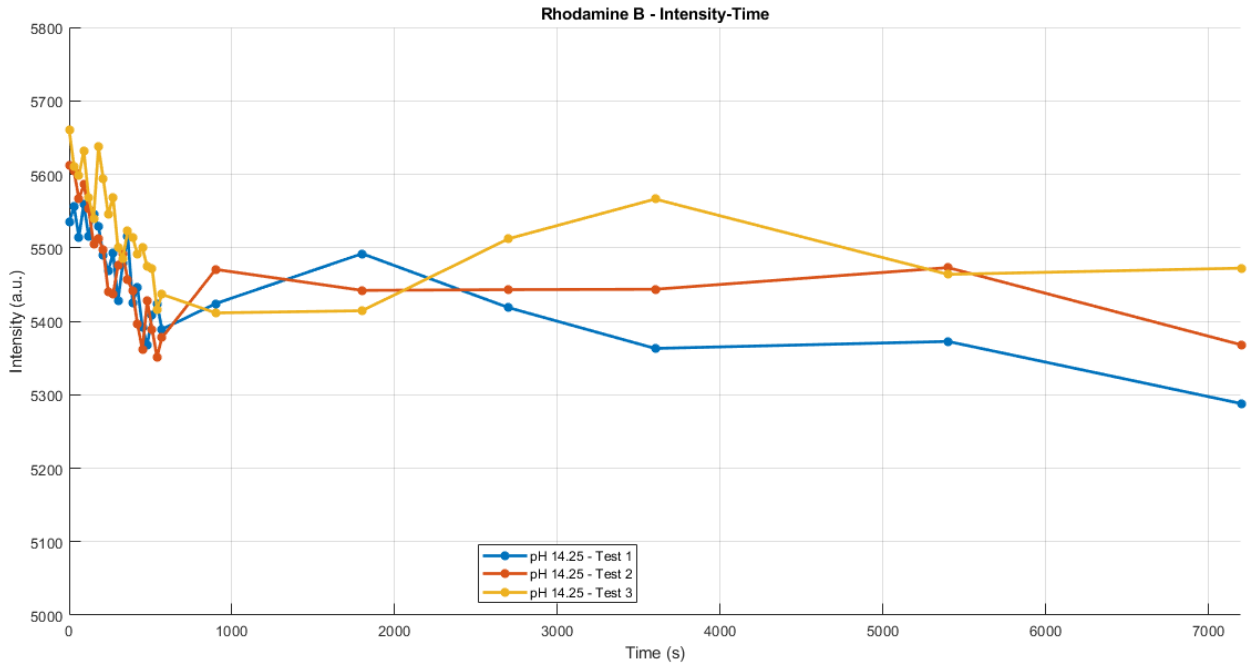

Figure 3.4.7. Rhodamine B intensity-time variation for three tests in solution at pH 14.25.

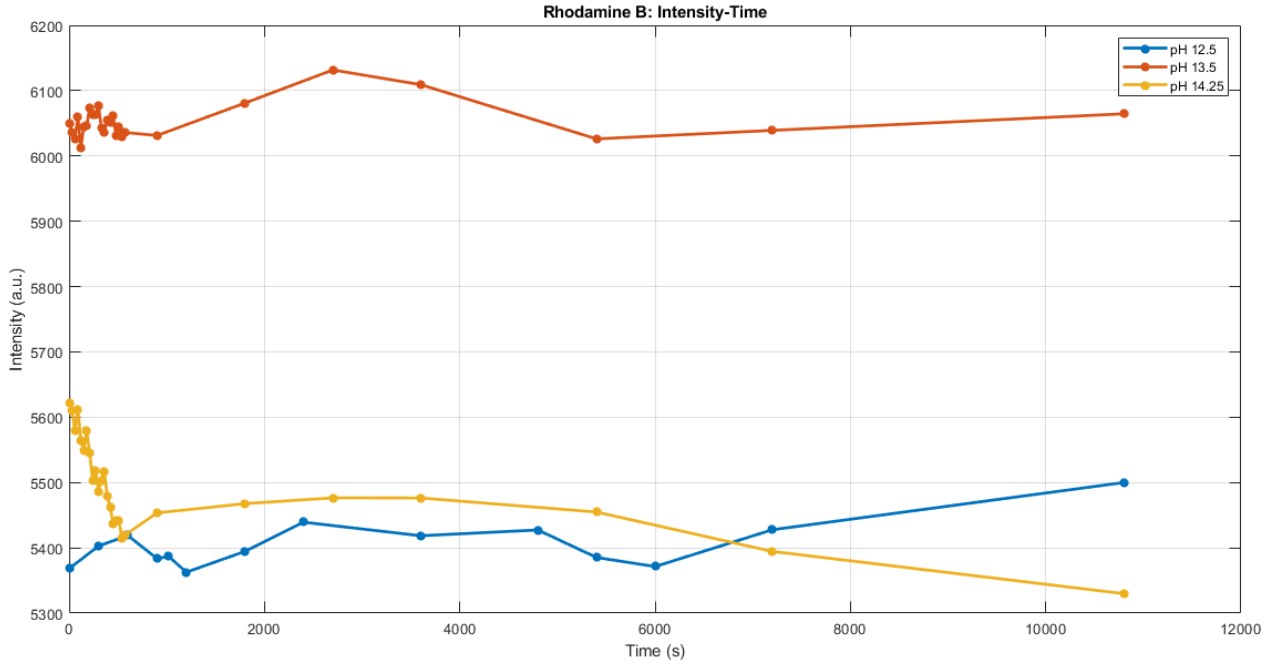

Figure 3.4.8 displays the average intensity-time curves for Rhodamine B at each pH point.

3.5. Effect of Metal Cations on Dye Fluorescence

The interactions of Rhodamine B and Rhodamine 6G in the presence of metal cations (Pb^{2+} and Sn^{4+}) have been studied.

The tests were conducted according to the same protocol as the previous paragraph: under isothermal conditions for two hours and for three different pH values (12.5, 13.5 e 14.25).

3.5.1. Rhodamine 6G

The first graph **(figure 3.5.1)** shows the three curves of Rhodamine 6G at three pH points, each with the addition of a solution of 30 mM of lead ions Pb^{2+}.

The second graph **(figure 3.5.2)** represents the three curves of Rhodamine 6G at three pH points, each with the addition of a solution of 30 mM of tin ions Sn^{4+}.

In both cases, it was observed that the stability of the dye does not change and that the intensity values are comparable with the previous ones.

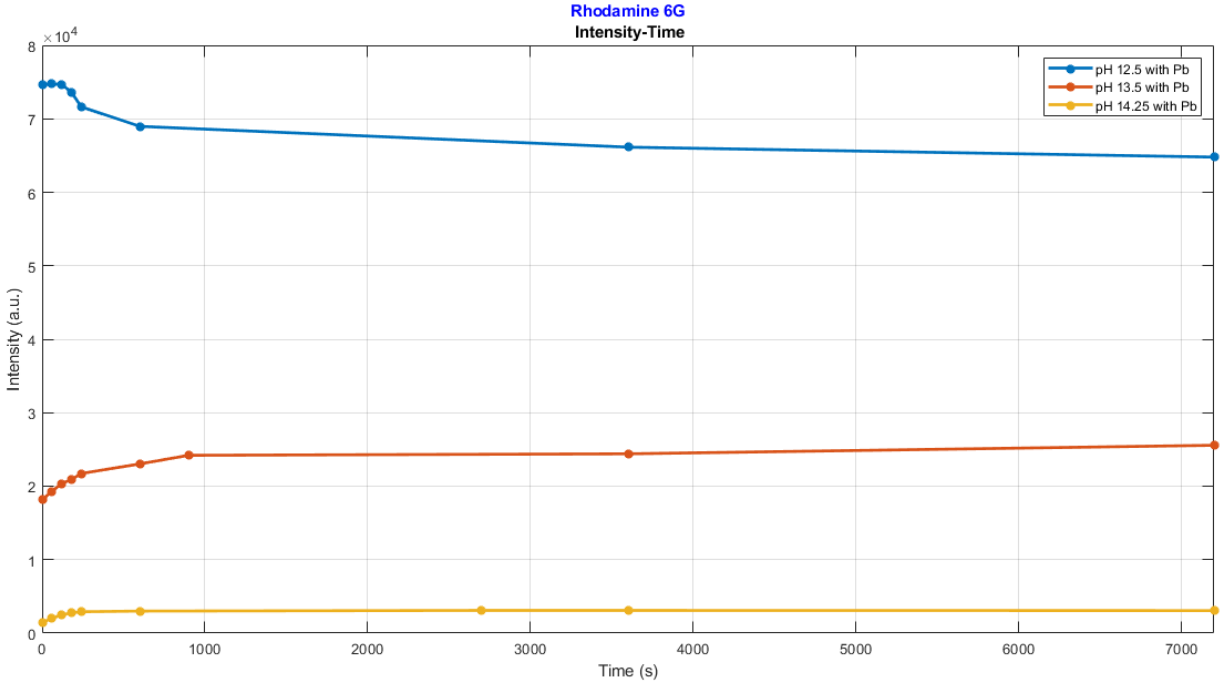

Figure 3.5.1. Rhodamine 6G Intensity-Time Curves with 30 mM Lead Ions.

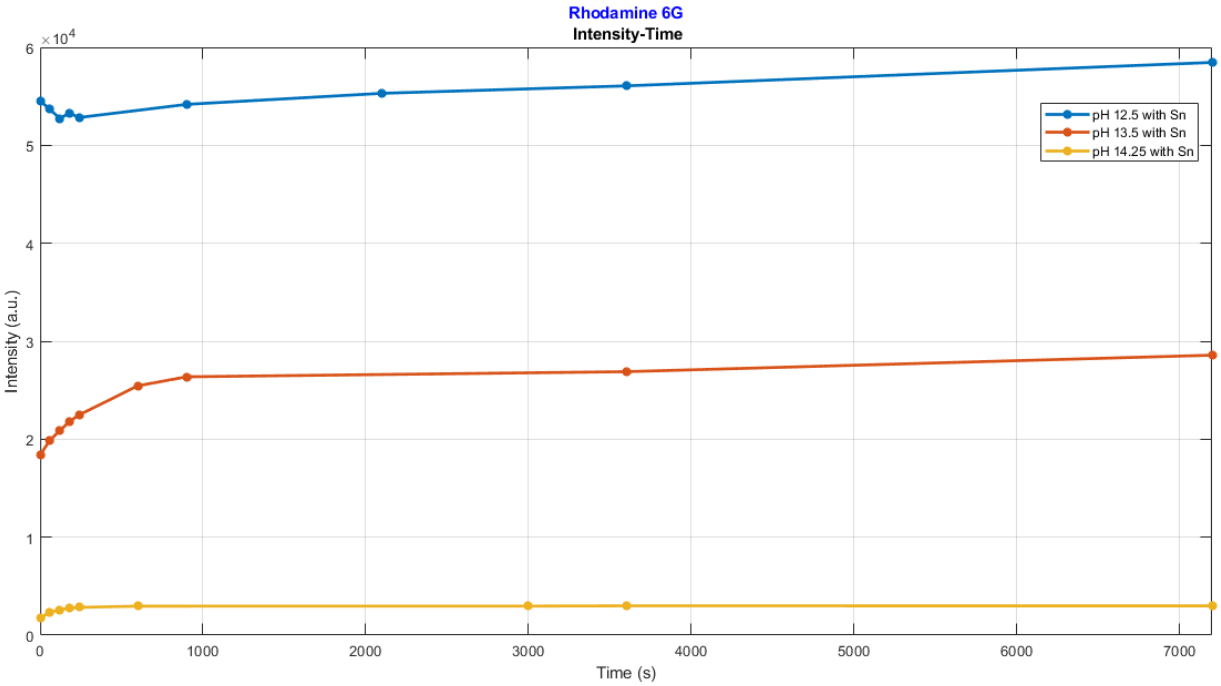

Figure 3.5.2. Rhodamine 6G Intensity-Time Curves with 30 mM Tin Ions.

3.5.3. Rhodamine B

The first graph **(figure 3.5.3)** shows the three curves of Rhodamine B at three pH points, each with the addition of a solution of 30 mM of lead ions Pb^{2+}.

The second graph **(figure 3.5.4)** represents the three curves of Rhodamine B at three pH points, each with the addition of a solution of 30 mM of tin ions Sn^{4+}.

The curves of Rhodamine B prove to be stable over time, however, differences in intensity values have been observed compared to the case discussed in the previous paragraph. With the addition of 30 mM of lead ions, the pH curve of 12.5 showed a higher intensity than the others. Instead, with the addition of 30 mM of tin ions, the pH 13.5 curve showed a higher intensity, while the pH 12.5 showed significantly lower values.

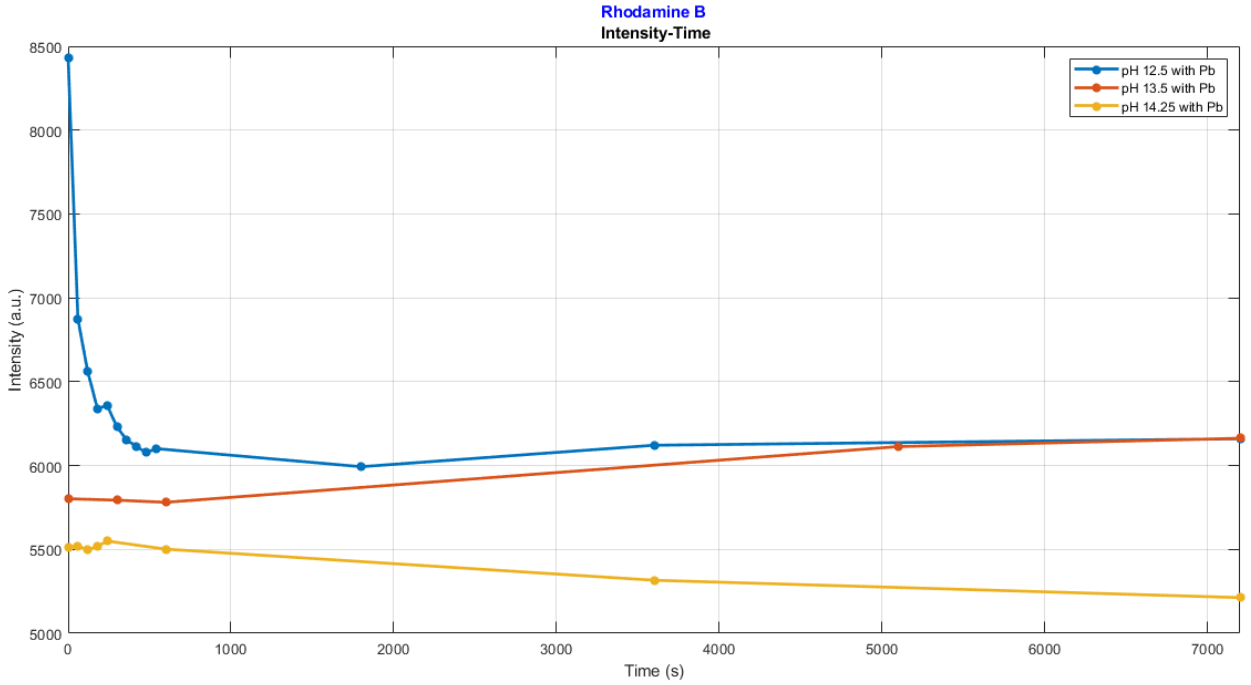

Figure 3.5.3. Rhodamine B Intensity-Time Curves with 30 mM Lead Ions.

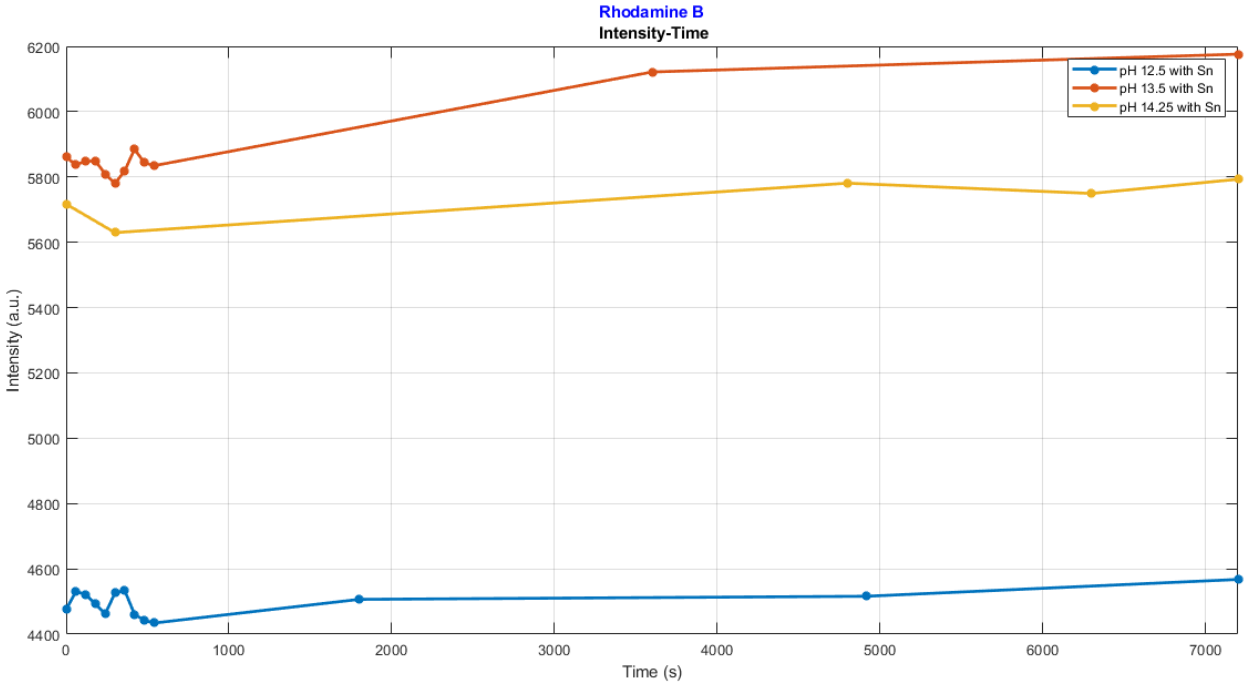

Figure 3.5.4. Rhodamine B Intensity-Time Curves with 30 mM Tin Ions.

3.6. Kinetic study

A kinetic analysis was conducted to evaluate how quickly the dyes respond to the pH change, capturing their dynamic behavior across the entire pH spectrum.

This test was carried out for Rhodamine B and Rhodamine 6G.

The experiment began with a solution of pH 12.5, to which a highly alkaline concentrated solution was added approximately every 30 s until it reached pH 13.5.

Subsequently, the same procedure was repeated starting from a pH 13.5 solution, continuing until a pH 14 solution was achieved.

The procedure performed is detailed in the Kinetic Studies section of Materials and Methods.

3.6.1. Rhodamine 6G

Figure 3.6.1 shows the kinetic response starting from pH 12.5, while **Figure 3.6.2** illustrates the corresponding variation in intensity.

Figure 3.6.3 and **Figure 3.6.4** show similar trends starting from a pH solution of 13.5.

Rhodamine 6G exhibits a rapid and stable response to changes in pH.

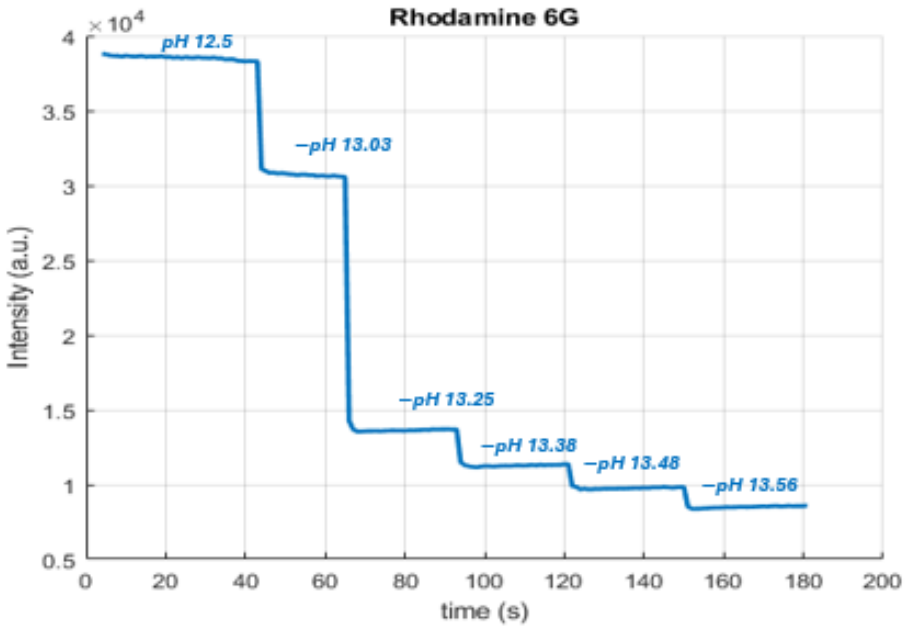

Figure 3.6.1. Kinetic response of Rhodamine 6G starting from pH 12.5 with the addition of a highly concentrated alkaline solution.

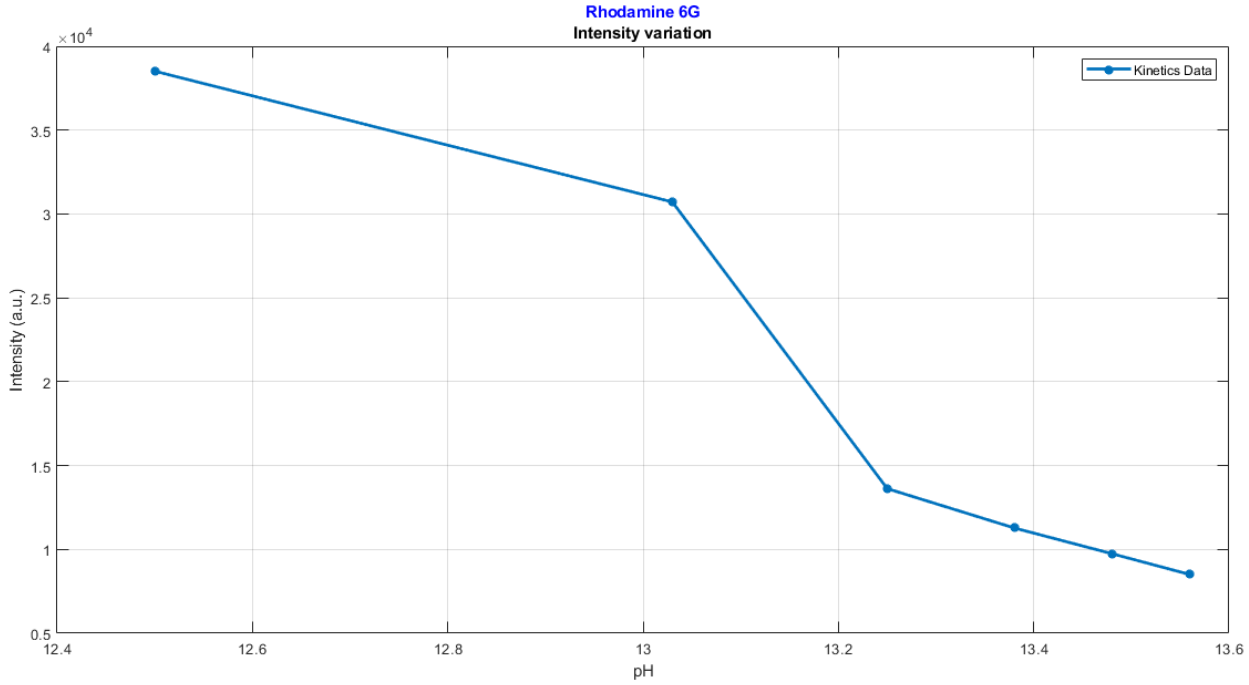

Figure 3.6.2. Intensity variation of Rhodamine 6G across the pH range from 12.5 to 13.5.

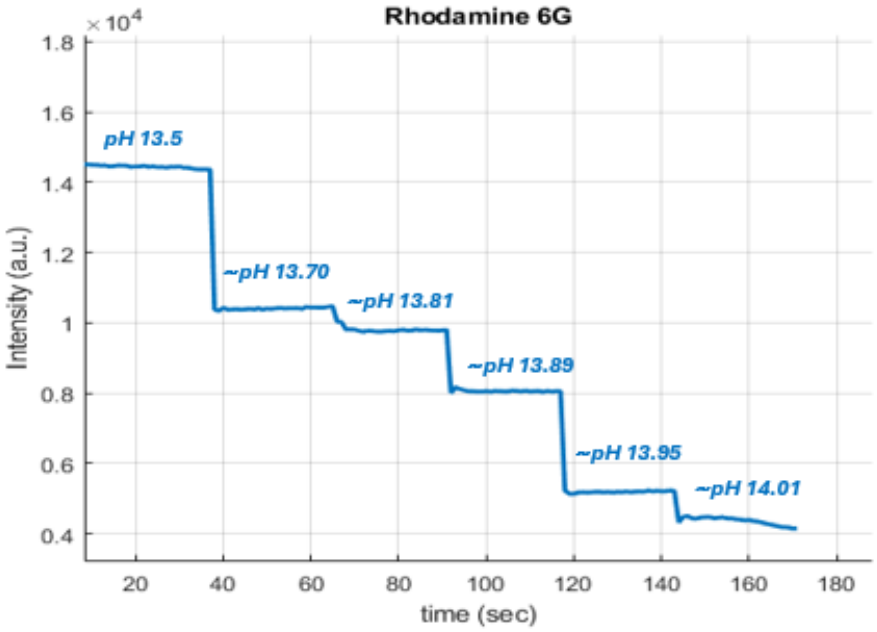

Figure 3.6.3. Kinetic response of Rhodamine 6G starting from pH 13.5 with the addition of a highly concentrated alkaline solution.

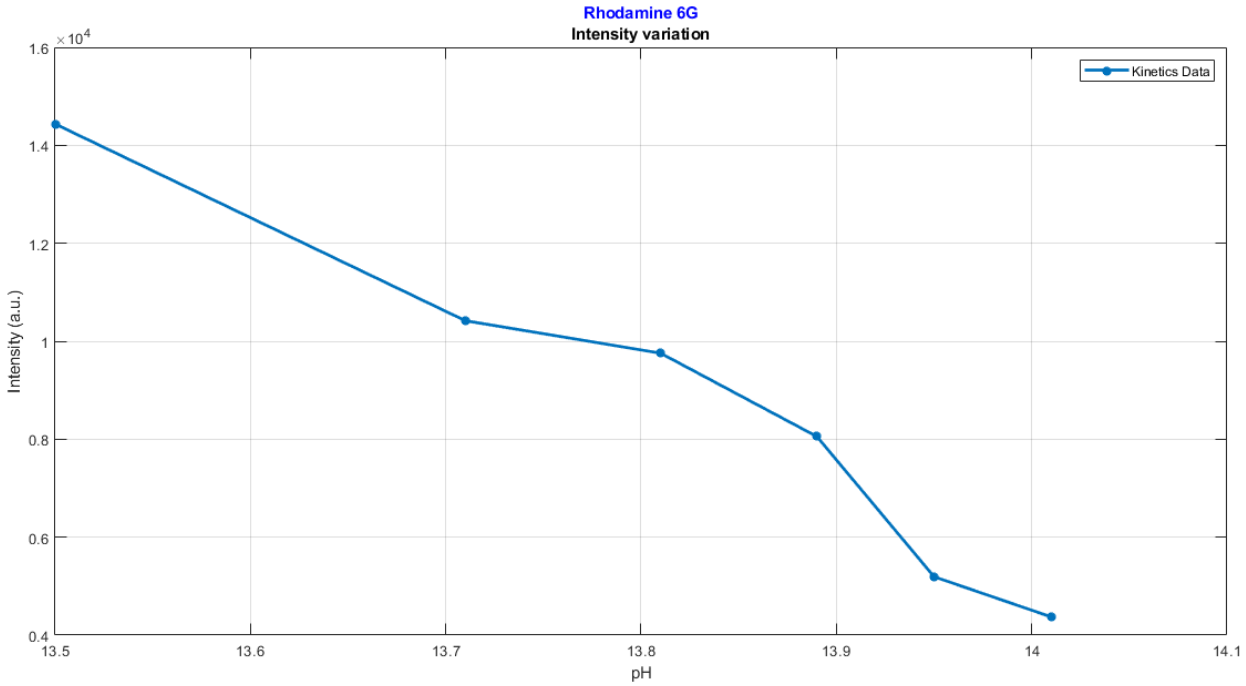

Figure 3.6.4. Intensity variation of Rhodamine 6G across the pH range from 13.5 to 14.

3.6.1. Rhodamine B

Figure 3.6.5 shows the kinetic response starting from pH 12.5, while **Figure 3.6.6.** show the same analysis starting form a pH solution of 13.5.

Compared to Rhodamine 6G, Rhodamine B exhibits a much noisier and unstable response.

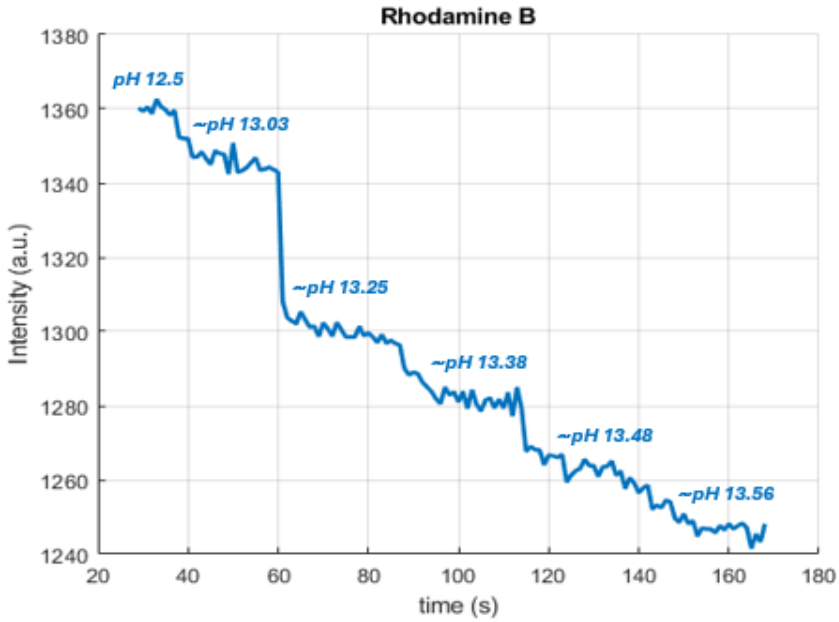

Figure 3.6.5. Kinetic response of Rhodamine B starting from pH 12.5 with the addition of a highly concentrated alkaline solution.

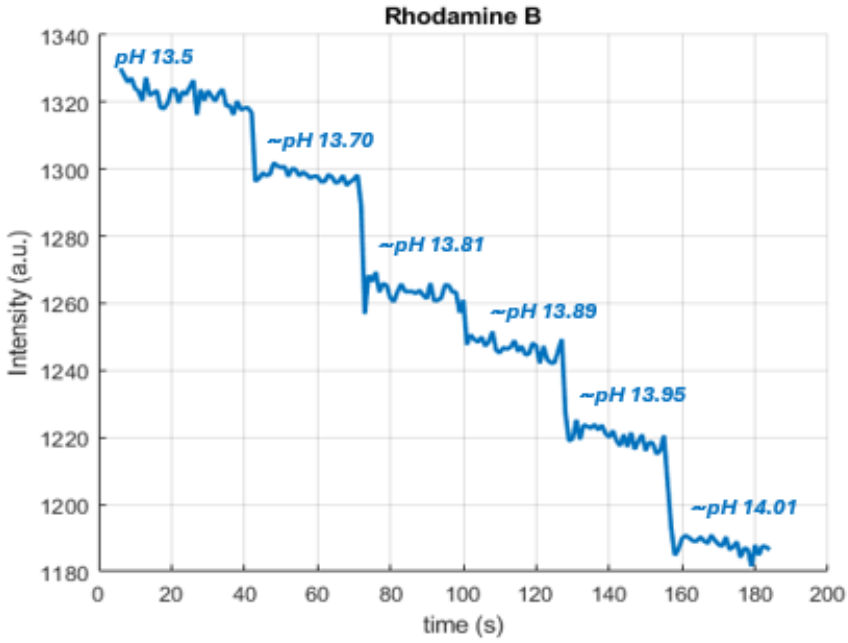

Figure 3.6.6. Kinetic response of Rhodamine B starting from pH 13.5 with the addition of a highly concentrated alkaline solution.

3.7. Florescence Intensity Analysis of Rhodamine 6G with pH

The final step in the results analysis involved preparing new solutions within the desired pH range (pH 12.5 to pH 14.25). The number of investigated points was increased, focusing on the following pH points: 12.5, 12.7, 12.8, 13, 13.1, 13.2, 13.3, 13.4, 13.5, 13.6, 13.7, 13.8, 13.9, 14, 14.1, and 14.25. This test was conducted for the Rhodamine 6G, selected for its suitability and stability compared the other dyes considered. Each pH data point was measured in triplicate. **Figure 3.7.1** shows the average fluorescence intensity values across different pH levels, along with their corresponding standard deviations.

Figure 3.7.2 shows the linear polynomial interpolating the data in the pH range 12.7 to 14, while **Figure 3.7.3** displays the second-order polynomial in the same range.

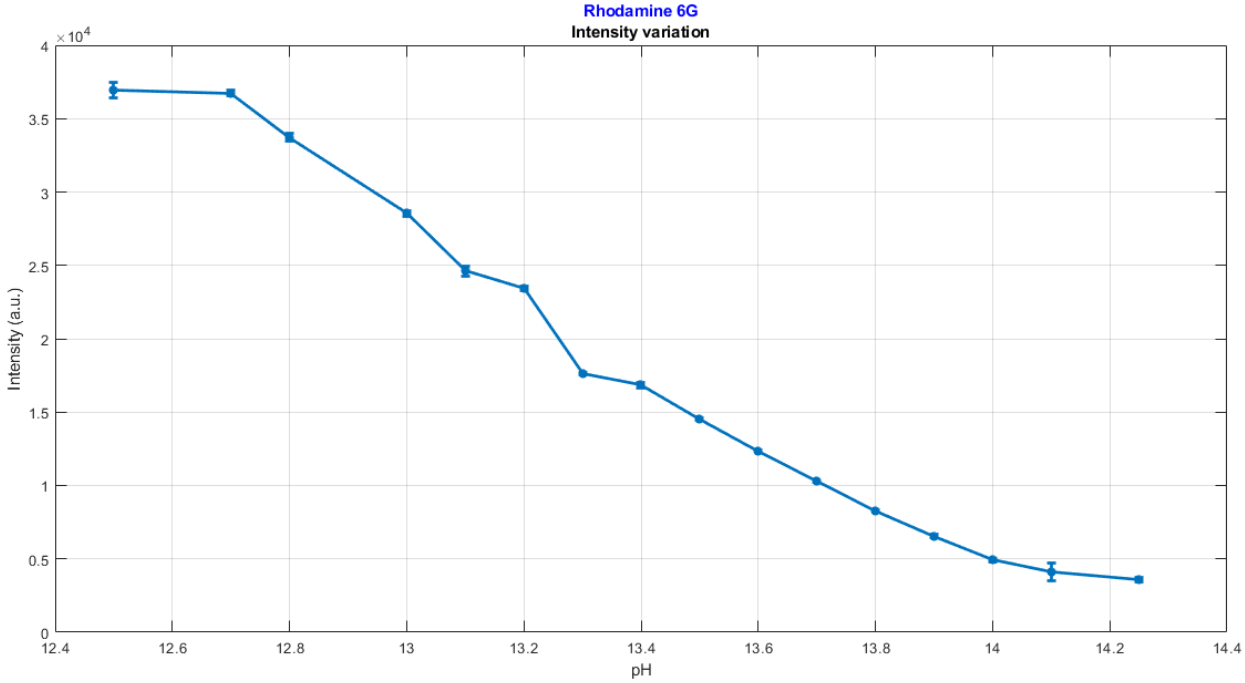

Figure 3.7.1. Intensity-pH variation with the standard deviations of Rhodamine 6G.

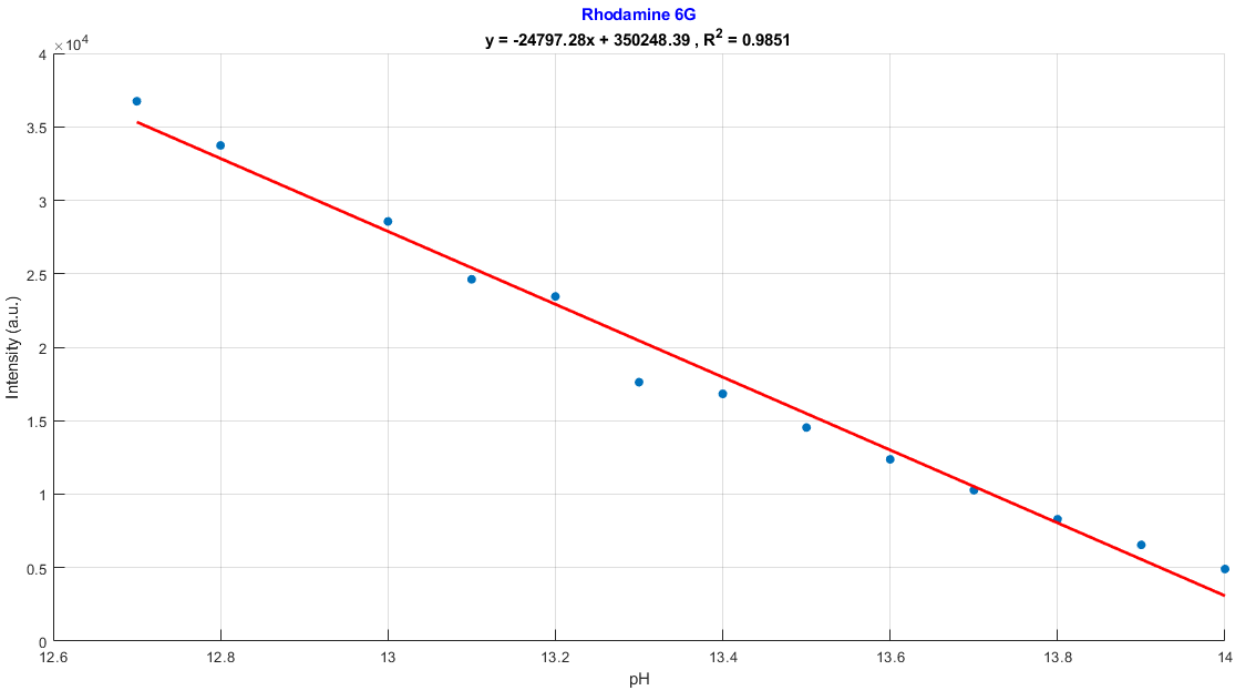

Figure 3.7.2. Linear polynomial interpolation in the range between 12.7 and 14.

Equation of linear polynomial:

$$y = -24797.28\,x - 350248.39 \qquad (3.7.1)$$

Coefficient of determination:

$$R^2 = 0.9851$$

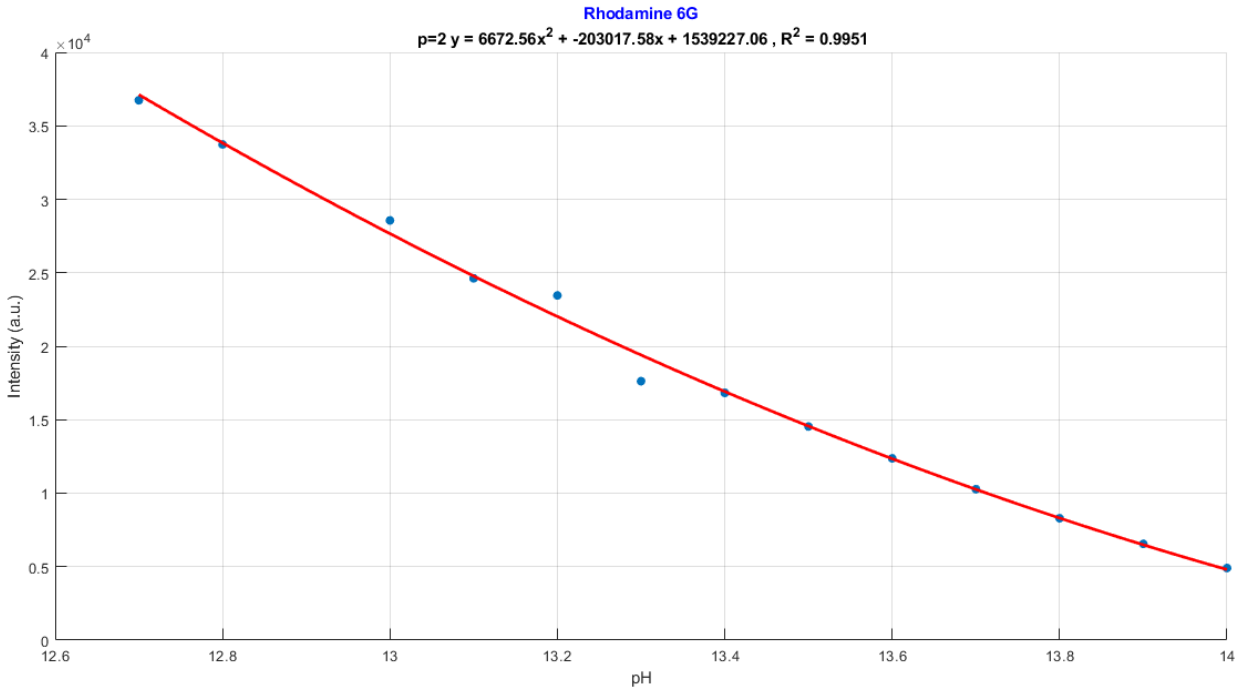

Figure 3.7.3. Second-order polynomial interpolation between pH 12.6 and 14.

Equation of second-order polynomial:

$$y = 6672.56\,x^2 - 203017.58x + 1539227.06 \qquad (3.1.4)$$

Coefficient of determination:

$$R^2 = 0.9951$$

Finally, the data obtained from this latest analysis were compared with those obtained in the previous section *(Kinetic study, specifically with the graphs Figure 3.6.2 and Figure 3.6.3).* These results are shown in **Figure 3.7.4** and **Figure 3.7.5**.

The results appear to demonstrate good repeatability and consistency.

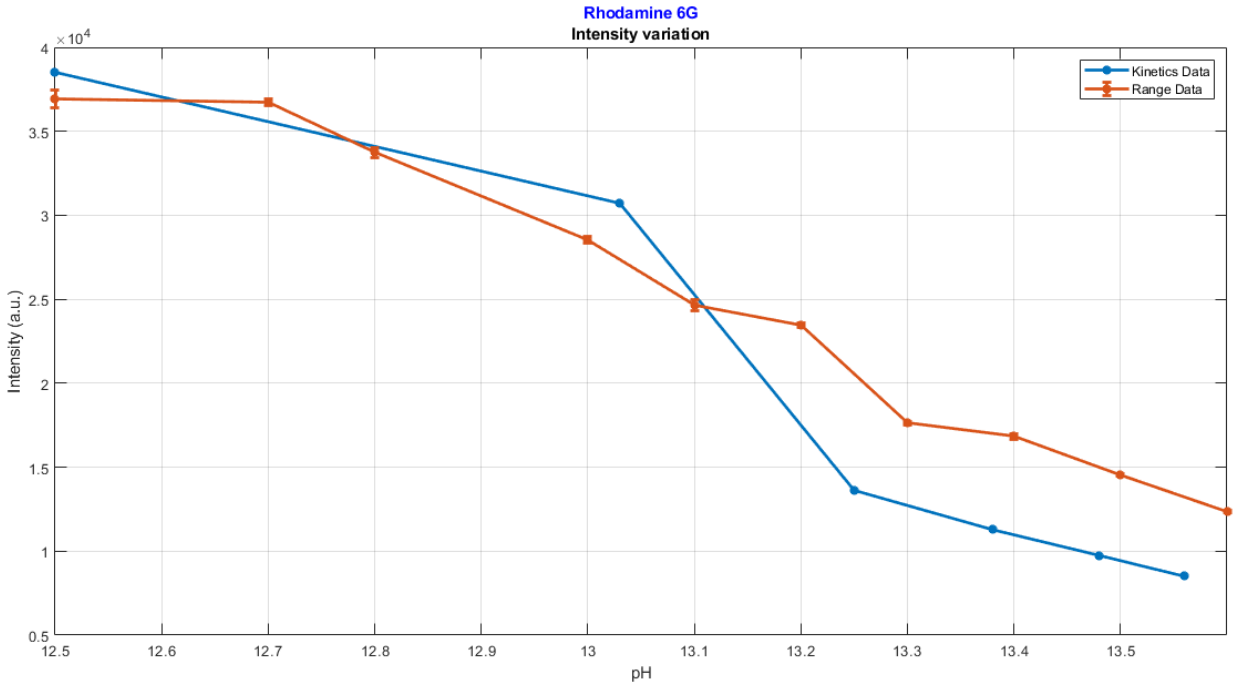

Figure 3.7.4. Comparison of fluorescence intensity profiles of Rhodamine 6G across the pH range from 12.5 to 13.5

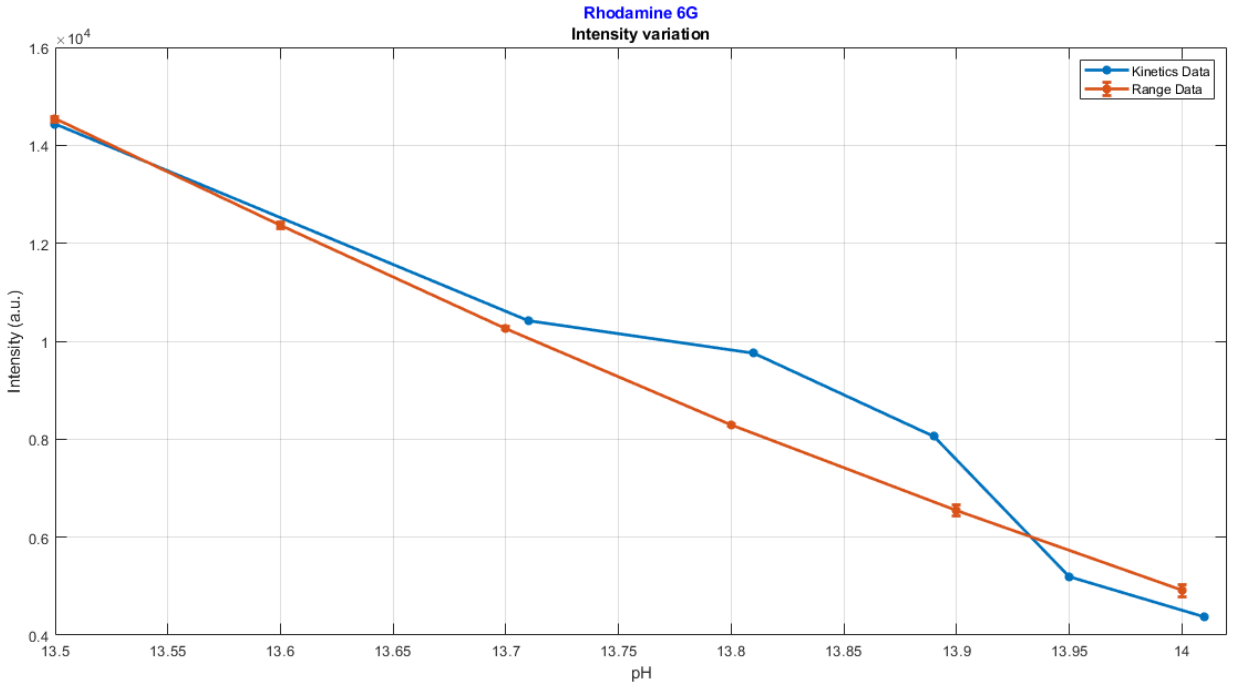

Figure 3.7.5. Comparison of fluorescence intensity profiles of Rhodamine 6G across the pH range from 13.5 to 14.25.

4. Conclusion

The studies conducted identified that Rhodamine 6G is the most suitable dye for the pH monitoring applications under continuous flow conditions.

Rhodamine 6G is characterized by:

- A good stability over time, even in the presence of metal cations.
- A rapid and stable response to gradual pH changes, characterized by quick variations in fluorescence intensity at different pH values.

In comparison to other dyes, Rhodamine 6G also showed consistent results in the fluorescence intensity tests.

These findings are promising and assure the reliability of fluorescence-based methods for pH monitoring. Fluorescence analysis offers a rapid, compact, and accurate measuring way, making it a reliable tool for pH monitoring. The analysis provides a technique to measure the fluorescence without making contact with the solution, which is ideal for continuous flow reactor applications.

This method can be used for measuring other chemical and physical parameters such as redox potential, identifying the presence of specific organic compounds (e.g. pollutants), or the viscosity of the liquids. Its flexibility makes it a valuable tool for improving quality control in various industrial processes.

Future development could focus on extending the analysis to a wider pH range or in acidic environments to improve system versatility.

This would involve alternative dyes and require the study of their interactions with different metals. The application might be furtherly widened to the screening of different thin-film deposition types.

5. Bibliography

[1] Noy Zakay, L. Lombardo, N. Maman, M. Parvis, Leonid Vradman, and Y. Golan, "A Combinatorial Approach for the Solution Deposition of Thin Films," *ACS applied engineering materials*, vol. 1, no. 5, pp. 1367–1374, Apr. 2023, doi: https://doi.org/10.1021/acsaenm.3c00072.

[2] Y.-K. Park *et al.*, "Fabrication of Colorimetric Textile Sensor Based on Rhodamine Dye for Acidic Gas Detection," vol. 12, no. 2, pp. 431–431, Feb. 2020, doi: https://doi.org/10.3390/polym12020431.

[3] J. Pablo, Imelda Santiago Núñez, Georgina Beltrán Pérez, Juan Castillo Mixcóatl, Severino Muñoz Aguirre, and Rodolfo Palomino Merino, "Optical fiber sensor for the measurement of the pH level using organic dyes deposited by the sol-gel process," *Proceedings of SPIE, the International Society for Optical Engineering/Proceedings of SPIE*, doi: https://doi.org/10.1117/12.742279.

[4] L. D. Lavis and R. T. Raines, "Bright Building Blocks for Chemical Biology," *ACS Chemical Biology*, vol. 9, no. 4, pp. 855–866, Mar. 2014, doi: https://doi.org/10.1021/cb500078u.

[5] K. V. Ksenofontova *et al.*, "Amine-Reactive BODIPY Dye: Spectral Properties and Application for Protein Labeling," *Molecules*, vol. 27, no. 22, p. 7911, Jan. 2022, doi: https://doi.org/10.3390/molecules27227911.

[6] S. Casa and M. Henary, "Synthesis and Applications of Selected Fluorine-Containing Fluorophores," *Molecules*, vol. 26, no. 4, p. 1160, Feb. 2021, doi: https://doi.org/10.3390/molecules26041160.

[7] S. Lach, P. Jurczak, N. Karska, A. Kubiś, A. Szymańska, and S. Rodziewicz-Motowidło, "Spectroscopic Methods Used in Implant Material Studies," *Molecules*, vol. 25, no. 3, p. 579, Jan. 2020, doi: https://doi.org/10.3390/molecules25030579.

[8] "Coumarins | AAT Bioquest," *www.aatbio.com*. https://www.aatbio.com/catalog/chemical-reagents-coumarins-and-derivatives (accessed May 06, 2024).

[9] J. R. Lakowicz, *Principles of Fluorescence Spectroscopy*. New York, Ny: Springer Us, 2006.

[10] Granite, “Jablonski Diagram | What is it?,” *Edinburgh Instruments*. https://www.edinst.com/blog/jablonski-diagram-2/

[11] “What is the Jablonski Diagram?,” *www.horiba.com*. https://www.horiba.com/int/scientific/technologies/fluorescence-spectroscopy/what-is-the-jablonski-diagram/

[12] “Spectrometers,” *Avantes*. https://www.avantes.com/products/spectrometers/

[13] “Avantes Bundles | Pro-Lite Technology,” Jul. 01, 2022. https://pro-lite.co.uk/products-services-index/spectroscopy/spectrometers/fibre-optic-spectroscopy/avantes-bundles/ (accessed May 07, 2024).

[14] “Fluorescencia y fosforescencia.” Available: https://shaker.umh.es/jmgr/PDF/TIBs.2011.3.FLUORESCENCIA.pdf

[15] M. Scocchi, “Lezione 5: fluorescenza e chemiluminescenza.” Accessed: May 08, 2024. [Online]. Available: https://moodle2.units.it/pluginfile.php/329891/mod_resource/content/1/Lezione%205%20fluorescenza%20e%20chemiluminescenza%20%202018_19.pdf

[16] G. Beltrán-Pérez *et al.*, “Fabrication and characterization of an optical fiber pH sensor using sol–gel deposited TiO2 film doped with organic dyes,” *Sensors and Actuators B: Chemical*, vol. 120, no. 1, pp. 74–78, Dec. 2006, doi: https://doi.org/10.1016/j.snb.2006.01.048.

[17] M. Sohany, I. S. M. A. Tawakkal, S. H. Ariffin, N. N. A. K. Shah, and Y. A. Yusof, “Characterization of Anthocyanin Associated Purple Sweet Potato Starch and Peel-Based pH Indicator Films,” *Foods*, vol. 10, no. 9, p. 2005, Aug. 2021, doi: https://doi.org/10.3390/foods10092005.

[18] N. Oladzadabbasabadi, A. Mohammadi Nafchi, M. Ghasemlou, F. Ariffin, Z. Singh, and A. A. Al-Hassan, “Natural anthocyanins: Sources, extraction, characterization, and suitability for smart packaging,” *Food Packaging and Shelf Life*, vol. 33, p. 100872, Sep. 2022, doi: https://doi.org/10.1016/j.fpsl.2022.100872.

[19] H. Cui *et al.*, “Recent Advancements in Natural Plant Colorants Used for Hair Dye Applications: A Review,” *Molecules*, vol. 27, no. 22, p. 8062, Jan. 2022, doi: https://doi.org/10.3390/molecules27228062.

[20] “Rhodamine B,” *Wikipedia*, Oct. 20, 2020. https://en.wikipedia.org/wiki/Rhodamine_B

[21] R. F. Kubin and A. N. Fletcher, “Fluorescence quantum yields of some rhodamine dyes,” *Journal of Luminescence*, vol. 27, no. 4, pp. 455–462, Dec. 1982, doi: https://doi.org/10.1016/0022-2313(82)90045-x.

[22] K. G. Casey and E. L. Quitevis, “Effect of solvent polarity on nonradiative processes in xanthene dyes: Rhodamine B in normal alcohols,” *The Journal of Physical Chemistry*, vol. 92, no. 23, pp. 6590–6594, Nov. 1988, doi: https://doi.org/10.1021/j100334a023.

[23] M. J. Snare, F. E. Treloar, K. P. Ghiggino, and P. J. Thistlethwaite, “The photophysics of rhodamine B,” *Journal of Photochemistry*, vol. 18, no. 4, pp. 335–346, Jan. 1982, doi: https://doi.org/10.1016/0047-2670(82)87023-8.

[24] E. Birtalan *et al.*, “Investigating rhodamine B-labeled peptoids: Scopes and limitations of its applications,” *Biopolymers*, vol. 96, no. 5, pp. 694–701, 2011, doi: https://doi.org/10.1002/bip.21617.

[25] “Rhodamine 6G,” *Wikipedia*, Jun. 12, 2023. https://en.wikipedia.org/wiki/Rhodamine_6G

[26] “Indigo carmine,” *Wikipedia*, Dec. 08, 2020. https://en.wikipedia.org/wiki/Indigo_carmine

[27] “Carmine Indigo Food Colouring: Buy Online,” *Alquera.com*, Jun. 18, 2023. https://www.alquera.com/en/colorante-alimentario-azul/ (accessed May 09, 2024).

[28] “Titan yellow,” *Wikipedia*, Jan. 08, 2024. https://en.wikipedia.org/wiki/Titan_yellow (accessed May 09, 2024).

[29] Wikipedia Contributors, “Fiber Bragg grating,” *Wikipedia*, Dec. 15, 2019. https://en.wikipedia.org/wiki/Fiber_bragg_grating

[30] “. Gassino, Development of a fiber optic probe for tumor laser ablation with integrated temperature measurement capabilities. PhD thesis, Politecnico di Torino, 2019.”

[31] “Luna Innovations | Fiber Optic Sensing and Measurement Systems,” *lunainc.com*. https://lunainc.com/

[32] F. Deng *et al.*, “Comparison of rhodamine 6G, rhodamine B and rhodamine 101 spirolactam based fluorescent probes: A case of pH detection,” *Spectrochimica acta. Part*

A, Molecular and biomolecular spectroscopy, vol. 268, pp. 120662–120662, Mar. 2022, doi: https://doi.org/10.1016/j.saa.2021.120662.

[33] "Glass Electrode - an overview | ScienceDirect Topics," *www.sciencedirect.com*. https://www.sciencedirect.com/topics/earth-and-planetary-sciences/glass-electrode

[34] W. Vonau and U. Guth, "pH Monitoring: a review," *Journal of Solid State Electrochemistry*, vol. 10, no. 9, pp. 746–752, Sep. 2006, doi: https://doi.org/10.1007/s10008-006-0120-4.

[35] A. J. Gomes, C. N. Lunardi, F. S. Rocha, and G. S. Patience, "Experimental methods in chemical engineering: Fluorescence emission spectroscopy," *The Canadian Journal of Chemical Engineering*, vol. 97, no. 8, pp. 2168–2175, Jul. 2019, doi: https://doi.org/10.1002/cjce.23506.

[36] C. J. Watras *et al.*, "A temperature compensation method for chlorophyll and phycocyanin fluorescence sensors in freshwater," *Limnology and Oceanography: Methods*, vol. 15, no. 7, pp. 642–652, May 2017, doi: https://doi.org/10.1002/lom3.10188.

[37] "Principio di Franck-Condon," *Wikipedia*, Sep. 14, 2023. https://it.wikipedia.org/wiki/Principio_di_Franck-Condon.

Acknowledgements

I would like to thank my supervisor, Professor Sabrina Grassini, for being there by my side throughout this journey, for encouraging and supporting me, and for all the trust she has shown in me. Without her, this thesis project would not be possible.

I am also very grateful to my co-supervisor, Professor Yuval Golan, for the trust he has shown in me and for his warm welcome and support. Even though my experience in Israel was brief, it was fantastic and very stimulating for me. It was a big honor to have this opportunity and I thank Prof. Golan for it.

I want to thank Leonardo Iannucci for guiding me step by step and for his advice, and also Chiara Bellezza for all the support in the laboratory.